Platinum-Based Nanostructured Materials: Synthesis, Properties, and Applications

Aicheng Chen* and Peter Holt-Hindle

Department of Chemistry, Lakehead University, 955 Oliver Road, Thunder Bay, Ontario P7B 5E1, Canada

Received November 30, 2009

Contents

1. Introduction

Rising energy demands, depletion of fossil fuel reserves, and environmental pollution have fueled the search for energy conversion devices with high efficiency and low emissions. Fuel cells powered by hydrogen or small organic molecules, such as ethanol, formic acid, and methanol, may have the potential to meet these requirements.[1−3] Platinum-based catalysts are vital to fuel cells, sensors, and the petroleum and automotive industries due to their high catalytic activity and stability.[4−6] Over the past decade, research into the design of novel platinum and platinum-based nanomaterials with unique properties has been greatly intensified due to the potential for new applications and improving current applications.[7] Since platinum is a precious metal, most of the recent efforts have focused on decreasing platinum utilization via increasing the catalytic efficiency of Pt-based catalysts by tailoring high-performance Pt-based nanostructured materials,[8,9] revealing that the shape of Pt nanoparticles plays a critical role in catalysis.[10]

This review will outline the common methods of synthesizing platinum nanostructured materials with extracts from published investigations by numerous researchers. These methods include the sol−gel method, electrodeposition, electroless deposition, and physical approaches, as well as hydrothermal and solvothermal techniques. Overall, the synthesis section highlights the diverse range of synthesis parameters as well as the different types of Pt nanostructures and Pt-based nanomaterials formed with each method, noting that the composition, morphology, and properties of the

* Corresponding author. Tel: 1-807-343-8318. Fax: 1-807-3467775. E-mail: aicheng.chen@lakeheadu.ca.

Aicheng Chen received his Ph.D. in Electrochemistry from the University of Guelph under the direction of Professor Jacek Lipkowski in 1998. He then spent two years working as a Research Scientist at Huron Tech Canada Inc. and two years as an Electrochemical Specialist at FINNCHEM Canada Inc. In 2002, Dr. Chen joined Lakehead University as an Assistant Professor, where he was tenured and promoted to Associate Professor in 2005, and became the Canada Research Chair in Material & Environmental Chemistry in 2006. He started to work on Pt-based electrocatalysis in 1990 when he was a M.Sc. student with Professor Shi-Gang Sun at Xiamen University. Dr. Chen's current research interests span the areas of Electrochemistry, Electrocatalysis, Photocatalysis, Electroanalysis, Green Chemistry, Materials Science, and Nanotechnology. For his accomplishments, Dr. Chen has been awarded the Premier's Research Excellence Award (2003); the Canada Research Chair Award in Material & Environmental Chemistry (2005); the Japan Society for the Promotion of Science (JSPS) Fellowship (2006); Lakehead University Merit Award for exceptional performance in research, teaching and service (2004, 2007); and the Canadian National Committee for the International Union of Pure & Applied Chemistry Travel Award (2008). More recently, Dr. Chen received the 2009 Electrochemical Society Canadian Section Lash Miller Award for the excellence of publications and technical contributions in the field of electrochemical science and technology and the 2009 Fred Beamish Award of the Canadian Society for Chemistry, which recognizes individuals who demonstrate innovation in Analytical Chemistry, where the research is anticipated to have significant potential for practical applications.

10.1021/cr9003902
Published on Web 02/19/2010

Peter Holt-Hindle received his H.B.Sc. and M.Sc. degrees in Chemistry from Lakehead University (Thunder Bay, Ontario) in 2006 and 2009, respectively. He was awarded the High Output Publication Excellence (H.O.P.E.) Award, Lakehead University President's Award, and Robert Poulin Awards for publication excellence, academic performance, and outstanding citizenship, respectively. His research interests lie in synthesis of Pt-based nanomaterials with focus on improving the performance of fuel cells and biosensor electrocatalysts.

formed Pt-based nanomaterials can be tuned by manipulating the precursors and reaction conditions. The properties section describes the connection between the composition and morphology of the Pt and Pt-based nanomaterials to their catalytic, magnetic and optical properties, and resulting applications. The application section reviews the catalytic properties of Pt and Pt-based nanomaterials employed in current and prospective applications such as fuel cells, biosensors, automotive catalytic converters, petroleum refining, hydrogen production and anticancer drugs. The catalytic properties of the Pt-based nanostructures are discussed in reference to how they can improve the efficiency and reduce the cost in potential applications, through measures such as decreasing Pt loading by using high surface area supporting materials with good electronic properties and by forming alloyed binary and ternary Pt-based catalysts. By employing diverse fabrication methods to tune the properties of Pt and Pt-based nanostructured materials, there is great potential to improve existing technologies to provide superior and cost-effective solutions to meet the needs of consumers and industries.

2. Synthesis of Pt and Pt-Based Nanomaterials

2.1. Hydrothermal and Solvothermal Techniques

The hydrothermal and solvothermal methods are easy, templateless, and surfactant-free approaches to fabricating Pt and Pt-based nanomaterials.[11−32] Hydrothermal processes involve a heterogeneous reaction, which takes place in aqueous solvents under high temperature and pressure conditions. Solvothermal processes differ in the use of nonaqueous solvents. While there are a large number of variations in the procedures, many similarities exist among the different procedures.[11,13] Hydrothermal and solvothermal processes usually take place in closed systems, such as Teflon lined autoclaves enclosed in stainless steel vessels. The major difference between the hydrothermal and solvothermal methods used to synthesize Pt and Pt-based nanomaterials is the Pt precursor. The majority of nanomaterials fabricated using hydrothermal processes use $H_2PtCl_6 \cdot xH_2O$,[11−17,19,21−29] whereas solvothermal processes use compounds such as platinum acetylacetonate, $Pt(acac)_2$.[30,31] Chen et al.[28] prepared nanoporous Pt networks using a hydrothermal-assisted seed growth method. Pt nanoparticles were synthesized onto a titanium substrate using the following electrochemical deposition conditions: -20 mA cm^{-2} for 3 min in a solution containing 0.8 g L^{-1} H_2PtCl_6 and 0.3 g L^{-1} HCl. Following the modification, the titanium substrate was placed inside a sealed Teflon lined vessel containing 0.8 g L^{-1} H_2PtCl_6, 0.3 g L^{-1} HCl, and ethylene glycol and heated to 100 °C for 10 h. The as-synthesized Pt nanomaterials had diameters in the range of tens to hundreds of nanometers and formed a nanoporous network on the Ti substrate. The nanoporous Pt networks possess a large electroactive surface, which contributes to their enhanced electrocatalytic properties compared with polycrystalline Pt. Hou et al.[31] synthesized PtFe nanowires using a solvothermal reduction process. A solution containing 50 mM $Pt(acac)_2$, 2 mM glycerol, or 1,2-hexadecandiol and 70 mL of ethylenediamine was mixed before adding 0.75 mM $Fe(CO)_5$. The solution was transferred into a Teflon autoclave inside a stainless steel vessel and heated to 180 °C for 48−96 h. The products were centrifuged, washed with distilled water and ethanol to remove residual alkaline salt and surfactant, and then dried at 60 °C for 4 h in a vacuum oven. Figure 1 shows that the as-synthesized FePt nanowires have diameters of 30−50 nm. The nanowires were annealed in an Ar atmosphere for 30 min at 500 and 600 °C in order to further investigate their morphologies and magnetic properties.

Formaldehyde[19,21,25] and ethylene glycol[22,24,28] are the two most common reducing agents used in the hydrothermal synthesis of Pt and Pt-based nanomaterials. Holt-Hindle et al.[15,16] prepared nanoporous PtIr electrocatalysts using formaldehyde as the reducing agent. They began by mixing 9.0 mL of 1.6 g L^{-1} $H_2PtCl_6 \cdot 6H_2O$ in 1.72 g L^{-1} HCl, various amounts of an $IrCl_3$ solution containing 2.96 g of $IrCl_3$ dissolved in 60 mL of isopropyl alcohol, and 0.24 mL of 17% formaldehyde in a sealed Teflon container that contained titanium plates pre-etched in 18% HCl at 85 °C for 15 min. The Teflon container was placed inside a stainless steel vessel

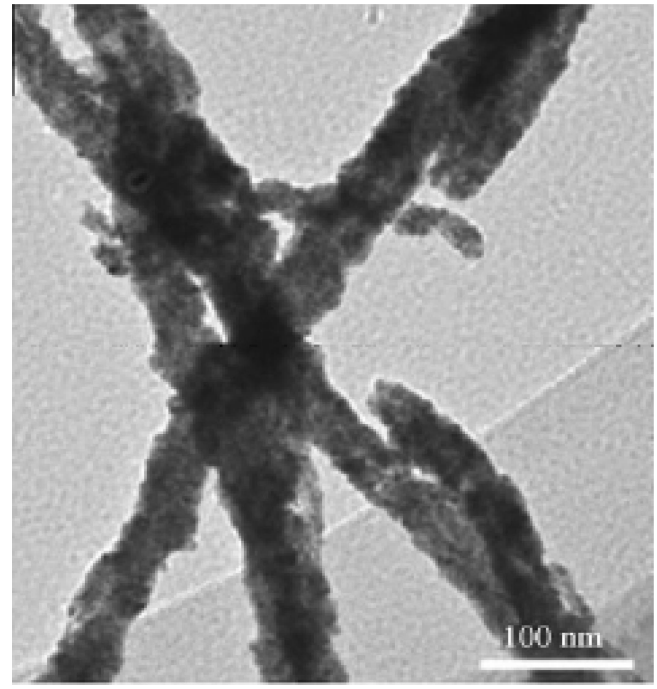

Figure 1. TEM image of the PtFe nanowires. Reprinted from Hou, Y.; Kondoh, H.; Che, R.; Takeguchi, M.; Ohta, T. *Small* **2006**, *2*, 235. Copyright 2006 Wiley-VCH.

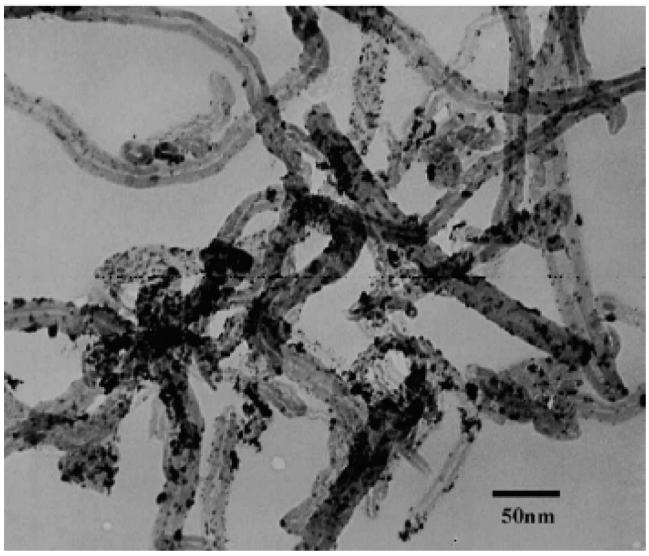

Figure 2. TEM image of Pt/MWCNT nanocomposite. Reprinted from Chen, L.; Lu, G. *Electrochim. Acta* **2008**, *53*, 4316. Copyright 2008 Elsevier.

and heated to 180 °C for 10 h. The as-synthesized nanoporous PtIr catalysts completely covered the surface of the Ti substrate and had diameters ranging from 50 to 500 nm. The metallic ratio of Pt/Ir was easily changed by varying the composition of the $IrCl_3$ and $H_2PtCl_6 \cdot 6H_2O$ precursors. Chen et al.[22] prepared size-dependent Pt nanoparticles on MWCNTs (multiwalled carbon nanotubes) using ethylene glycol as the reducing agent. Prior to the deposition of the Pt nanoparticles, the MWCNTs were functionalized via refluxing for 24 h in a 2.6 M nitric acid solution at 123 °C. Preparation of the Pt nanoparticles began with the mixing of 2.7 mL of 0.3862 M H_2PtCl_6, 10 mL of ethylene glycol or glycerol, and 80 mg of MWCNTs before drops of NaOH were added to adjust the pH. The mixture was ultrasonicated for 30 min to disperse the MWCNTs in the solution before 75 mL of the precursor solution was transferred to a Teflon lined autoclave. The vessel was heated to 160 °C for 5 h. The final product was filtered, washed with ethanol and deionized water, and dried at 373 K for 12 h. Figure 2 shows a TEM image of the Pt nanoparticles with an average size of 7.1 nm moderately dispersed on the MWCNTs formed using ethylene glycol as the reducing agent. Overall, the type of reducing agent and pH of solution had a significant effect on the nanoparticle size, dispersion, and electrocatalytic activity.

One of the advantages of the hydrothermal and solvothermal methods is that Pt,[18,28] Pt-based binary,[15−17,30,31] and Pt-based ternary nanomaterials[14] can be easily fabricated. In comparison to the above-described Pt nanomaterials, the synthesis of binary Pt-based nanomaterials requires the addition of another metallic precursor solution. For example, Wang et al.[21] fabricated a variety of titanium-supported binary Pt-based nanomaterials using the hydrothermal method. A typical synthesis involved transferring the etched titanium substrate into a Teflon lined autoclave containing 54.4 mM H_2PtCl_6, various amounts of other metallic precursor solutions from the group of $Pb(NO_3)_2$, $RuCl_3$, $IrCl_3$, or $PdCl_2$, and the reduction agent formaldehyde. The total volume of the aqueous mixture was 10 mL. The autoclave was sealed before it was heated to 180 °C for 10 h. Figure 3 shows the SEM images of the as-synthesized Pt-based nanomaterials with particle sizes ranging from tens of nanometers to hundreds of nanometers. After cooling, the coated titanium plates were annealed in an argon atmosphere for 2 h at 250 °C prior to electrochemical testing. Overall, the hydrothermal method allowed for the fabrication of a variety of Pt-based nanomaterials with tunable bimetallic compositions. Yi et al.[14] prepared titanium-supported ternary PtRuIr nanomaterials using a one-step hydrothermal process. The titanium supports were etched and placed inside a Teflon holder containing a solution composed of 10 mL of 0.8 g L^{-1}

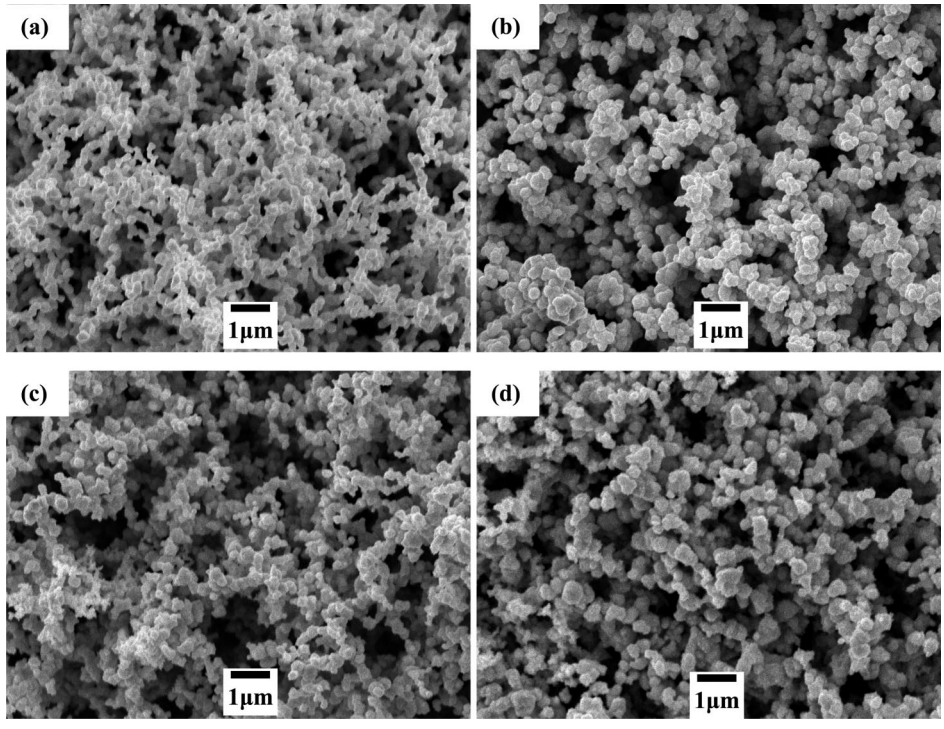

Figure 3. SEM images of various PtM (50:50) nanomaterials synthesized using formaldehyde as a reducing agent: (a) PtPb; (b) PtIr; (c) PtPd; and (d) PtRu. Reprinted from Wang, J.; Holt-Hindle, P.; MacDonald, D.; Thomas, D. F.; Chen, A. *Electrochim. Acta* **2008**, *53*, 6944. Copyright 2008 Elsevier.

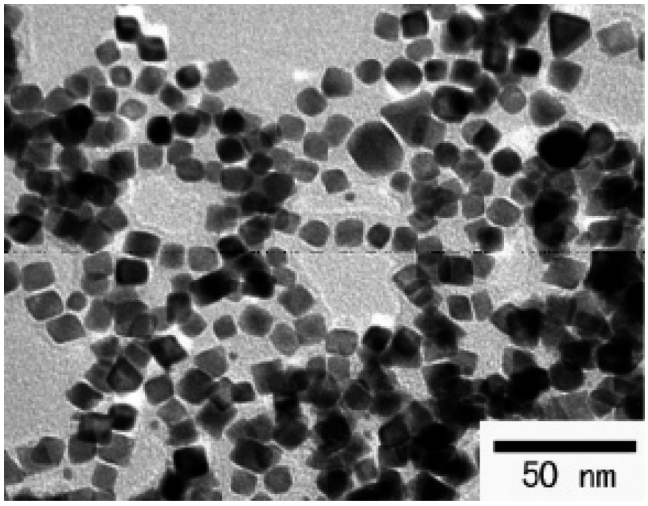

Figure 4. SEM image of the PDDA-protected Pt nanopolyhedrons. Reprinted from ref 29. Copyright 2007 American Chemical Society.

H_2PtCl_6 in 0.86 g L^{-1} HCl, 3.5 g L^{-1} $RuCl_3$, 0.05 mL of 0.14 M $IrCl_3$, and 0.5 mL of ethylene glycol. The solution was mixed, sealed in a stainless steel vessel, and heated to 180 °C for 10 h. The resulting nanomaterials had particle diameters ranging from 170 to 230 nm, which demonstrates that platinum, iridium, and ruthenium were collectively deposited onto the electrode supporting material using a one-step hydrothermal process.

The hydrothermal and solvothermal processes can be employed to synthesize a wide variety of nanomaterials, ranging from nanoparticles[18−28] to nanoparticles with distinct shapes,[29] nanowires,[30,31] and nanodendrites.[17] For instance, Chen et al.[29] synthesized Pt nanopolyhedrons using a hydrothermal process. A solution containing 200 μL of poly(diallyldimethylammonium chloride) (0.27 M), 5 mL of water and 600 μL of H_2PtCl_6 (19.3 mM) was stirred for 30 min. The mixture was transferred into a 15 mL Teflon autoclave, sealed and heated to 140 °C for 40 h. After the samples cooled, they were centrifuged at 12 000 rpm and rinsed with purified water. Figure 4 shows the SEM image of the as-synthesized Pt nanopolyhedrons with average diameters of 10 nm. The Pt nanopolyhedrons were synthesized using a hydrothermal method without any seeds or surfactants and display good electrocatalytic activity for O_2 reduction. Wang et al.[17] prepared alloyed PtAu nanodendrites using a single-step hydrothermal process. A typical synthesis involved placing etched titanium plates into a Teflon autoclave containing a solution of 5.0 mM H_2PtCl_6, 5.0 mM $HAuCl_4$, 1.0 M ammonium formate, and formic acid to adjust the pH to between 5.5 and 6.5. The autoclave was sealed in a stainless steel vessel and heated to 180 °C for 8 h. The samples were allowed to cool to room temperature before undergoing annealing at 250 °C for 2 h in an Ar atmosphere. Figure 5 presents the SEM image of the PtAu nanodendrites with the cluster sizes ranging from 80 to 100 nm and trunk lengths from 1 to 10 μm. The PtAu nanodendrites were synthesized with an environmentally friendly and surfactant-free hydrothermal method and showed high electrocatalytic activity toward formic acid oxidation.

Hydrothermal and solvothermal methods are easy and reproducible processes that offer the potential to fabricate a wide variety of Pt and Pt-based nanostructured materials on various supporting materials such as titanium, silica, or carbon nanotubes. Overall, these methods use inexpensive

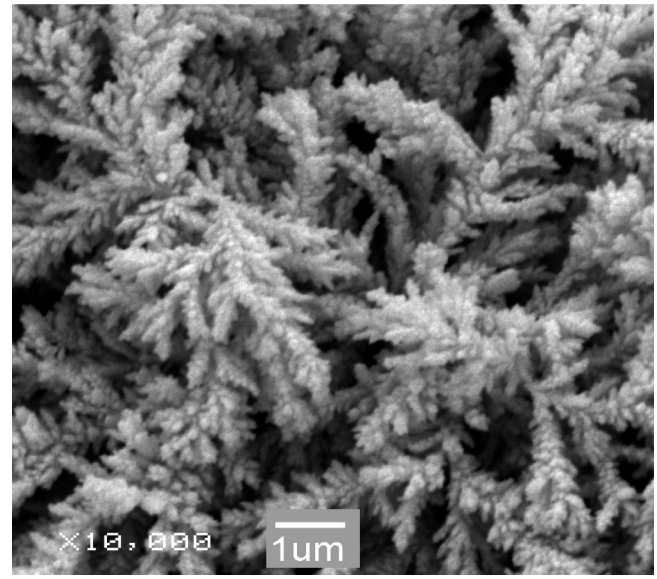

Figure 5. SEM image of the as-synthesized PtAu catalyst. Reprinted from Wang, J.; Thomas, D. F.; Chen, A. *Chem. Commun.* **2008**, 5010. Copyright 2008 Royal Society of Chemistry.

equipment and can be completed quickly, often within a day. The composition and morphology of the as-synthesized Pt and Pt-based nanostructured materials can be tuned by manipulating the precursors, pH, and temperature of the reaction.The method is also particularly suitable for the synthesis of large quantities of various Pt-based nanostructured materials while maintaining good control over their composition. Disadvantages of the method include the need for autoclaves for handling the high-temperature and high-pressure experimental conditions and the impossibility of observing the growth of the nanostructured materials.

2.2. Sol−Gel Method

The solution−gel (sol−gel) process is a wet chemical technique used to efficiently and economically fabricate platinum nanostructures.[33−55] The sol−gel technique is based on hydrolyzable precursors, such as metal alkoxides, which undergo hydrolysis and polycondensation reactions as well as subsequent drying to form various products. This method has been widely used to create platinum[33−40] and platinum-based[41,50,54] nanoparticles with uniform size. Many research groups use $H_2PtCl_6 \cdot xH_2O$ as their platinum precursor.[37,40,42,55] For instance, Bass et al.[55] created Pt nanoparticles by slowly adding drops of a solution containing a predetermined amount of $H_2PtCl_6 \cdot 6H_2O$ in 4 mL of ethanol into a mixture consisting of 25 mL of aluminum-tri-*sec*-butoxide (ATB), 10 mL of deionized water, and 100 mL ethanol. Once the solution turned yellow, the mixture was aged for 1 day in a rotavapor at 60 °C. The solvent was removed by heating the solution to 80 °C for 1 h and to 100 °C for an additional 1 h. The sample was allowed to air-dry overnight at 100 °C before undergoing calcination for 8 h at 500 °C in O_2/Ar. The resulting Pt nanoparticles were encapsulated in the alumina support and had diameters of 4.5 ± 1.4 nm.

Other research groups have synthesized Pt and Pt-based nanomaterials using organometallic precursors[36,45,47,49,51] rather than $H_2PtCl_6 \cdot xH_2O$. For example, Malenovska et al.[46] employed $Pt(acac)_2$ as a precursor to form Pt nanoparticles in a silica film. The fabrication began by dissolving 0.1 mmol of $Pt(acac)_2$ in 10 mL of ethanol and the subsequent addition of {(3-[(2-aminoethyl) amino]propyl}triethoxysilane

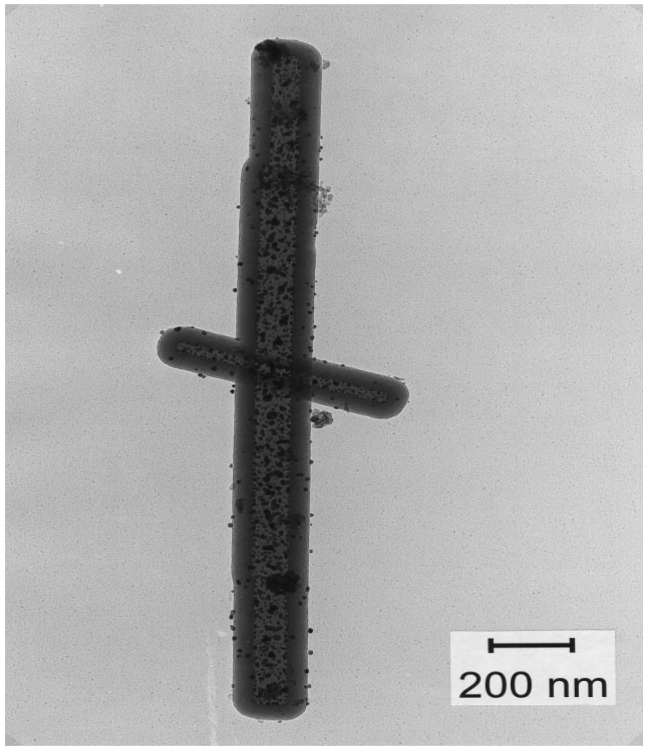

Figure 6. TEM image of Pt nanoparticles on calcinated TiO_2 nanotubes. Reprinted from Hippe, C.; Wark, M.; Lork, E.; Schulz-Ekloff, G. *Microporous Mesoporous Mater.* **1999**, *31*, 235. Copyright 1999 Elsevier.

(AEAPTS). The amount of AEAPTS added corresponded to a 1:4 molar ratio of Pt/AEAPTS. The mixture was stirred until no further color change was observed. Following the stirring, 0.2 mmol of tetraethoxysilane (TEOS) and 40 mL of 0.2 N aqueous NH_4OH were added to the solution. Subsequently, the sample was heated to 70 °C for three days. The platinum nanoparticles were formed following reduction in a hydrogen atmosphere at 500 °C for 2 days and had an average diameter of 22 nm. Overall, the Pt nanoparticles were found to be highly dispersed in the silica film and higher average particle diameters were obtained with increasing reduction temperatures.

Platinum nanoparticles can be fabricated on many supporting materials such as silicates,[36,40,47,49,51] aluminum,[45,55] titanium,[39] and carbon.[42,43] Hippe et al.[38] fabricated TiO_2 nanotubes containing platinum nanoparticles. The preparation began by dissolving 0.0193 g of $[Pt(NH_3)_4](HCO_3)_2$ in 2.15 g of water, followed by adding 40 mL of ethanol. A mixture containing 170.2 μL of tetrabutylorthotitanate (TBOT) and 2.15 g of 0.4 N NH_3 was added dropwise to the solution at 203 K. The mixture was stirred for 12 h, and its temperature was then increased to room temperature, before the solvent was removed at 333 K and 1600 Pa. The sample was dried in a vacuum to remove the alcohol and water. As shown in Figure 6, the uniformly dispersed platinum nanoparticles were produced on the inside and outside of the TiO_2 nanotubes following the calcination of the sample at 773 K for 2 h. Hu et al.[45] created alumina-supported platinum nanoparticles using a single step sol−gel method. A solution of water and aluminum tri-*sec*-butoxide (ATB) was prepared at a molar ratio of 100:1 (H_2O/ATB) by stirring the components at room temperature for 30 min. Drops from a 0.1 g mL^{-1} HNO_3 solution were added to the mixture, which was stirred for 10 min to allow the ATB to decompose and form a *sec*-butanol phase on top of the solution. The *sec*-butanol phase was removed from the mixture prior to adding more HNO_3 solution to bring the molar ratio of HNO_3/Al to 0.5. The solution was stirred for 1 h and sonicated for 30 min at room temperature following the addition of $Pt(NH_3)_4Cl_2$ to the mixture. Following 48 h in a fume hood, the solvent water evaporated resulting in the formation of a gel. Additional drying of the sample occurred at 110 °C for 12 h and 200 °C for 12 h, before calcination at 550 °C for 2 h to form the resulting platinum nanoparticles with diameters ranging from 10 to 50 nm.

Some research groups have also successfully used the sol−gel method to create binary Pt-based nanomaterials, including PtAg,[41] PtSn,[54] and PtRu.[48,50] Yu et al.[41] used the sol−gel process to create silica-stabilized PtAg nanoparticles. The fabrication began by mixing 6.07 g of cetyltrimethylammonium bromide (CTAB) and 150 mL of toluene. Solutions containing 0.091 g of $(NH_4)PtCl_4$ and 0.082 g of $AgNO_3$ in a total of 4.20 mL of deionized water to yield an atomic ratio of 2:1 (Ag/Pt), were added separately. Following the addition of 0.66 mL of 5 M NaOH and 2 h of stirring, drops of 98% hydrazine monohydrate were added to reduce the metals. A change in color of the mixture from pink to black was observed. Finally, drops of TEOS (total of 6.934 g) were added to the mixture, which was stirred for 6 days. The as-synthesized alloyed PtAg nanoparticles were stabilized in silica gel and had a uniform particle size (4−5 nm). Balakrishnan and Gonzalez[54] prepared bimetallic Pt−Sn nanomaterials using the sol−gel method. Solutions containing 49.8 g of ATB in 100 mL of 2-butanol, $H_2PtCl_6 \cdot xH_2O$ in 5 mL of warm acetone and 0.27 g of $SnCl_4 \cdot 5H_2O$ in 5 mL of warm acetone were combined and mixed thoroughly. Another solution containing 0.6 mL of HCl, 10.6 g of H_2O, and 100 mL of methanol was added to the mixture and stirred. The resulting mixture was transferred to a rotavapor where it was mixed continuously, undergoing a series of temperature variations. The rotavapor was opened to the atmosphere to aid in solvent removal before several more temperature variations: 60 °C for 20 h, 80 °C for 1 h, and 100 °C for 30 min. The sample was transferred to an oven where it was dried at 120 °C for one day. Finally, the metallic components were reduced by heating the sample to 500 °C for 2 h in 5% O_2, 15 min in He, and 3 h in H_2. The temperature was temporarily increased to 520 °C in He before it was reduced to 500 °C for 1 h. Finally, the sample was allowed to cool to room temperature under the He atmosphere. Overall, the size of the binary PtSn nanocatalysts was not significantly impacted by the Sn content. Kim et al.[50] formed Pt−Ru nanomaterials on carbon for the purpose of application in direct methanol fuel cells (DMFCs). The Pt and Ru sources were a solution prepared by mixing 0.00338 mol of $Pt(acac)_2$ and various amounts of ruthenium acetylacetonate ($Ru(acac)_2$) in 100 mL of acetone at 50 °C. A gel was formed following the addition of a solution containing 25% tetramethylammonium hydroxide (TMAH) in methanol and stirring the mixture for 10 min. The gel was dried in air at 170 °C for 10 h. The resulting dried gel was crushed with a mortar and pestle and then heated to 190−400 °C in air or in 0.1−1% O_2 for 2−10 h to form PtRu nanoparticles with diameters <50 nm.

Sol−gel synthesis is a useful technique for creating Pt and Pt-based nanoparticles with uniform size and distribution. The syntheses can be carried out with a variety of precursors, completing or networking agents, and heat treatments to vary the resulting particle size. The ability to fabricate Pt and Pt-

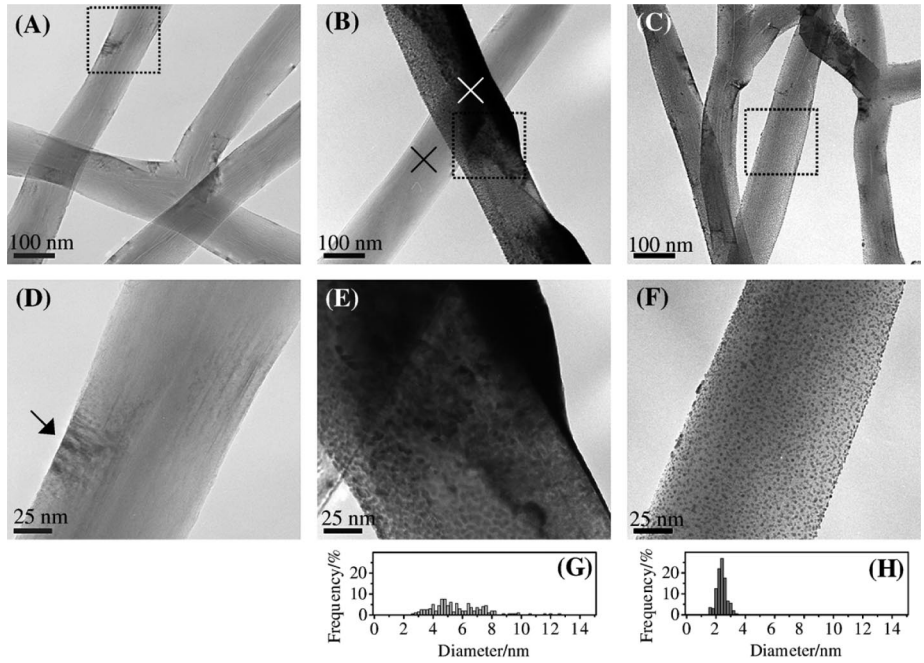

Figure 7. TEM images of CNFs (A) before and (B, C) after Pt deposition with various sputtering conditions; panels D, E, and F are enlarged images from the boxes in panels A, B, and C, respectively; and panels G and H are histograms of the Pt nanoparticle diameters from panels E and F, respectively. Reprinted from Yamamoto, H.; Hirakawa, K.; Abe, T. *Mater. Lett.* **2008**, *62*, 2118. Copyright 2008 Elsevier.

based nanomaterials with small dimensions makes this technique promising in the development of highly efficient Pt-based catalysts for fuel cells and other applications.

2.3. Physical Synthesis Techniques

Physical syntheses for fabricating Pt and Pt-based nanomaterials are quite varied. The products created range from nanosized films, nanoparticles, and nanowires to nanorods. Physical syntheses are processes whereby the precursor material undergoes no chemical change. This broad range of fabrication methods includes sputtering,[58−86] ion or electron beam deposition,[87−98] laser ablation,[99−106] and various types of irradiation.[107−123]

The preparation of Pt nanomaterials with sputtering methods allows for the precise control of Pt content.[56,57] A variety of Pt nanomaterials have been fabricated including nanoparticles,[60−66,70,73,75] nanostructured thin films,[59,67,68,71,84] and bimetallic Pt-based nanomaterials.[72,78,82,85] Yamamoto et al.[70] used a polygonal barrel sputtering system to deposit Pt nanoparticles onto carbon nanofibers (CNF). The sputtering target was a 99.95% Pt plate (50 mm × 100 mm). The sputtering conditions were Ar pressure of 1.2 Pa, 50 W RF power, and deposition time of 30 min and the barrel was rotated at an angle of ±75° at 5 rpm. In addition, the barrel was hit with a mechanical vibrator 20 times per minute. Figure 7 reveals that the dispersion of the Pt nanoparticles varies depending on the deposition parameters. In Figure 7E, the unmodified CNFs have nonuniformly dispersed Pt nanoparticles with a wider size distribution that is due to the aggregation of the CNFs. As shown in Figure 7F, when bent pieces of stainless steel were placed in the sputtering system with the CNFs, the Pt nanoparticles were evenly dispersed and had a narrow size distribution. The addition of small pieces of columnar stainless steel (ϕ 2 × 10 mm) to the CNFs evidently helped to minimize CNF aggregation by gently pulling apart the fibers without breaking them.

Electron and ion beam induced deposition (EBID and IBID) methods have been used to fabricate a variety of Pt and Pt-based nanomaterials including nanoparticles,[91,94−96] nanostructured films,[97] nanowires or nanorods,[87−90,92] and bimetallic Pt-based nanomaterials.[90,94] EBID had the advantages of reduced thermal stress, no ion implantation, lack of damage to the substrate and absence of Ga contamination; however it has lower deposition rates compared with IBID.[93] Plank et al.[87] utilized EBID to fabricate Pt nanorods on highly orientated pyrolytic graphite (HOPG). The Pt precursor used was a $C_9H_{16}Pt$. A FEI Nova200 dual beam system and a four-gas injection setup were used for the Pt deposition. The synthesis conditions were a temperature of 45 °C, a working distance of 4.8 mm, and a dwell time of 4 ms. In addition, the growth times, accelerating voltages, and beam currents were tuned to optimize the volume of the Pt nanorods. Figure 8 shows the TEM image of a representative Pt nanorod with an apex diameter of 10 nm. Beam defocus was found to have a significant influence on volume growth rates.

Liao et al.[88] synthesized carbon-sheathed Pt nanowires using focused IBID. A Dual-Beam 235 system from FEI Company was used for the synthesis. The Pt precursor used was $(CH_3)_3CH_3C_5H_4Pt$ gas. The synthesis conditions were 1.4×10^{-6} mbar, 30 kV Ga^+ ions scanned over the substrate in the presence of the Pt precursor, 0.2 μs dwell time, and a −50% overlap. Following the deposition, the Pt nanowires were annealed at various temperatures to investigate the effect on product morphology. The product Pt nanowires had granular metal composite systems, which can be visualized as a long network of Pt grains. The trend that emerges is the higher the temperature of the annealing, the larger the Pt grains and their resulting conductivity.

Dolbec et al.[103] investigated the growth dynamics of pulse laser deposited Pt nanoparticles on a highly ordered pyrolytic graphite (HOPG) substrate. The Pt nanoparticles were fabricated at room temperature. The system was set up with the laser beam focused on a 5 cm × 5 cm polycrystalline Pt

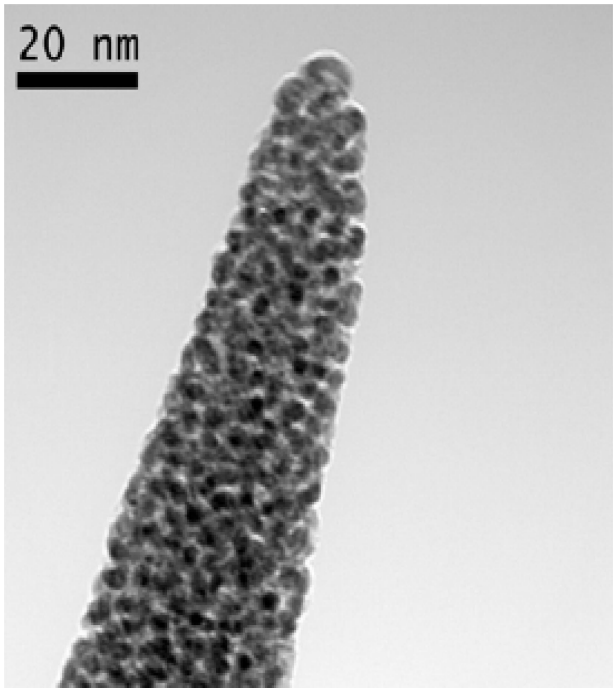

Figure 8. TEM image of a typical Pt nanorod tip synthesized with a focused beam at 30 keV and 150 pA. Reprinted from Plank, H.; Gspan, C.; Dienstleder, M.; Kothleitner, G.; Hofer, F. *Nanotechnology* **2008**, *19*, 485302. Copyright 2008 IOP Publishing.

target (99.99%) at an angle of 45 °C. The target was ablated in a high vacuum vessel (10^{-6} Torr) using a KrF excimer laser with a wavelength of 248 nm, pulse duration of 17 ns, and a 20 Hz repetition rate. To ensure the production of reproducible samples, the target was moved across the laser beam continuously through the rotation and translation movement of the Pt target. The number of laser pulses was varied from 5 to 1000 to vary the amount of Pt deposited on the HOPG substrate. As the number of pulses increased, the thickness of the Pt layer and the Pt nanoparticle diameter increased. In addition, the kinetic energy of the ablated species was found to influence particle size and morphology. High kinetic energy in the ablated species resulted in a reduction of particle size and flattened particle shape. Optimizing the synthesis conditions of pulsed laser deposition enables researchers to have a high degree of control over the size of the resulting nanoparticles.

Irridiation techniques have been successfully employed to fabricate a variety of Pt nanoparticles,[107,109−111,114−118] nanowires,[112,113] and bimetallic Pt-based nanomaterials.[119,121,122] Numerous irradiation methods have been used to synthesize these Pt nanomaterials including γ,[113,117,119−121] UV/vis,[108,114−116,118,122,123] microwave,[107,111] and sonication.[109,110,112] Deivaraj et al.[107] employed microwave irradiation to fabricate carbon-supported PtNi nanoparticles. The synthesis began by preparing a solution containing 0.1 g of Vulcan XC-72, 0.2 g of 10 000 wt poly(*N*-vinyl-2-pyyrolidone) (PVP), 30 mL of water, 10 mL of a 5 mM K_2PtCl_4 solution, and 10 mL of a 5 mM $NiCl_2 \cdot 6H_2O$ solution. PVP was utilized as a stabilizing agent. This mixture was transferred to a CEM Discover microwave reactor and subjected to 100 W for 10 min while stirring. The as-synthesized PtNi nanoparticles had diameters of 2.9−5.6 nm. In addition, the PtNi nanoparticles fabricated with microwave irradiation had smaller particle size and more uniform distribution on the carbon substrate in comparison to PtNi nanoparticles synthesized with conventional heating and room-temperature reduction reactions.

Luo et al.[116] prepared crown-shaped Pt nanoparticles from a Pt precursor solution containing fourth generation NH_2-terminal poly(amido amine) [(G4-NH_2)PAMAN] dendrimers using UV irridiation. An aqueous solution containing 0.1 mM of $H_2PtCl_6 \cdot 6H_2O$ and 0.07 mM of the dendrimer was irradiated under UV light in a dark box at 25 °C for 7 h. A low-pressure mercury lamp (HOYA-SCHOTT, EX250, wavelength 200−450 nm) was used. UV visible spectroscopy was used to verify the reduction of the Pt ions in solution. Figure 9A,B reveals the morphology of the product, crown-shaped Pt nanoparticles with diameters of 100−130 nm and 10−30 nm shell thickness. It is proposed that the dendrimers serve as stabilizers as well as templates for the formation of the Pt nanoparticles.

Park et al.[110] used an ultrasonic irradiation method to prepare polypyyrole (PPy)/Pt nanocomposites. The fabrication began by preparing a solution containing 0.25 mM $H_2PtCl_6 \cdot 6H_2O$, 10 mM PPy, and 1.25 mM sodium dodecyl sulfate (SDS). The SDS was employed as a stabilizing agent. The temperature of the water bath during the sonication was 298 K. A 13 mm Φ, Branson Sonifier 450D was immersed in the solution. Ultrasonification was carried out with a collimated 20 kHz beam from the transducer with an input power of 30 W for various lengths of time. UV/visible spectroscopy was used to verify the reduction of the Pt ions from the solution. Figure 10 shows the morphology of the Pt and PPy/Pt nanocomposites with particle sizes of 2−3 and 40 nm, respectively. The PPy/Pt nanocomposites have uniform dispersion and a narrow particle size distribution;

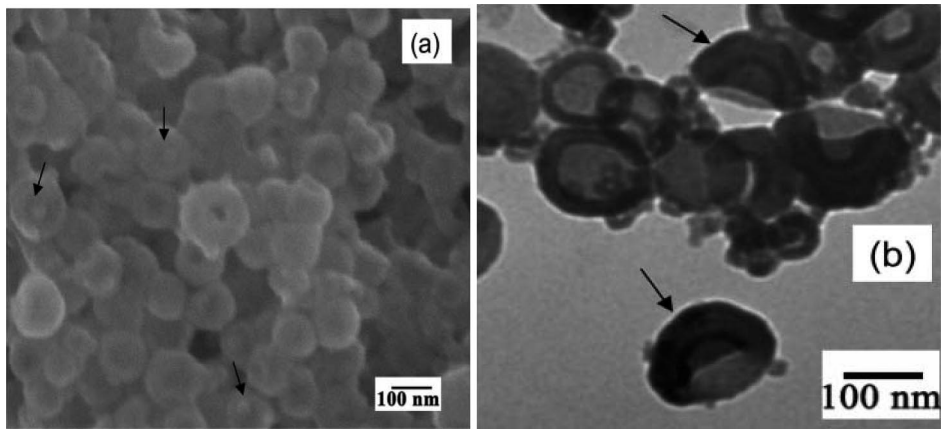

Figure 9. (a) SEM and (b) TEM images of the crown-shaped platinum nanoparticles. Reprinted from Luo, X.; Imae, T. *J. Mater. Chem.* **2007**, *17*, 567. Copyright 2007 Royal Society of Chemistry.

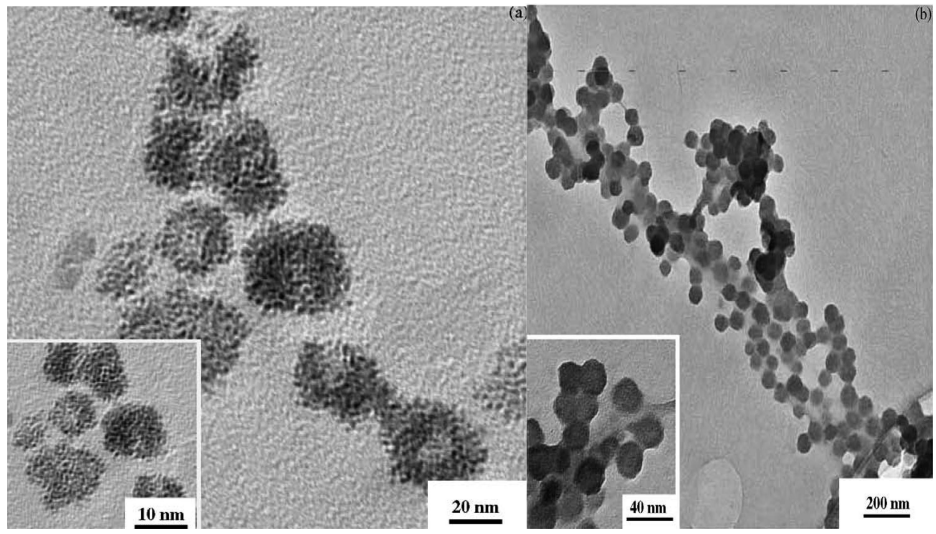

Figure 10. TEM images of the as-synthesized (a) Pt-NPs and (b) Pt-NPs/PPy nanocomposite. Reprinted from Park, J.; Atobe, M.; Fuchigami, T. *Electrochim. Acta* **2005**, *51*, 849. Copyright 2005 Elsevier.

however they lose electroactivity after continuous cycling in aqueous solutions due to the overoxidation of the PPy.

Wang et al.[120] used γ-irradiation to fabricate Pt nanoparticles supported on MWCNTs. A mixture of MWCNTs, chloroplatonic acid, 2-propanol, and sodium salt sulfonate was ultrasonicated for 15 min and purged with N_2. The alcohol was used as a hydroxyl radical scavenger and the salt as a surfactant. The mixture was irradiated with a ^{60}Co source with a dose rate of 2 kGy h^{-1}. The as-synthesized Pt/MWCNT nanocomposite had Pt nanoparticles with diameters of 2.5−4.0 nm. The radiolysis of water forms radicals, which reduced the metal ions in solution to metal on the MWCNTs. The optimization of experimental conditions resulted in uniform particle dispersion and narrow size distributions.

Sputtering, ion and electron beam deposition, laser ablation, and several types of irradiation methods have been used to synthesize a variety of Pt nanomaterials. The fabrication conditions, concentration of reagents, and presence of stabilizers in these physical synthesis methods can be tuned to control the product composition, morphology, and properties.

2.4. Electrochemical Deposition

Electrodeposition is a practical method for generating a variety of Pt and Pt-based nanomaterials.[124−199] This method involves the use of a two- or three-electrode electrochemical system, with the electrolyte serving as the source of Pt as well as the conducting medium. Deposition occurs by controlling either the electrode potential or the current density of the electrochemical cell. This method is used to fabricate thin films or layers composed of nanoparticles or nanocrystals,[125,130−143,149−164,172−176,199] as well as nanowires and nanorods.[126,129,166−169,182,197,198]

A variety of electrochemical techniques have been employed to facilitate the deposition of Pt and Pt-based nanomaterials onto electrode supporting materials including chronoamperometry, cyclic voltammetry, potential step experiments, potential pulse experiments, chronopotentiometry, and current pulse experiments. Tirawi et al.[125] used potentiostatic pulse plating to deposit Pt onto a SiO_2 surface. The nanosized Pt islands were fabricated at room temperature in a three-electrode cell containing 1 M K_2PtCl_4 and 1 M H_2SO_4. The deposition was achieved by pulsing the potential between 0.08 and −0.01 V, with time durations of 3 and 1 ms, respectively. The as-synthesized Pt nanosized islands had sizes between 200 and 800 nm. A Pt blanket electrode was also prepared on the SiO_2 substrate using the same cell setup, but with different potentials and time durations of 0.06 V for 5 ms and −0.04 V for 2 ms. While the blanket Pt electrode exhibited superior surface coverage, the nanosized Pt island networks had an electroactive surface area (ESA) over 4 times larger, owing to the smaller particle size of the catalysts.

One of the most popular electrodeposition techniques used to synthesize Pt and Pt-based nanomaterials is chronoamperometry. Zhao et al.[140] synthesized Pt nanoparticle/MnO_2 nanowire composites using electrodeposition. A three electrode electrochemical cell with a saturated calomel electrode (SCE) as the reference electrode, Pt plate counter electrode, and anodic aluminum oxide (AAO)/Ti/Si template as the working electrode was used for the synthesis. The MnO_2 nanowires were fabricated in a 0.5 M $Mn(CH_3COO)_2$ solution by holding the potential constant at 1.4 V for 5000 s. The AAO film was removed by immersing the substrate in 0.01 M NaOH for 0.5 h. The resulting "brush shaped" MnO_2 nanowires had a uniform diameter of 30 nm, similar to the pores in the AAO template, and were arranged into "brush shaped" arrays. The Pt nanoparticles with diameters less than 15 nm were deposited onto the MnO_2 nanowires in a 5 mM H_2PtCl_6 solution at −0.3 V for 50 s. The product Pt nanoparticle/MnO_2 nanowire composites showed enhanced electrocatalytic activity toward methanol oxidation compared with Pt nanowire arrays prepared with a similar electrodeposition method.

Another technique widely employed to prepare Pt and Pt-based nanomaterials is cyclic voltammetry. Zhao et al.[160] fabricated Pt nanoparticles on MWCNTs using a three-step process. The first step involved the electrochemical treatment of multiwalled CNTs to produce various functional groups. Then, cyclic voltammetry was performed between 0.3 and 1.3 V at 100 mV s^{-1} for 10 cycles in a pH 4 solution containing 2 M K_2PtCl_4 and 0.1 M K_2SO_4 to promote the electro-oxidation of $PtCl_4^{2-}$ to Pt(IV). Finally, the Pt(IV) complex was converted to Pt(0) by cycling at 100 mV s^{-1} between 0.9 and −0.35 V in a 0.1 M H_2SO_4 solution until a steady state was reached. Increasing the number of cycling steps for the $PtCl_4^{2-}$ to Pt(IV) conversion resulted in higher dispersion of the Pt nanoparticles on the MWCNTs, with a particle size of 2 nm obtained after 190 cycles, as well as increased electrocatalytic activity. The

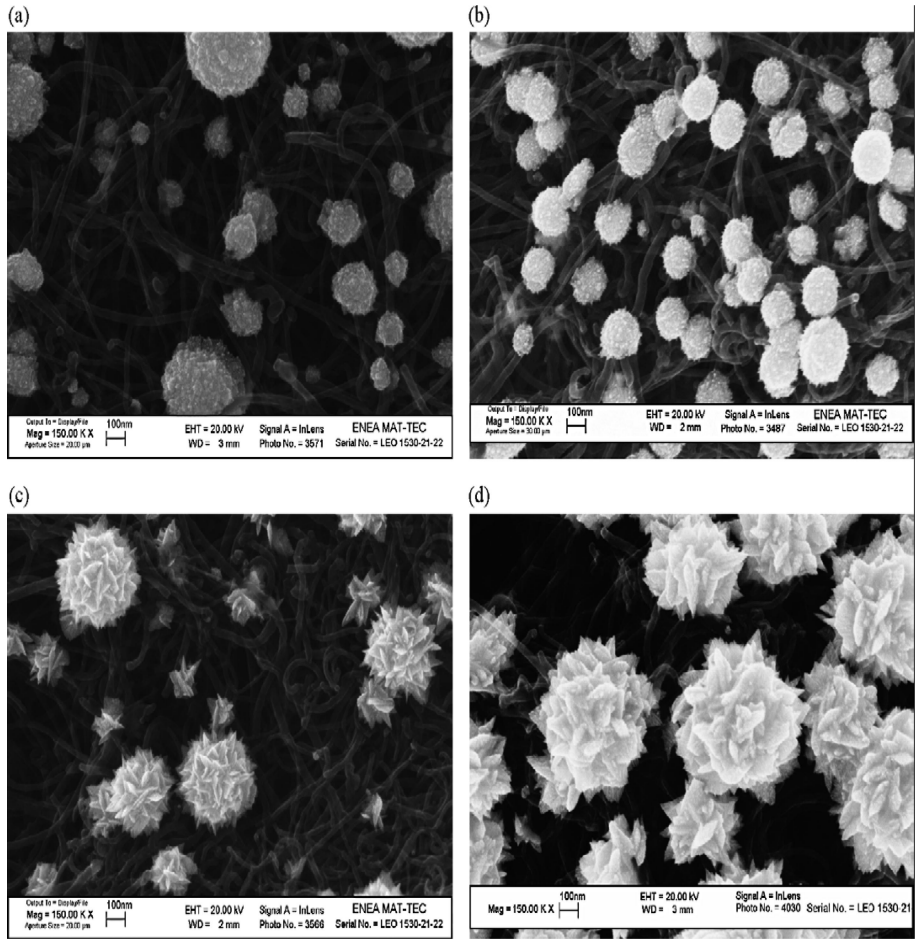

Figure 11. SEM images of Pt nanoparticles deposited on CNTs with charge density values of (a) 120, (b) 180, (c) 240, and (d) 360 mC cm^{-2}. Reprinted from Paoletti, C.; Cemmia, A.; Giorgi, L.; Giorgi, R.; Pilloni, L.; Serrab, E.; Pasquali, M. *J. Power Sources* **2008**, *183*, 84. Copyright 2008 Elsevier.

high dispersion of the Pt nanoparticles may be due to the functionalization of the MWCNTs.

Cui et al.[184] deposited Pt nanoparticles onto MWCNTs using a potential step experiment. MWCNTs were attached to the GC electrode using conductive silver paint. The electrodeposition took place in a three-electrode electrochemical cell using a MWCNT/GC working electrode, Pt counter electrode, and Ag/AgCl/KCl (3 M) reference electrode. The supporting electrolyte was a solution containing 1 mM K_2PtCL_4 and 0.1 M KCl. The Pt nanoparticles were deposited on the surface of the working electrode via potential steps from 0.5 to −0.7 V. The number of potential step cycles was fixed at 10, 50, or 200; the width or duration of the potential steps was varied to examine the effect on the morphology of the product nanoparticles. Overall, varying the width of the potential steps had almost no effect on the particle size, which averaged 10 nm; whereas a higher number of repeated potential steps from 0.5 to −0.7 V resulted in larger Pt nanoparticles with snowflake-like morphology, which possessed higher porosity and electrocatalytic activity toward oxygen reduction.

Paoletti et al.[131] deposited Pt nanoparticles onto carbon black (CB) and CNTs using chronopotentiometry. The CNTs were pretreated to remove carbaceous and metallic impurities by refluxing in HNO_3 for 2 h. CB and CNTs were attached onto separate GC substrates by spraying solutions of alcohol and Nafion onto the surfaces. A standard three-electrode electrochemical cell was used for the electrodeposition, with the GC working electrode, Pt counter electrode, and Ag/AgCl reference electrode. The supporting electrolyte was a solution of 5 mM H_2PtCl_6 and 1 M H_2SO_4. The deposition was carried out by applying a current between 0.025 and 0.3 mA cm^{-2} for 300 s. The product morphology was highly dependent on the charge density values. The SEM images of the formed Pt nanoparticles shown in Figure 11 reveal three distinct morphologies: spherical (a), dendritic (b), and lamellar (c, d). The Pt nanoparticles were finely dispersed on both the CNT and CB substrates. The morphology of the nanoparticles affected the electrocatalytic performance of the electrodes, and overall the globular particles exhibited the best performance.

Song et al.[132] fabricated Pt nanoparticles in PVP using current pulse electrodeposition. PVP is a nonionic surfactant, capable of forming complexes with Pt ions in solution, and it adsorbs on the substrate. Two different molecular weights of PVP were used: PVP-L (29 000) and PVP-H (130 000). The electrolyte used for the pulse electrodeposition was a solution composed of 0.2 M H_2SO_4, 5 mM H_2PtCl_6, and 50 mM PVP. The current was pulsed from 0 mA cm^{-2} for 300 ms to −10 mA cm^{-2} for 100 ms, and back to 0 mA cm^{-2} for 300 ms. The total number of pulses was 50. The resulting particle sizes for the deposition were 360 nm for pure Pt, 3.4 nm for Pt with PVP-L, and 2.9 nm for Pt with PVP-H. The use of PVP in the electrolyte for electrodeposition of the Pt nanoparticles was found to produce particles over 100 times smaller than those produced without PVP.

While a variety of electrochemical techniques have been used to deposit Pt nanoparticles onto various electrode supporting

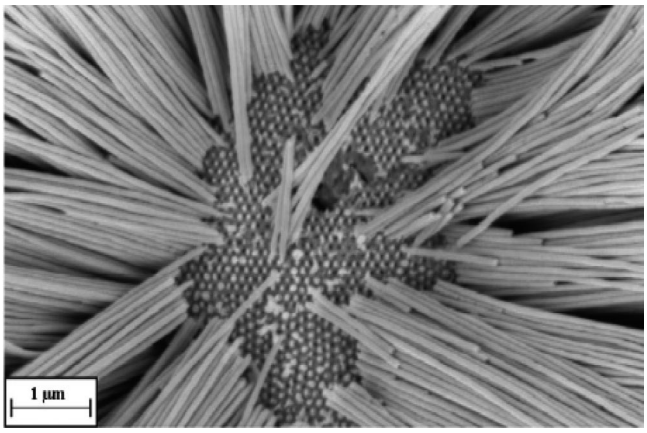

Figure 12. SEM image of the Pt nanowires, formed with a deposition charge of 26.1 C cm^{-2} after matrix dissolution. Reprinted from Napolskii, K. S.; Barczuk, P. J.; Vassiliev S. Yu.; Veresov, A. G.; Tsirlina, G. A.; Kulesza, P. J. *Electrochim. Acta* **2007**, *52*, 7910. Copyright 2007 Elsevier.

materials, these techniques can also be used to fabricate other Pt nanomaterials such as nanowires or nanorods[166−169,182,195] and bimetallic Pt-based nanomaterials.[157,165,168,172,182,189,196] Napolskii et al.[148] employed an electrodeposition technique to synthesize Pt nanowires using anodic aluminum oxide (AAO) templates. High-purity aluminum foils were anodized in 0.3 M oxalic acid at 40 V for 48 h. A two-electrode electrochemical cell with a Pt foil counter electrode was used with the temperature of the electrolyte maintained between 0 and 5 °C. The alumina film was then etched in a solution of 35 mL L^{-1} H_3PO_4 and 20 g L^{-1} CrO_3 at 70 °C. Then, the film was anodized again for 50 h using the previous conditions. The electrodeposition of the Pt onto the template was carried out using a three-electrode electrochemical cell with a Pt wire counter electrode and Ag/AgCl reference electrode. The electrolyte used for the deposition was a solution containing 0.01 M Na_2PtCl_6 and 0.02 M HCl. The deposition was achieved at a constant potential of 0.3 V until the total charge spent was between 1 and 26 C cm^{-2}. Figure 12 shows that the diameter of Pt nanowires is similar to the diameter of the pores in the alumina matrix. The diameter of the Pt nanowires was 50−60 nm, and their overall length increased with increasing charge spent for the electrodeposition.

Zhao et al.[155] fabricated 3D flowerlike Pt nanoparticle clusters on CNTs using a three-step electrochemical process. In the first step, the CNTs were modified with functional groups by cycling the potential between −0.4 and 1.8 V in K_2SO_4. In the second step, the Pt(II) complex was oxidized to form a Pt(IV) complex using potential step deposition from 0.3 to 1.1 V with different pulse widths until a steady pulse current was reached. The electrolyte used was a solution containing 2 M K_2PtCl_6 and 0.1 M K_2SO_4. Finally, the Pt(IV) complex was transformed to Pt nanoparticles on the CNT surface by cycling the potential between −0.26 and 1.0 V until a steady state was reached. The as-synthesized Pt nanoparticles had different morphologies depending on their synthesis methods: potential step or CV. The potential-step method produced flowerlike Pt nanoparticle clusters with particle sizes ranging from 1 to 20 nm depending on the pulse width, whereas the CV method produced finely dispersed Pt nanoparticles. Overall, the Pt nanoparticles synthesized using a pulse width of 0.001 s had the highest electrochemical active surface and electrocatalytic activity.

Sun and co-workers developed a novel electrochemical approach to prepare tetrahexahedral (THH) Pt nanocrystals (NCs) with high-index facets on glass carbon substrates.[199] The Pt nanocrystals were synthesized in a standard three-electrode cell with the electrolyte containing 0.2 mM H_2PtCl_6 and 0.5 M H_2SO_4. Subsequently, the as-synthesized nanoparticles were subjected to a square-wave treatment, with an upper potential of 1.2 V and the lower potential between −0.10 and −0.20 V. The treatment took place in a solution containing 0.1 M H_2SO_4 and 30 mM ascorbic acid at 10 Hz for 10 to 60 min. Figure 13A−D shows the SEM images of the as-fabricated Pt nanocrystals with particle sizes ranging

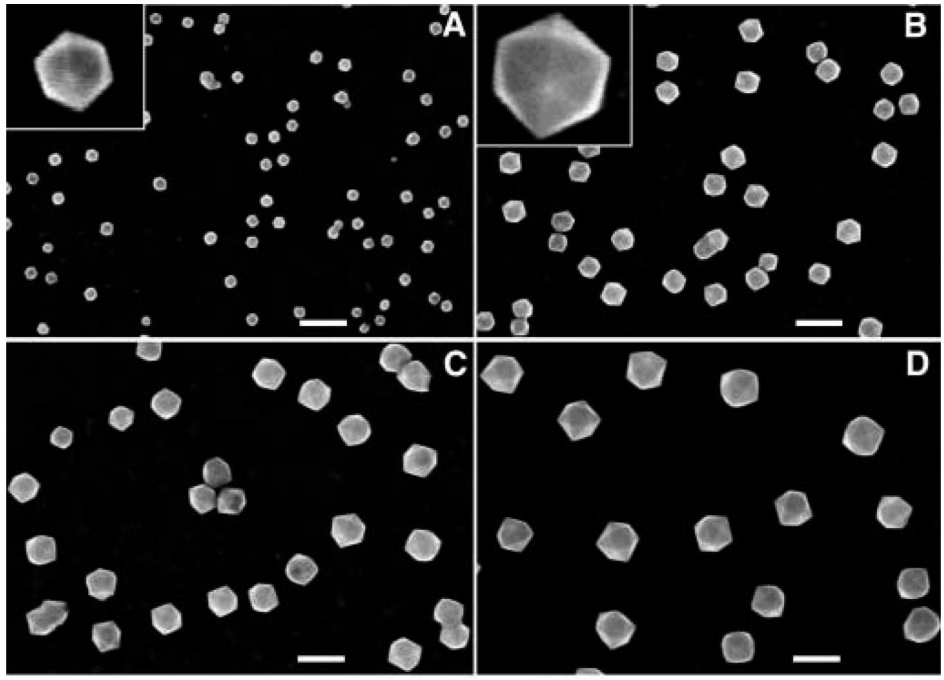

Figure 13. SEM images of the THH Pt nanocrystals synthesized with growth times of (A) 10, (B) 30, (C) 40, and (D) 50 min. The insets in panels A and B are the high-magnification SEM images. The scale bars are 200 nm. Reprinted from Tian, N.; Zhou, Z.; Sun, S.-G.; Ding, Y.; Wang, Z.-L. *Science* **2007**, *316*, 732. Copyright 2007 AAAS.

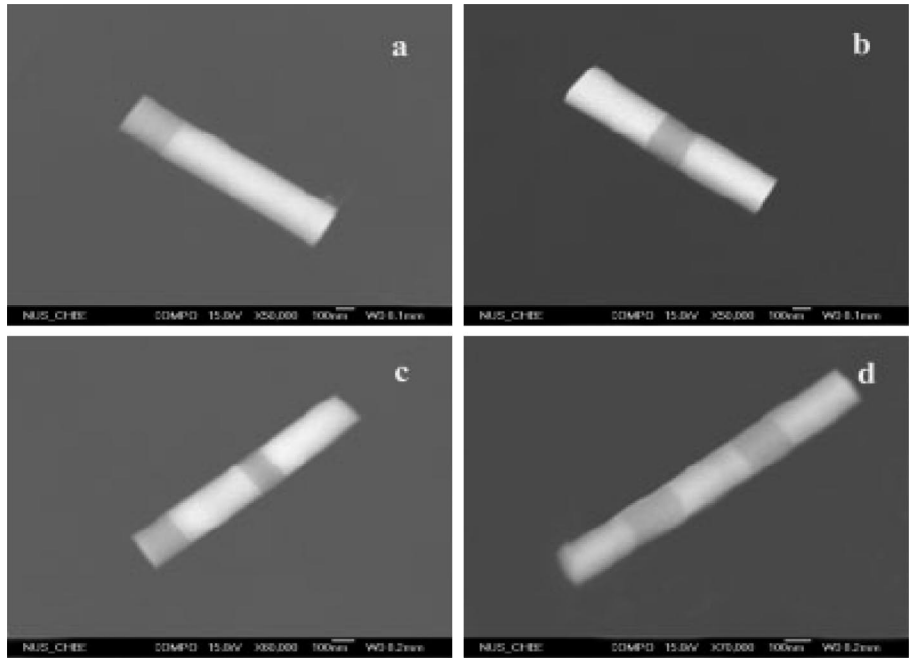

Figure 14. SEM images of the nanorods containing segments of (a) Pt−Ru, (b) Pt−Ru−Pt, (c) Pt−Ru−Pt−Ru, and (d) Pt−Ru−Pt−Ru−Pt. The diameter of each nanorod was approximately 200 nm. Reprinted from Liu, F.; Lee, J. Y.; Zhou, W. *Adv. Funct. Mater.* **2005**, *15*, 1459. Copyright 2005 Wiley-VCH.

from 53 to 144 nm. The formed Pt nanocrystals contain high-index facets such as {210}, {520}, or {730} compared with typical Pt nanoparticles which have {100}, {110}, or {111}. The high-index facets are thermally stable and have higher energy, which contributes to their enhanced electrocatalytic activity compared with Pt nanoparticles.

Cui et al.[152] used electrodeposition to form alloyed PtPb nanoparticles on MWCNTs. MWCNTs were grown on Ta plates and attached to the GC working electrode using conductive silver paint. The electrodeposition of the PtPb nanoparticles occurred in a solution of 0.1 M KCl, 0.67 mM K_2PtCl_6, and 0.33 mM $Pb(NO_3)_2$ by stepping the potential from 0.5 to −0.4 V, with step durations of 0.2 and 10 s, respectively, for a total of 60−120 cycles. Following the electrodeposition of the PtPb nanoparticles, a Nafion film was applied to the PtPb/MWCNT composite by dipping the electrode into a 0.25% (v/v) Nafion in 20% ethanol solution. To improve electrocatalytic performance, an additional layer of PtPb nanoparticles was deposited using conditions identical to the first electrodeposition, except that only 30 cycles were used. The alloyed PtPb nanoparticles had snowflake-like morphology with particle sizes of 10−40 nm and were observed mostly on the tips of the MWCNTs. The use of the Nafion layer was found to increase the electrocatalytic performance of the composite electrodes.

Liu et al.[182] synthesized multisegment bimetallic PtRu nanorods with customizable lengths on AAO templates using sequential chronopotentiometry experiments. An alumina membrane with copper electroplated from an aqueous solution of 1 M $CuSO_4$ at −28.3 mA cm^{-2} for 400 s was used as the working electrode. The electrodeposition conditions for the Pt nanorod segments were −0.44 mA cm^{-2} at 50 °C for various lengths of time in a solution of 0.01 M H_2PtCl_6 and 0.2 M H_2SO_4. The conditions for the electrodeposition of the Ru nanorod segments were −15 mA cm^{-2} at 50 °C for various lengths of time in a solution of 3.5 g L^{-1} $Ru(NO)Cl_3$ and 10 g L^{-1} NH_2SO_3H. To prepare nanorods with alternating segments of Pt and Ru, after one metal was plated, the electrode was rinsed with ultrapure water and subjected to a chronopotentiometry experiment where the current was held at −0.44 mA cm^{-2} until the potential was lower than −4 V. Figure 14a−d shows the morphology of the as synthesized segmented nanorods with customizable lengths. Nanorods synthesized with higher numbers of Pt/Ru interfaces showed enhanced electrocatalytic activity, which provided evidence of the bifunctional mechanism.

Electrodeposition is a simple yet powerful method for generating a variety of Pt and Pt-based nanostructured materials. The morphology, particle size, metallic composition, and electrocatalytic activity of the product nanostructured materials can be tuned based on the precursor solutions, substrate materials, and deposition conditions.

2.5. Electroless Deposition

Electroless deposition is among the most straightforward and efficient methods used to fabricate Pt and Pt-based nanomaterials.[200−266] This method involves the reduction of Pt and possibly other cocatalysts from a metal salt solution onto an electrode surface. The process takes place in acidic, basic, or neutral aqueous solutions and requires a reducing agent. It differs from hydrothermal and solvothermal routes because these take place in open systems. A variety of reducing agents have been employed to synthesize Pt nanoparticles,[201−203,205,209,215,225,251,255−257,265] Pt nanowires/nanorods,[204,253] Pt nanostructured materials with different shapes,[214,216,224,236,242,244] and Pt-based bimetallic nanomaterials.[230,232−235,239,240,246,258−262]

Pt nanoparticles are the most common product of electroless deposition. Metz et al.[209] synthesized Pt nanoparticles on vertically aligned carbon nanofibers (VACNFs) using a three-step electroless deposition process. In the first step, the VACNFs were sensitized with tin. Then the fibers were involved in a redox reaction in a 0.03 M palladium chloride solution, which resulted in the transfer of Pd atoms to the surface of the fibers. Finally the pretreated VACNFs were immersed in a pH 11.95 solution containing 10 μL of 5 wt % diammineplatinum(II) nitrate in 10 mL of 1.92 M

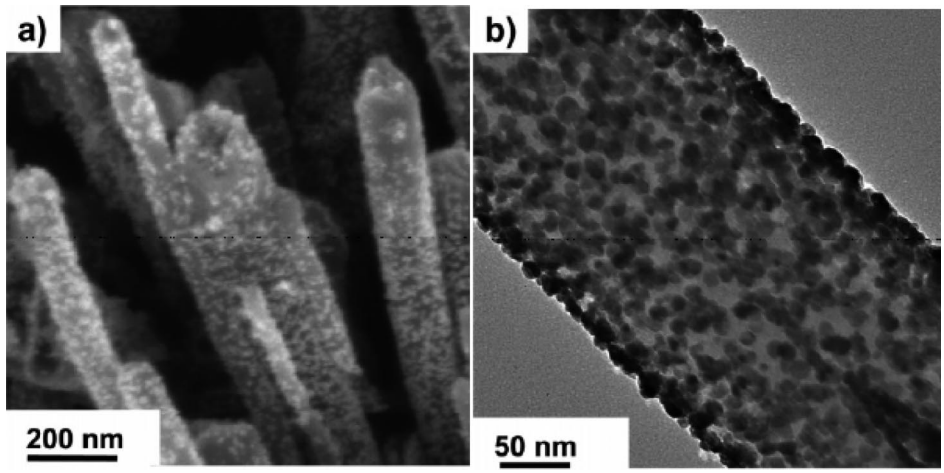

Figure 15. (a) SEM and (b) TEM image of platinum nanoparticles on carbon nanofibers. Reprinted from ref 209. Copyright 2007 American Chemical Society.

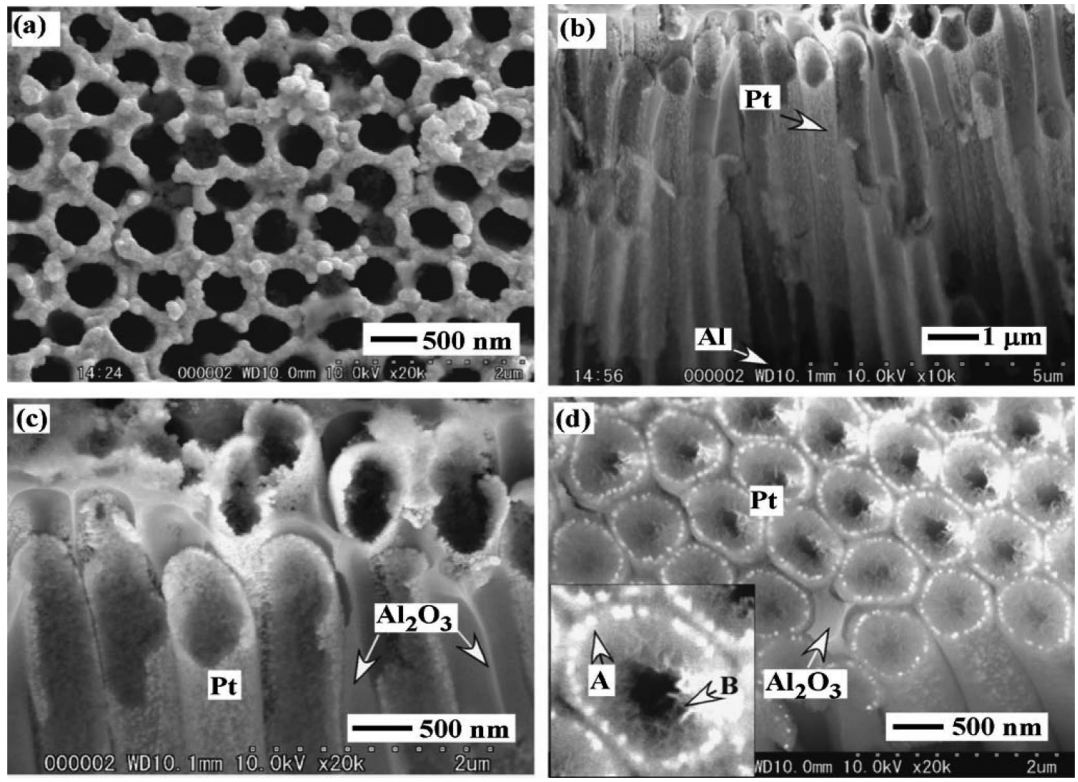

Figure 16. SEM images of Pt nanotubules in porous alumina films after deposition for (a−c) 3 min and (d) 7 min. The images show different angles of the Pt nanotubules: (a) top view, (b, c) vertical sections, and (d) transverse section. Reprinted from Chu, S. Z.; Kawamura, H.; Mori, M. *J. Electrochem Soc.* **2008**, *155* (5), D414. Copyright 2008 Electrochemical Society.

ammonium hydroxide, 0.25 M hydrazine hydrate, and 0.4 M hydroxylamine hydrochloride at 55 °C for 1−3 h. Figure 15 shows that the Pt nanoparticles are well dispersed on the VACNFs and have an average diameter of 8 nm. Prior to the electroless deposition of Pt, the functionalization of the VACNFs was determined to greatly enhance the nucleation of the Pt nanoparticles, which resulted in 10−20× higher Pt loading.

Chu et al.[204] fabricated Pt nanotubules on aluminum sheets using hydrazine as a reducing agent. Aluminum sheets underwent critical-potential anodization in various acids to form self-organized porous anodic alumina (PAA). The PAA films were etched in different acids to widen the pores and aid in the uniform deposition of Pt. Pd colloids were produced on the nanoporous walls to help initiate the electroless deposition on the chemically inert alumina. Electroless deposition was achieved by immersing the alumina in an alkali bath containing hydrazine, 0.02 M H_2PtCl_6, 0.3 M NH_2NH_2, and 0.8 M $HONH_3Cl$. The pH of the mixture was adjusted using ammonia. The solution was mixed for 3−7 min at 333−353 K. Figure 16 shows the Pt nanotubules formed via different electroless deposition times, with tube thickness of 100−200 nm, tube diameters of 600 nm, and tube lengths of 10−12 μm. Overall, the size and aspect ratio of the Pt nanotubules synthesized on PAA films can be tuned by varying the fabrication conditions in order to enhance surface area, mechanical strength, and electrocatalytic performance.

Qu et al.[214] utilized a substrate-enhanced electroless deposition process to prepare shape- and size-controlled Pt nanoparticles on CNTs. Cu-supported CNTs were formed by dispersing a solution containing 0.5 mL of MWCNTs in

ethanol (0.8 mg/10 mL) on Cu foil. Then the substrate was immersed in a solution containing 3.8 mM K_2PtCl_4 and 5 mM $CuCl_2$ for 1 min. Following the formation of the Pt nanocubes, the substrate was washed with distilled water. The fabrication of Pt nanospheres followed the same procedure, except that the Cu-supported CNTs were immersed in a solution containing 1.9 mM K_2PtCl_4 for 30 min. The formation of the Pt nanocubes and Pt nanospheres with diameters ranging from 100 to 200 nm and 200 to 500 nm was found to be highly dependent on the metal salt concentrations and reaction times.

The most commonly used reducing agents are ethylene glycol[216−247] and sodium borohydride.[248−266] Knupp et al.[222] synthesized Pt nanoparticles on CNTs and CNFs using a polyol synthesis method with ethylene glycol as the reducing agent. The CNTs and CNFs were pretreated with concentrated nitric and sulfuric acid at 60 °C for 1−4 h to remove impurities and add functional groups. The CNTs and CNFs were transferred into a mixture of ethylene glycol and water and sonicated to disperse the nanomaterials in solution. Following the dropwise addition of the appropriate amount of K_2PtCl_6, the solution was sonicated again. The mixture was refluxed for 2 h at 125 °C. The as-synthesized Pt nanoparticles on the CNTs and CNFs had diameters from 2.3 to 3.9 nm. The Pt nanoparticles fabricated on the CNTs with 10 wt % Pt loading had the smallest particle size and best particle dispersion, which resulted in the highest ESA.

Guo et al.[263] used sodium borohydride as a reducing agent and citric acid (CA) as a stabilizing agent to prepare Pt nanoparticles. The Pt nanoparticles were synthesized from a precursor solution containing different ratios of citric acid and H_2PtCl_6 (1:1, 2:1, 3:1, 4:1) in 250 mL of ammonium hydroxide. The solution was ultrasonicated for 30 min following the addition of Vulcan XC-72. The mixture was stirred for 10 h at 50 °C with the continuous addition of ammonium hydroxide to maintain the volume of the solution. An excess amount of 0.1 M $NaBH_4$ was added dropwise to facilitate the reduction of the Pt ions in the solution over a period of 3 h. The resulting Pt nanoparticles had sizes ranging from 3 to 6 nm. Among the different CA/Pt ratios used to fabricate the Pt nanoparticles, the ratio of 2:1, with a particle size of 3.82 nm, exhibited the highest ESA and electrocatalytic performance.

Herricks et al.[244] employed a polyol process with sodium nitrate to control the morphology of the synthesized Pt nanoparticles, where ethylene glycol served as both the reducing agent and solvent. A solution containing 1 mL of 80 mM H_2PtCl_6 was rapidly added to a mixture composed of 7 mL of ethylene glycol at 30 mM PVP (MW = 55 000) and with varying amounts of $NaNO_3$ at a temperature of 160 °C. The ratio of $NaNO_3$/Pt was varied from 0 to 11. Figure 17a−f shows that the morphology of the synthesized Pt nanomaterials varies greatly with dimensions between 3 and 30 nm. The variation in the structure of the Pt nanomaterials was due to the concentration of the nitrate ion, which was responsible for slowing the reduction of the Pt(II) and Pt(IV) ions in solution by ethylene glycol. This effect may be attributed to the formation of stable complexes between the nitrate and Pt(II) and Pt(IV) ions in solution thus altering the reaction kinetics.

Song et al.[253] synthesized Pt nanowire networks via chemical reduction of a Pt complex using sodium borohydride as a reducing agent. The synthesis started by aging a solution containing 10 mL of 20 mM K_2PtCl_6 for one day.

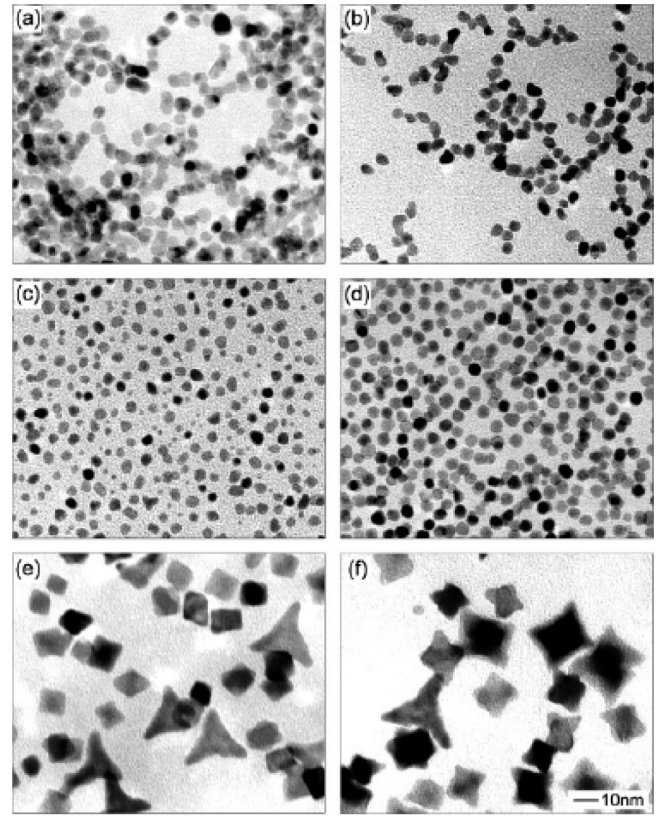

Figure 17. TEM images of Pt nanoparticles synthesized with different ratios of ($NaNO_3/H_2PtCl_6$): (a) 0, (b) 0.3, (c) 1.6, (d) 3.3, (e) 5.5, and (f) 11.0. Reprinted from ref 244. Copyright 2004 American Chemical Society.

After aging, 10 mL of chloroform and 40 mM cetyltrimethylammonium bromide (CTAB) were added to form a two-phase aqueous chloroform mixture. The resulting mixture was stirred for 10 min to transfer the Pt complex into the chloroform phase. For the Pt reduction, 80 mL of Nanopure water and 10 mL of 300 mM sodium borohydride were added to the mixture and stirred at 1000 rpm. The SEM and TEM images in Figure 18a−d show that the as-synthesized Pt nanowires have diameters of 2.2 nm and form large extended wire networks. The stirring speed was found to have a significant effect on the morphology of the Pt nanostructures. At low stir speeds, the majority of the product was nanoparticles; whereas, at higher stir speeds, the product was nanowire networks. This is likely related to the enlarged surface area of the chloroform micelles and the efficiency of the borohydride diffusion into the micelles.

While electroless deposition methods have been used to form a variety of simple Pt nanostructured materials, such as nanoparticles, nanowires or nanorods, and nanoparticles with varying shapes, many research groups have employed similar methodologies to form bimetallic Pt-based nanomaterials.[239,258−262] Zhu et al.[208] fabricated well-dispersed PtRu alloy nanoparticles on Vulcan XC-72 using electroless deposition. The carbon black (CB) was sensitized in a solution containing 2.5 g of $SnCl_2$ in 0.1 M HCl. The CB was then immersed in the solution and ultrasonicated for 30 min. Activation took place in a solution composed of 2.82 g of $PdCl_2$ in 0.1 M HCl via immersion and ultrasonification of the CB for 30 min. Following the pretreatment, the CB was immersed in a stirred solution made up of 1.93 mM H_2PtCl_6 and 3.63 mM $RuCl_3$ for 1 h. Na_2CO_3 was added to the solution to adjust the pH to 10. Finally, 20 mg L^{-1}

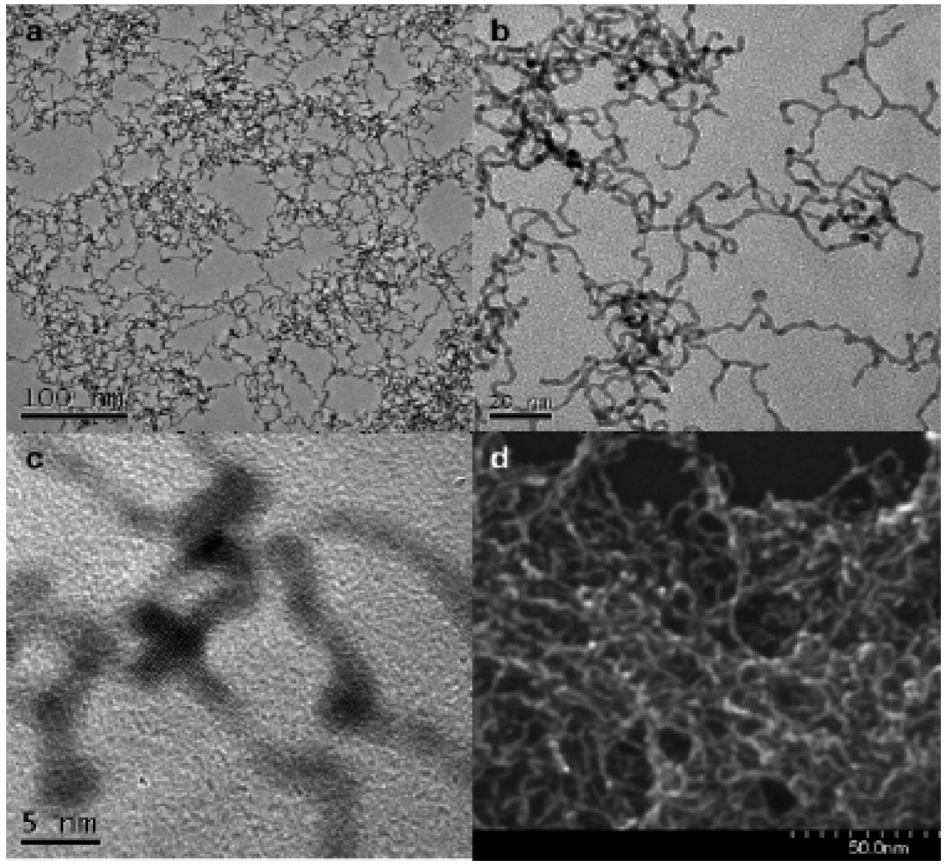

Figure 18. (a−c) TEM and (d) SEM images of the as-synthesized Pt nanowire networks. Reprinted from ref 253. Copyright 2007 American Chemical Society.

borohydride sodium was added to the mixture, which was then stirred for 2 h. The as-synthesized PtRu nanoparticles had diameters of 3.5−4.0 nm. Overall, the PtRu nanoparticles fabricated using the pretreatments possessed alloying, superior dispersion, and small particle size.

Tegou et al.[207] used a two-step electroless process to form Pt-coated Cu nanoparticles. In the first step, electrodeposition was used to deposit Cu onto a glass carbon (GC) substrate. The experiment was carried out in a solution containing 0.1 M $HClO_4$ and 0.1 M $CuSO_4$ at −0.4 V vs Ag/AgCl with a total passed charge density in the range of 5.5−41.3 mC cm^{-2}. The Cu/GC substrate was immersed in a solution containing 0.1 M HCl and 0.01 M K_2PtCl_6 for 30 min. The resulting PtCu deposits had a cracked mud structure. After cycling the potential between hydrogen and oxygen evolution, nanoparticles with sizes in the hundreds of nanometers were revealed. This process aids in the anodic dissolution of Cu to uncover the particles protected by the Pt surface layers.

Electroless deposition is a low-cost solution-based technique that has been successfully utilized to fabricate various Pt and Pt-based nanomaterials. The morphology and composition can be controlled to form a variety of Pt nanomaterials including nanoparticles, nanoparticles with different shapes, and nanowires. Use of AAO templates enables the synthesis of nanowires; the addition of other metal salts facilitates the fabrication of bimetallic Pt-based nanomaterials. Furthermore, electrocatalytic performance of the product Pt nanomaterials can be tuned by varying the concentration of the precursors, reagents, stabilizing agents, and reaction conditions.

3. Properties of Pt and Pt-Based Nanomaterials

3.1. Structure

The wide variety of synthesis techniques available to synthesize Pt and Pt-based nanomaterials contain reaction conditions such as Pt precursors, presence of surfactants or stabilizers, temperature, pH and substrate types, which may affect crystal growth, orientation, and grain size. A number of methods exist to characterize the structure of Pt and Pt-based nanomaterials, such as scanning electron microscopy (SEM), transmission electron microscopy (TEM), energy-dispersive X-ray spectroscopy (EDS or EDX), X-ray diffraction (XRD), X-ray photoelectron spectroscopy (XPS), low-energy electron diffraction (LEED), and selected-area electron diffraction (SAED). The information revealed by these characterization methods gives insight into how structure contributes to the enhanced properties of Pt and Pt-based nanomaterials.

SEM and TEM reveal information about the shape of nanoparticles and other nanomaterials, size of the nanomaterials, agglomeration of nanoparticles, and the distribution of the nanomaterials on the substrate. The information provided by TEM and SEM analyses is standard in most studies of the morphology and structure of Pt and Pt-based nanomaterials.[21,199,236,264,267−279] Tang et al.[269] used electrochemical deposition to deposit Pt nanoparticles on well-aligned CNT arrays. The morphology of the Pt/CNT nanocomposites was analyzed using SEM and TEM, as shown in Figure 19A−D. The SEM images show that the particle size and morphology were dependent on the deposition charge. A deposition charge of 9.744 μC cm^{-2} resulted

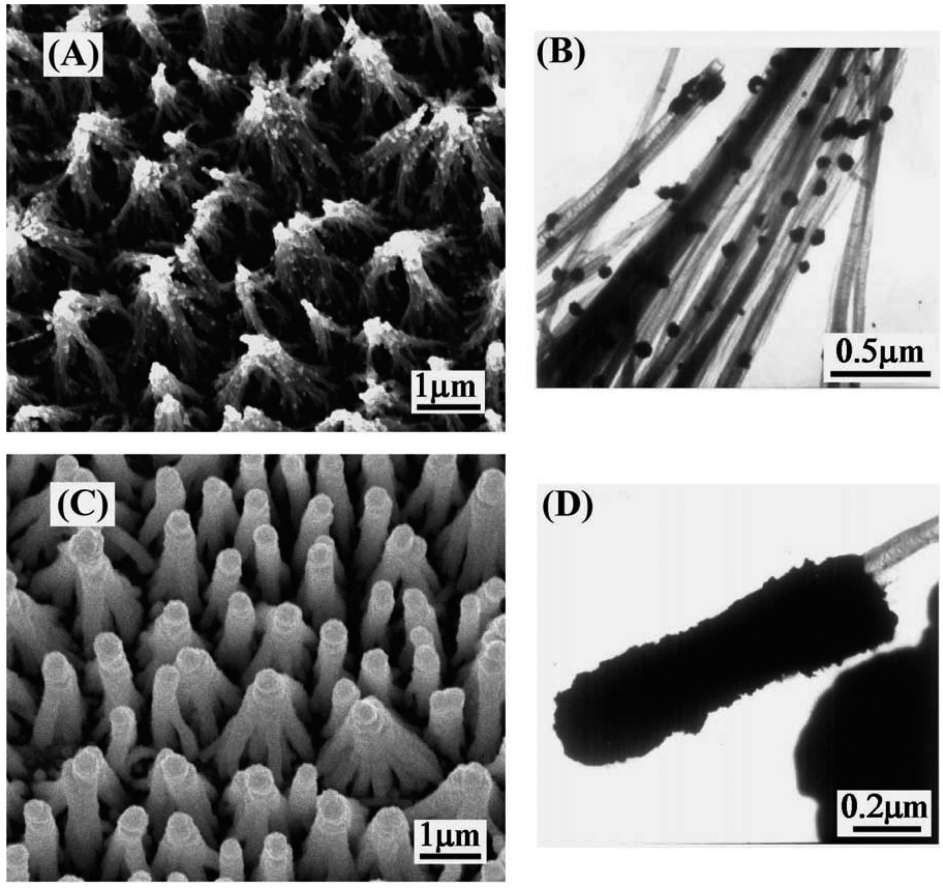

Figure 19. (A, C) SEM and (B, D) TEM images of Pt nanomaterials formed on CNT arrays with deposition charges of (A, B) 9.744 μC cm^{-2} and (C, D) 572.5 μC cm^{-2}. Reprinted from Tang, H.; Chen, J. H.; Huang, Z. P.; Wang, D. Z.; Ren, Z. F.; Nie, L. H.; Kuanga, Y. F.; Yao, S. Z. *Carbon* **2004**, *42*, 191. Copyright 2004 Elsevier.

in a particle size of 30−70 nm; whereas an increase in the charge to 572.5 μC cm^{-2} resulted in changing the morphology of the product Pt nanomaterials to a 65 nm thickness film. The TEM images reveal the agglomeration and distribution of the nanoparticles on the substrate, which may be difficult to distinguish in SEM images of nanoparticles dispersed on three-dimensional substrates such as CNTs. Figure 19B shows that the Pt nanoparticles are not agglomer-

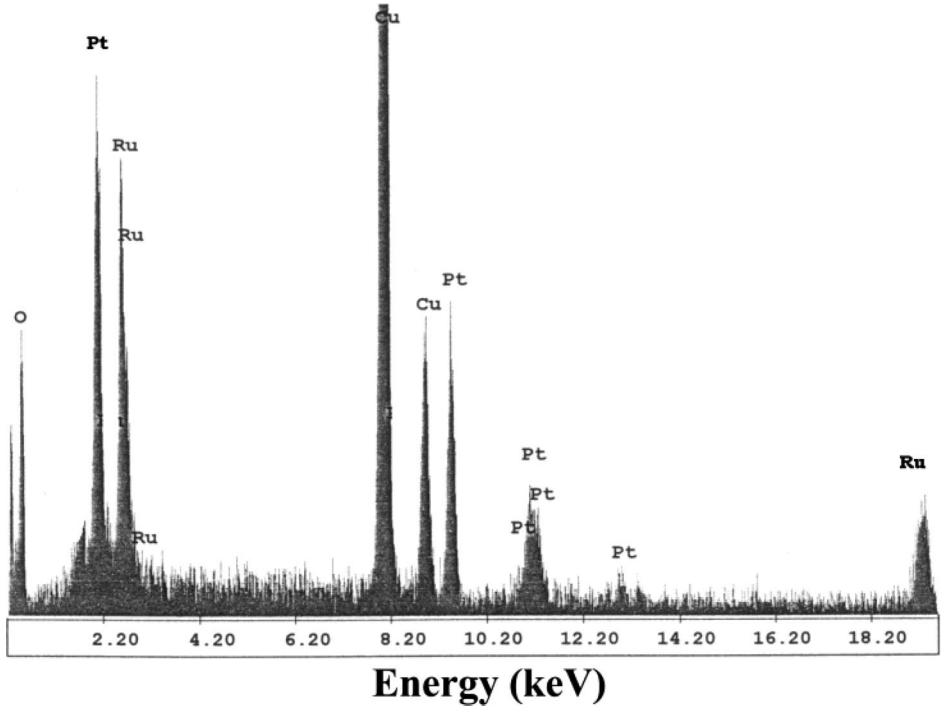

Figure 20. TEM−EDX spectra of PtRu nanoparticles. The Cu lines are attributable to the TEM grid. Reprinted from ref 267. Copyright 2003 American Chemical Society.

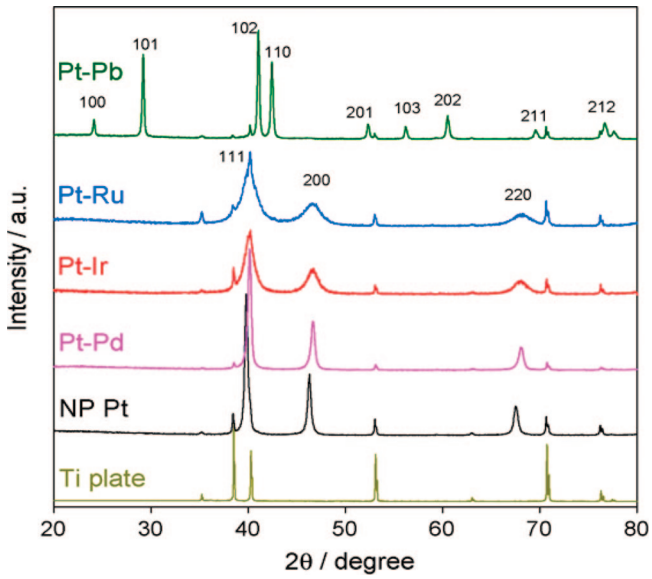

Figure 21. XRD patterns of the as-synthesized nanoporous PtM networks. Reprinted from Wang, J.; Holt-Hindle, P.; MacDonald, D.; Thomas, D. F.; Chen, A. *Electrochim. Acta* **2008**, *53*, 6944. Copyright 2008 Elsevier.

ated and are well dispersed on the CNT substrate for a deposition charge of 9.744 μC cm^{-2}. For a deposition charge of 572.5 μC cm^{-2}, the CNTs were coated uniformly by a Pt thin film as shown in Figure 19D.

The composition of Pt and Pt-based nanomaterials can be determined using numerous methods including EDS or EDX,[267,269,272,275,276] XPS,[264,279] and direct current plasma atomic emission spectroscopy (DCP-AES) or inductively coupled plasma atomic emission spectroscopy (ICP-AES).[274,277] Zhang et al.[267] fabricated PtRu nanoparticles on carbon paper using hydrazine as the reducing agent. Figure 20 shows the EDX spectra of the as-synthesized PtRu nanoparticles. The EDX analysis confirmed the fabrication of bimetallic PtRu nanomaterials from the appearance of distinct Pt and Ru peaks. The EDX results were also used to compare the Pt/Ru ratio between the precursor solutions and the product materials. This provides information about the reduction environment and whether species are preferentially reduced.[21,275] EDX analyses may also reveal information about the presence of impurities or the surface coverage of the nanomaterials over the substrate, if peaks for other elements are present in the spectra.[272]

Information about the phase of Pt and Pt-based nanomaterials is determined by XRD analysis.[267,268,272−276,279] Wang

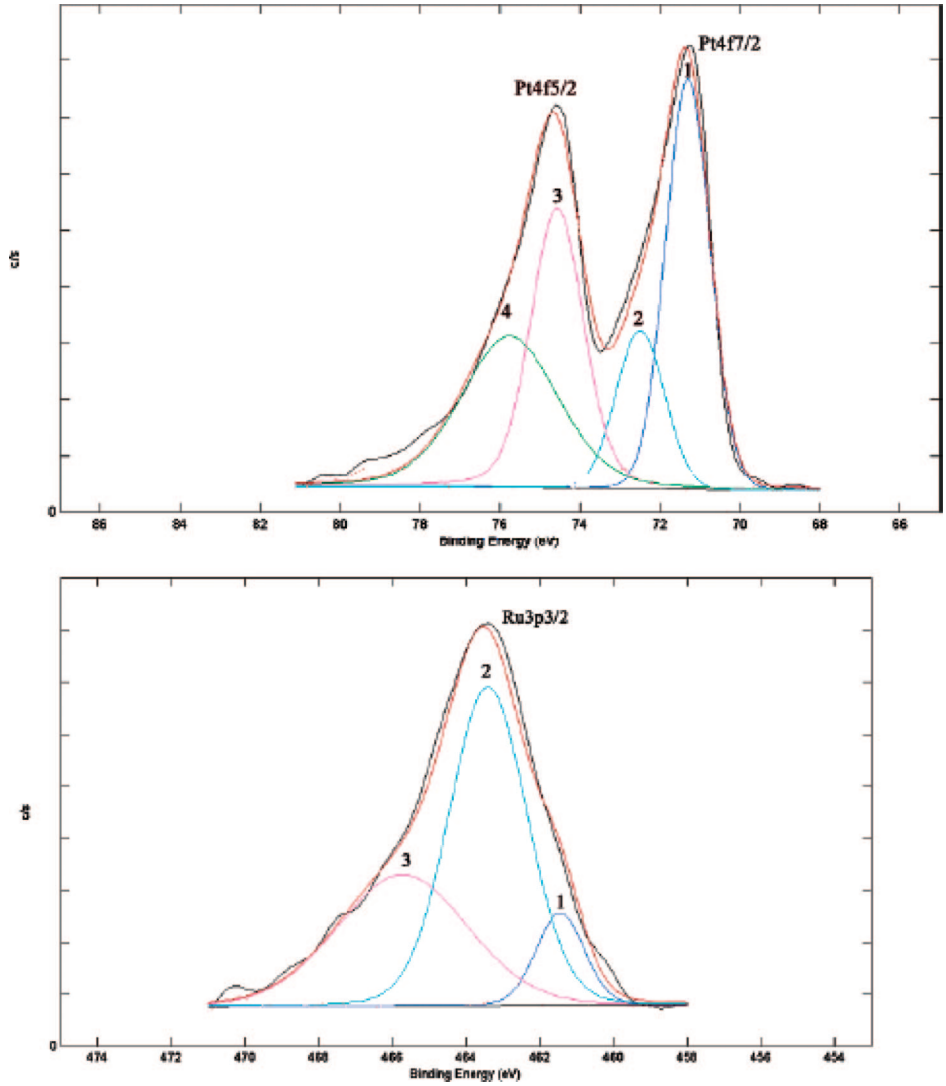

Figure 22. XPS spectrum of the Pt−Ru nanoparticles: (top) Pt 4f, peaks 1 and 3 represent the Pt $4f_{7/2}$ and Pt $4f_{5/2}$ lines of Pt^0, respectively; peaks 2 and 4 represent the Pt $4f_{7/2}$ and Pt $4f_{5/2}$ lines of Pt^{II}, respectively; (bottom) Ru $3p_{3/2}$. Reprinted from ref 267. Copyright 2003 American Chemical Society.

et al.[21] fabricated nanoporous PtM networks (M = Pb, Pd, Ru, or Ir) using the hydrothermal method. Figure 21 shows the XRD patterns for the five Pt-based nanomaterials. All five electrodes show characteristics of the hexagonal Ti crystal, albeit with lower intensities due to the surface coverage of the Ti substrate with the PtM nanoporous networks. The Pt, PtRu, PtIr, and PtPd electrodes display the (111), (200), and (220) reflections found in the face-centered-cubic (fcc) crystal structure. The peaks displayed by the PtPb electrode are characteristic of the hexagonal NiA crystal structure. The (111), (200), and (220) peaks for the PtRu, PtIr, and PtPd electrodes were found to have positive shifts in their 2θ values compared with nanoporous Pt. The increase in the 2θ values due to the decreased d-spacing was attributed to the addition of Ru, Ir, and Pd to Pt. Quantitative calculations for the lattice constants (a) revealed values of 0.389, 0.388, 0.388, and 0.392 for the nanoporous PtPd, PtRu, PtIr, and Pt electrodes, respectively. Moreover, the peak lines for the PtM patterns are between the 2θ values for pure Pt and M, and no characteristic (111), (200), and (220) reflections for each different M appear in the patterns. The sum of this evidence indicates that the PtM nanomaterials were either partially or fully alloyed. The XRD patterns also reveal information about the average crystallite size, which was calculated with the Scherrer formula. Calculations revealed average crystal sizes of 24, 35, 18, 6, and 4 nm for the nanoporous Pt, Pt−Pb, Pt−Pd, Pt−Ir, and Pt−Ru networks, respectively. The particle sizes calculated with the Scherrer formula were much lower than those in the SEM images, indicating the agglomeration of the Pt nanocrystallites.

XPS experiments can be used to determine the atomic composition as well as the metallic and oxide components of Pt and Pt-based nanomaterials.[267,276,279] Gullón et al.[264] prepared alloyed PtRu nanoparticles using sodium borohydride as the reducing agent. XPS experiments were performed to determine the atomic composition of the as-synthesized PtRu nanoparticles. The deconvoluted Pt and Ru signals and sensitivity factor were integrated and compared to determine the atomic compositions. Zhang et al.[267] employed XPS to determine the metallic and oxide components of Pt and Ru of their PtRu nanoparticles. Figure 22 shows the XPS spectra for the Pt and Ru components. The Pt $4f_{7/2}$ and Pt $4f_{5/2}$ peaks at 71.3 eV (1) and 74.57 eV (3) were both attributed to metallic Pt^0. The other Pt peaks at 72.49 eV (2) and 75.88 eV (4) were attributed to Pt^{II} in PtO or $Pt(OH)_2$. Comparing the relative heights of the peaks revealed that Pt^0 is the dominant species. The Ru $3p_{3/2}$ spectrum revealed peaks at 461.32 (1), 463.41 (2), and 465.72 eV (3), which were credited to Ru^0, Ru^{IV} in RuO_2, and Ru^{VI} in RuO_3, respectively. Comparing the relative heights of the peaks shows that Ru oxides are the majority species. Wang et al.[21] used XPS analysis to gain additional information about the composition of a nanoporous PtIr electrode. Figure 23 shows the XP spectra for the Pt and Ir components of the PtIr electrode. A comparison of the Pt $4f_{7/2}$ and Pt $4f_{5/2}$ peaks for the nanoporous PtIr and Pt networks revealed a positive shift in the binding energy for the Pt $4f_{7/2}$ peak for the PtIr electrode. A similar comparison of the Ir $4f_{7/2}$ and Ir $4f_{5/2}$ peaks for the PtIr electrode and pure Ir metal revealed a negative shift in the binding energy for the Ir $4f_{7/2}$ peak for the PtIr electrode. The shift in binding energy is related to a change in electron density, which indicates the presence of an intra-atomic charge transfer between the Pt and Ir atoms.

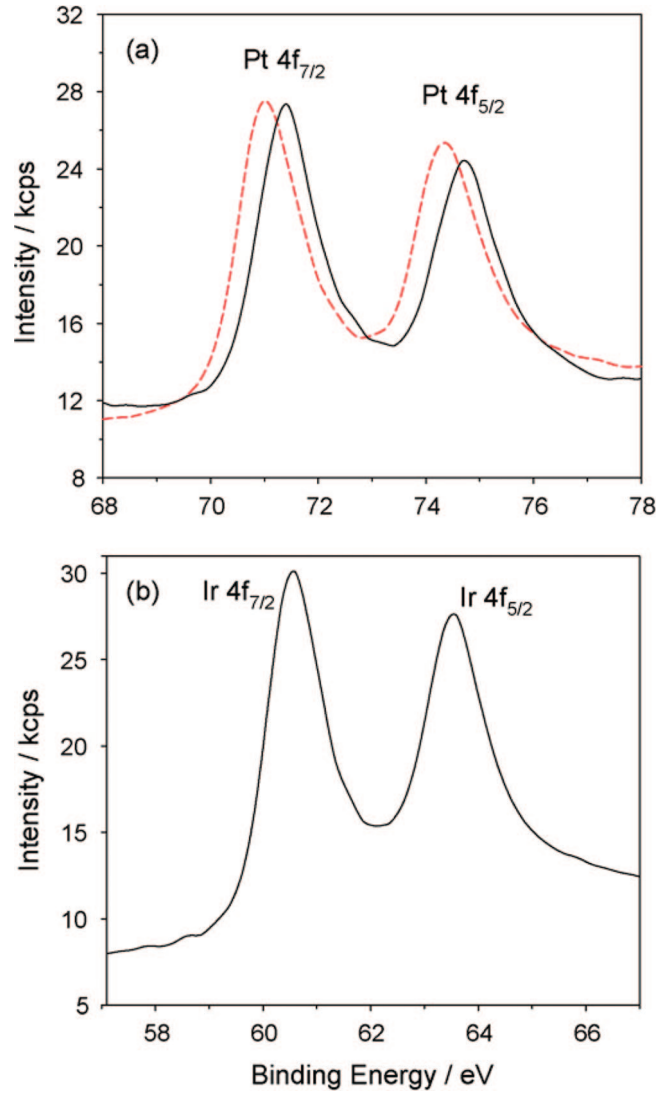

Figure 23. XPS spectra of the Pt 4f (a) and Ir 4f (b) regions of the nanoporous Pt (dashed line) and PtIr (black line) networks. Wang, J.; Holt-Hindle, P.; MacDonald, D.; Thomas, D. F.; Chen, A. *Electrochim. Acta* **2008**, *53*, 6944. Copyright 2008 Elsevier.

Fundamental studies of the {111}, {100}, and {110} index planes or facets typically found on single-crystal surfaces of bulk Pt reveal that these single-crystal surfaces have much lower activity than high index planes.[3,280] The high index planes have high densities of atomic steps, ledges, and kinks that act as active sites for breaking chemical bonds. Sun and co-workers developed a route for shape-controlled synthesis of Pt NCs through a square-wave potential.[199] Starting from Pt nanospheres electrodeposited on glassy carbon substrate instead of bulk Pt, they obtained THH Pt NCs at high yield. SAED and TEM measurements were used to investigate the index facets of the as-synthesized THH Pt nanocrystals, as shown in Figure 24. The nanocrystals were imaged along the [001] direction, which was parallel to 8 of the 24 facets in the THH Pt nanocrystals. The SAED pattern in Figure 24B revealed a 4-fold symmetry that proved the THH Pt nanocrystal was a single crystal. The high-resolution TEM image in Figure 24C revealed lattice spacing of 0.20 nm for the {200} planes of the THH Pt nanocrystal. The Miller

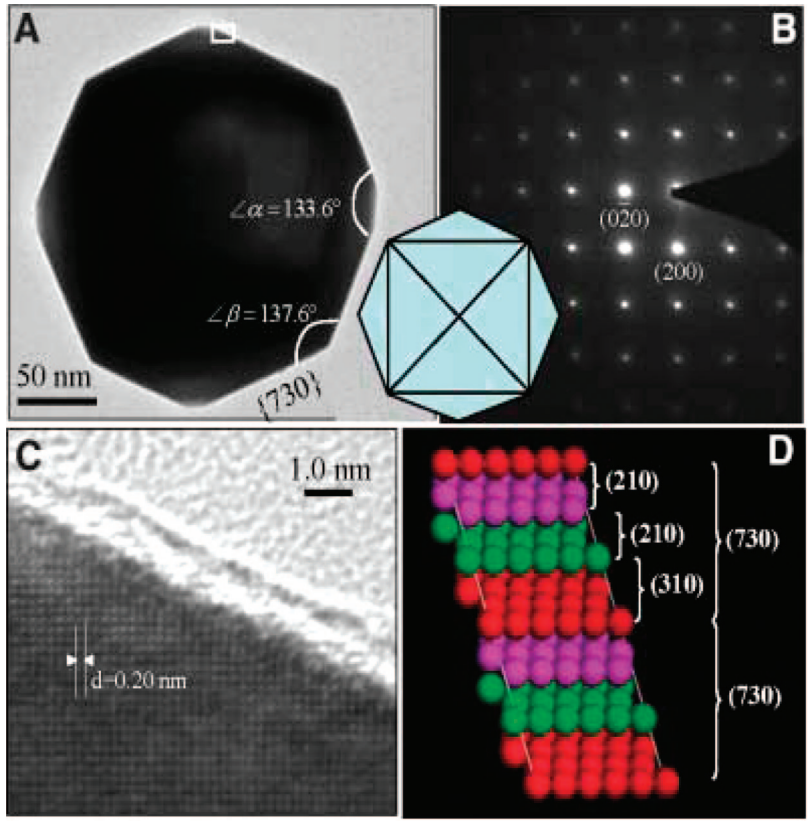

Figure 24. (A) TEM image of a single THH Pt nanocrystal, (B) SAED pattern with square symmetry, (C) high-resolution TEM image of the box from part A, D atomic model of the Pt{730} plane. Reprinted from Tian, N.; Zhou, Z.; Sun, S.-G.; Ding, Y.; Wang, Z.-L. *Science* **2007**, *316*, 732. Copyright 2007 AAAS.

indices of the exposed facets in Figure 24A were calculated by measuring the angle between the facets. The values of 133.6° ± 0.3° and 137.6° ± 0.3° between the {730} facets were in good agreement with the theoretical values for angle $\alpha = 133.6°$ and angle $\beta = 136.4°$. Therefore, the dominant facets of the THH Pt nanocrystals were {730} with contributions from {210}, {310}, and {520}. This composition is evident in the atomic arrangement of the Pt{730} surface in Figure 24D. The high-index facets possess enhanced electrocatalytic activity compared with spherical Pt nanoparticles, attributable to their thermal stability and higher energy.

A variety of methods can be used to characterize the size, distribution, agglomeration, composition, metallic and oxide components, phase, and index facets of Pt and Pt-based nanomaterials. The structural properties of Pt and Pt-based nanomaterials can vary greatly. Therefore, it is important to optimize the synthesis conditions of reagent concentration, types of reagents, temperature, pH, and substrate type to obtain the desired structural properties, which contribute to desirable optical, magnetic, and electrocatalytic properties.

3.2. Catalytic Properties

The development of novel Pt and Pt-based nanomaterials has garnered great interest from researchers in part due to the excellent electrocatalytic and catalytic properties of Pt. Platinum has high stability and electrocatalytic activity toward key reactions in fuel cells powered by the electrochemical oxidation of hydrogen and small organic molecules. These reactions include the hydrogen oxidation reaction (HOR), methanol oxidation reaction (MOR), ethanol oxidation reaction (EOR), formic acid oxidation, and oxygen reduction reaction (ORR). Platinum electrocatalysts have also shown potential for use in nonenzymatic biosensors due to their electrocatalytic activity toward glucose oxidation. The electrocatalytic activity of Pt and Pt-based nanomaterials toward these reactions as well as their current and potential use in applications will be discussed in detail in the applications section.

Platinum catalysts also play a key role in chemical sensing applications, as well as the automotive and petroleum industries. The role of Pt as a catalyst for CO detection, the oxidation of CO and NO_x in catalytic converters, the refining of petroleum, hydrogen production, and anticancer properties will also be discussed in the applications section. It is well-known that platinum is very expensive, due to its rare reserve on earth; thus some the discussion will focus on how the use of Pt-based electrocatalysts can reduce production costs through enhancing the activity of Pt via dispersing nanostructured materials on high surface area supporting materials and through coupling with other metals to form binary and ternary electrocatalysts.

3.3. Optical Properties

Nanostructured materials of noble metals exhibit optical properties different from their corresponding bulk metals and therefore have been the focus of many investigations due to their potential for applications in optoelectronic and biophotonic devices. The control of the composition and morphology of the nanomaterials, via different fabrication methods, is important for adapting them to specific applications. The optical properties of a variety of Pt-based nanomaterials, including thin films or coatings, nanowires, nanoparticles,

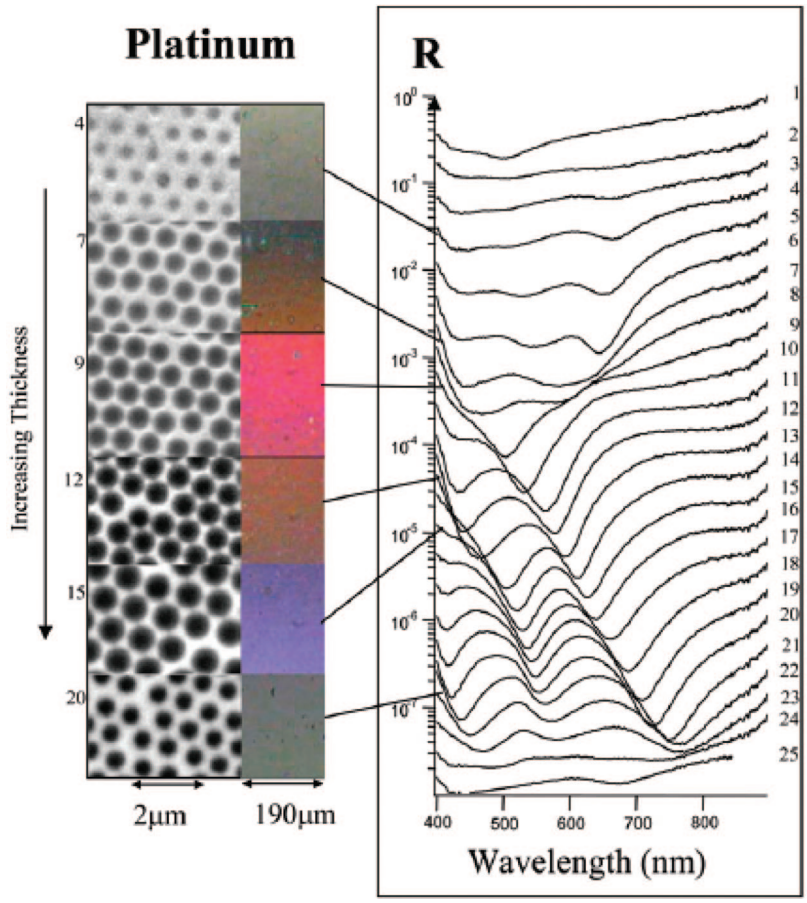

Figure 25. Normal incidence reflectance spectra and optical and SEM images for nanostructured platinum films with various thicknesses. The errors in film thickness were calculated using the formula $t = r \pm (r^2 - r_{pore}^2)^{1/2}$. Reprinted from Bartlett, P. N.; Baumberg, J. J.; Coyle, S.; Abdelsalam, M. E. *Faraday Discuss.* **2004**, *125*, 117. Copyright 2004 Royal Society of Chemistry.

and nanothorns, have been investigated using absorption, extinction, and reflectance spectra as well as Raman spectroscopic techniques.[281−287]

Barlett et al.[281] employed electrochemical deposition to fabricate nanostructured Pt films. The Pt was deposited under potentiostatic conditions at −0.05 V vs SCE through templates composed of hexagonally arranged 700 nm diameter polystyrene spheres on an evaporated gold substrate. The template was dissolved by soaking the electrodes in tetrahydrofuran for 2 h. An optical microscopy arrangement containing a fiber-coupled spectrometer was used to record the normal incidence reflection spectra as a function of film thickness, as shown in Figure 25. As the film thickness increases, dips in the reflectivity shift to longer wavelengths are observed. This resulted in changes to the color of the sample. For the thinnest films, spectra 1−7, a dip around 670 nm developed and increased in intensity and shifted toward shorter wavelengths as film thickness was increased. The cause of the trend may be a grafting like effect, known as surface plasmon, which is described as the coupling of electrons and light to produce a traveling wave solution along a dielectric/metal interface. Surface plasmon produces a coupling condition described by the equation

$$\sin(\theta) = [\varepsilon_1(\omega)/(1 + \varepsilon_1(\omega))]^{1/2} - m\lambda/d$$

The variables are defined as follows: θ is the angle of incidence, $\varepsilon_1(\omega)$ is the real part of the dielectric function of the metal, λ is the incident wavelength, d is the grafting periodicity, and m is an integer. Calculations revealed a value of 675 nm, which is close to the experimental values shown in Figure 25. As the film thickness increases, spectra 8−24, the dips broaden, intensity decreases, and the peaks shift in reflectivity to longer wavelengths. These changes are the result of the increased magnification required to image the samples in that region. In this region, the reflection of light from the top of the nanostructured films caused interference with the light reflected from within the film. This interference dominated the optical response of the nanostructured Pt films instead of the adsorption of light.

Suzuki et al.[197] utilized electrochemical deposition to fabricate nanostructured Pt films consisting of aligned nanowires. The deposition was performed on mesoporous silica films with aligned mesopores in a 2% chloroplatonic acid solution. Figure 26 shows the TEM images of the nanostructured Pt film composed of Pt nanowires approximately 3 nm in diameter. As shown in Figure 26A, the lattice fringes of the Pt nanowires are parallel, revealing that the nanowires were deposited through the micropores that connect the bordering mesopores. A Shimadzu UV-2500 PC spectrophotometer was employed for the absorption spectra measurements. The ultraviolet adsorption spectra revealed a single peak at 197 nm. This is consistent with localized surface plasmon resonance (LSPR) measurements along the short axis of the Pt nanowires. The polarized visible absorption spectra taken parallel and perpendicular to the nanowires revealed the anisotropic optical properties of the film. No LSPR absorption was observed in the visible region

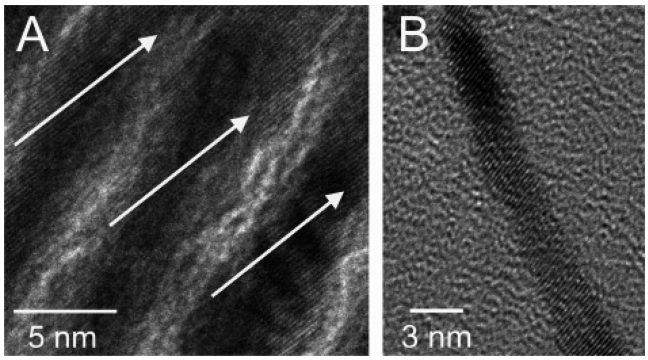

Figure 26. TEM images of (A) Pt nanowires on silica and (B) a single Pt nanowire. Reprinted from ref 197. Copyright 2008 American Chemical Society.

when the polarization was perpendicular to the nanowires, whereas a single peak at 660 nm resulted for the parallel polarization. The Pt/silica nanocomposite thin films exhibited the anisotropic properties of a single Pt nanowire despite possessing the interconnected structure of the film. It was proposed that interconnection does not have a significant effect on the electronic structure of the individual nanowires, perhaps due to the small number of interconnections between the nanowires.

Bigall et al.[285] used an electroless deposition method to fabricate monodisperse Pt nanoparticles. The approach employed a multistep seed-mediated approach using chloroplatonic acid as the precursor. The as-synthesized Pt nanoparticles had diameters ranging from 29 to 107 nm. The extinction spectra shown in Figure 27 were produced using a Cary 5000 spectrometer scanning between 230 and 800 nm. As the diameter of the particles increased, the localized surface plasmons or extinction peaks shifted to higher wavelengths. In Figure 27c, the experimental and calculated extinction spectra are compared. The calculated spectra were determined using a multiple-multipole (MMP) method because the electrostatic model results were too erroneous for the larger particles. While there was a good agreement between the slopes for the calculated and experimental curves, the values were different. The difference was attributed to the crystallinity and roughness of the nanoparticles. The linear dependence between the LSP resonance wavelength and particle diameter enables the easy optical characterization of particle diameter via extinction spectra.

Surface-enhanced Raman spectroscopy (SERS) is an important analytical technique for determining the identity of the molecules adsorbed on metal substrates. The optimization of the SERS response on nanostructured materials may lead to chemical and biosensing applications in the future. Sun and co-workers[287] synthesized platinum nanothorns using electrochemical deposition. The Pt nanothorns were synthesized on a glassy carbon substrate using square wave potential between −0.2 and 0.8 V for 20 min at 10 Hz. Figure 28 shows the SEM images of the as-synthesized Pt nanothorns with diameters up to 160 nm. The Pt nanothorns possess a face-centered-cubic (fcc) structure and high crystallinity and grew along the {111} direction. Pyridine was used as the probe molecule for the SERS measurements. A comparison of the SERS response of the Pt nanothorns and Pt nanoparticles revealed that the Raman signal for the Pt nanothorns at 1011 cm^{-1} is 140 cps compared with about 10 cps for the Pt nanoparticles. The electromagnetic

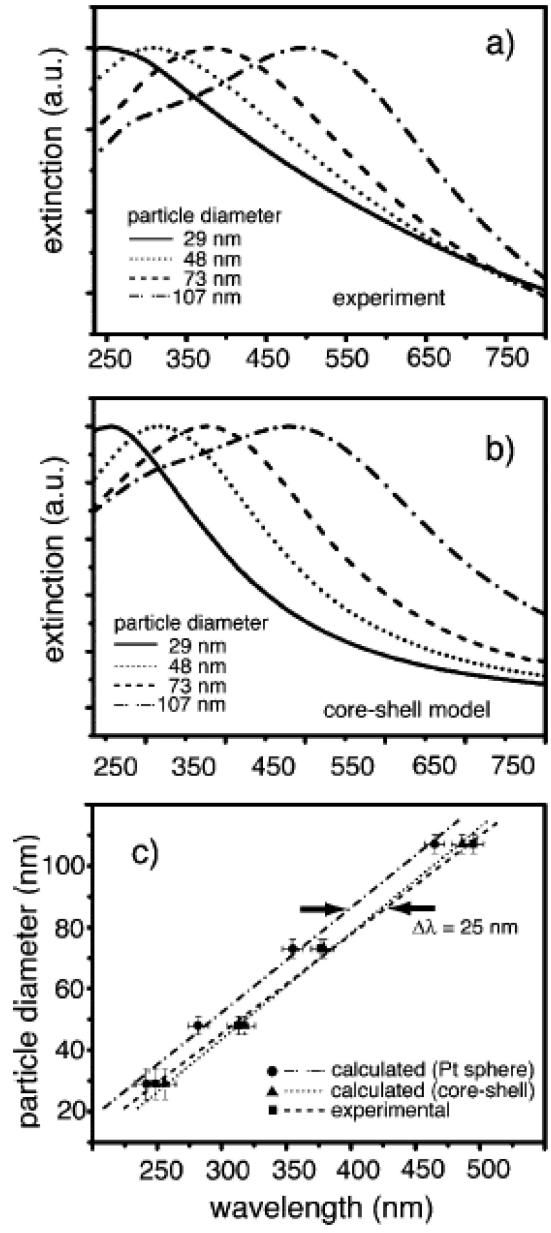

Figure 27. (a) Experimental extinction spectra of the platinum particles in aqueous solution, (b) calculated extinction spectra for a core−shell modeled platinum sphere, and (c) extinction peak positions for experimental data (■), calculated data for Pt spheres (●) and calculated data for core−shell modeled particles (▲). Linear fits were used to represent the lines for the respective data points. Reprinted from ref 285. Copyright 2008 American Chemical Society.

enhancement of the Pt nanothorns could be caused by the lightning rod effect, whereby the electromagnetic field is located near the high curvature points of the nanothorns resulting in a larger electric field by the sharpest surface.

The optical properties of Pt nanomaterials can be measured with a variety of techniques. The morphology of the as-synthesized nanostructured Pt materials has the largest effect on the optical properties of the nanomaterials. Overall, the synthesis technique can be used to tune the size and shape of the formed Pt nanomaterials and thus control the optical properties to tailor the novel materials toward specific applications.

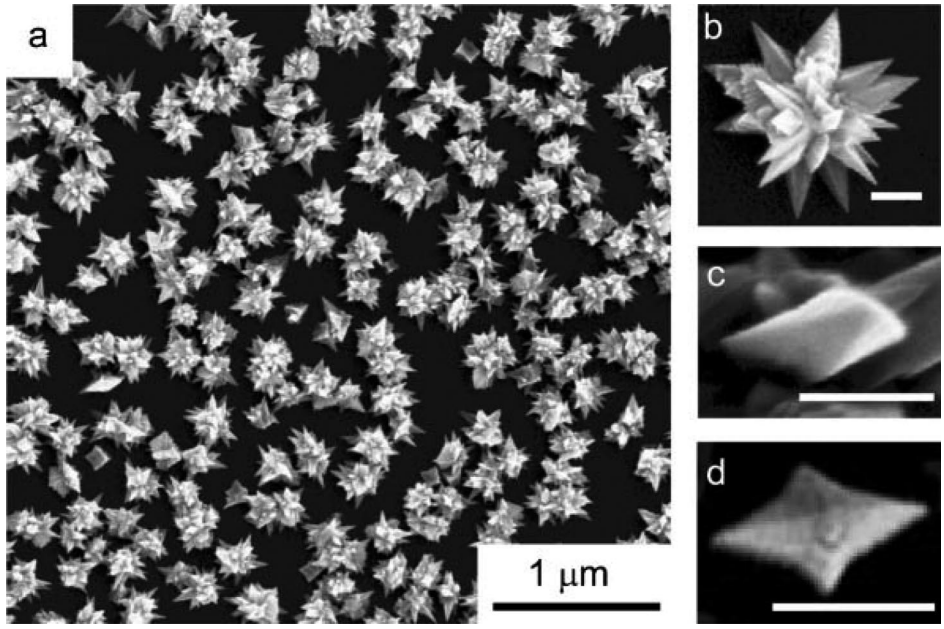

Figure 28. (a) SEM and (b) high-resolution SEM images of platinum nanothorn assemblies and (c) side and (d) top views of the Pt nanothorns. The scale bar in panels b−d is 100 nm. Reprinted from Tian, N.; Zhou, Z.; Sun, S.-G.; Cui, L.; Ren, B.; Tian, Z. *Chem. Commun.* **2006**, 4090. Copyright 2006 Royal Society of Chemistry.

3.4. Magnetic Properties

Platinum is a transition metal with a partially filled 5d shell. In the form of a bulk metal, Pt shows no evidence of surface magnetism, and the Pt 5d band is too wide to induce spin polarization. Investigating the magnetic properties of Pt and Pt-based nanomaterials has garnered great interest due to the potential for applications in magnetic storage media.[247,249,288−294] The magnetic properties of single metallic materials can be significantly improved through the formation of alloys with other metals. Magnetic alloys may have higher magnetic anisotropy, superior magnetic susceptibility, and larger coercivities compared with bulk metals.[295] Many studies have investigated the magnetic properties of Pt nanomaterials,[292,293,296−298] as well as in combination with ferromagnetic metals such as Co[95,288,290,291,295] and Fe.[247,249,289,294]

Delin et al.[292] investigated the magnetism of Pt nanowires using density functional calculations and found that they exhibited Hund's rule of magnetism. Fully relativistic calculations performed with the spin axis aligned along the wire direction indicated that the Pt nanowire had a magnetic moment of 0.6 μB at an equilibrium bond length of 2.48 Å. When the bond length was stretched, the magnetic moment increased. The fully relativistic Pt wire band structures were measured for five different bond lengths between 2.3 and 3.1 Å and revealed that the band edge A is on the Fermi level for all of the bond lengths. A magnetic moment may develop if a band edge lies near the Fermi level. This is due to the large energy gain expected if a band spin-splits such that one spin-channel band edge lies above and the other below the Fermi level. A comparison of the magnetic and nonmagnetic band structures showed that the (d_{xy}, $d_{x^2-y^2}$) bands triggers the formation of the magnetic state. The other band edges, d_{z^2} at A and d_{xz} and d_{yz} at Γ, also contribute to the magnitude of the magnetic moment as they split around the Fermi level.

Zhang et al.[296] studied the magnetic properties of Pt nanostructures with different morphologies. The Pt nanoparticles were formed via the decomposition of the Pt precursors in oleylamine or 1-dodecanethiol. As shown in Figures 29 and 30, the morphology of the as-synthesized Pt nanoparticles was controlled through the temperature and time of the synthesis reaction. A superconducting quantum interference device (SQUID) was used to characterize the magnetic properties of the Pt nanoparticles. The branched Pt nanoparticles exhibited much higher magnetization than the spherical Pt nanoparticles with values of 10×10^{-3} and 1×10^{-3} emu/g, respectively. The spherical Pt nanoparticles were paramagnetic whereas the branched nanoparticles were ferromagnetic at room temperature. The evidence suggests that ferromagnetism occurs in nanomaterials with high surface to volume ratios. The surfactants also affected the magnetic properties of the Pt nanomaterials. The thiol-capped Pt nanomaterials had enhanced magnetism compared with the amine-capped Pt nanomaterials. The evidence implied that the magnetic

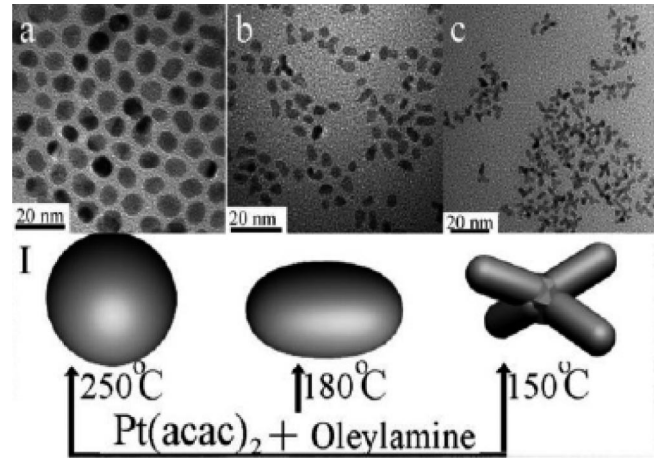

Figure 29. TEM images of Pt nanoparticles with different morphologies: (a) spherical, (b) elongated, and (c) tetrapod. Panel I shows the morphology evolution scheme of the Pt nanomaterials formed with different reaction temperatures. Reprinted from ref 296. Copyright 2008 American Chemical Society.

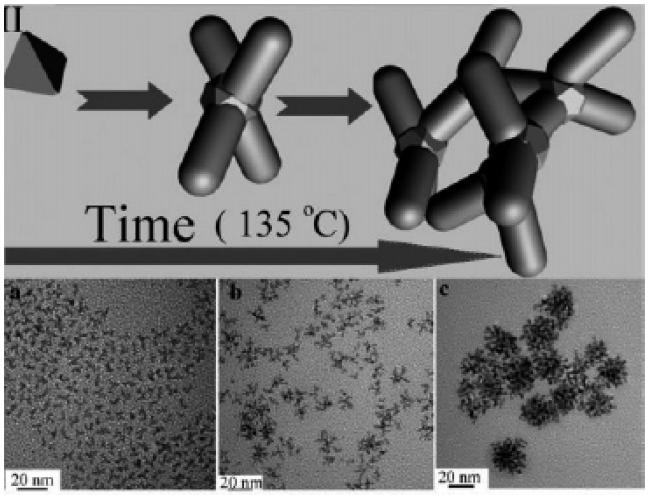

Figure 30. (II) Morphology evolution scheme of Pt nanomaterials formed with different reaction durations and TEM images of Pt nanoparticles formed via heating at 135 °C for (a) 0.5, (b) 4, and (c) 24 h. Reprinted from ref 296. Copyright 2008 American Chemical Society.

moments were produced by broken symmetry and charge transfers, since charge transfer was more efficient in 1-dodecanethiol than oleylamine.

Teng et al.[298] synthesized platinum nanowires using a modified phase-transfer method. A solution containing platinum chloride, octadecylamine (ODA), and the phase transfer agent n-dodecyltrimethylammonium bromide (DTAB) was prepared. The reducing agent, sodium borohydride, was added in large excess to facilitate the reduction of the platinum precursor. A superconducting quantum interference device (SQUID; model MPMS XL, Quantum Design) was used to determine the temperature dependence of the magnetic characteristics of the Pt nanowires, as shown in Figure 31a−f. The results from the magnetization curve at an applied field of 50 kOe and the coercivity in the hystersis loop at 300 K for Pt suggest that the nanowires were ferromagnetic rather than superparamagnetic. The unusual shift in the hysteresis at low temperature was attributed to a "magnetic memory" effect caused by magnetoelastic coupling. The cooling caused the local magnetic moments to align, which was related to the relaxation of the local lattice. The small observed magnetic moment implied that the magnetic moment took place in structural defects and changes in boundary conditions. The defects generated local magnetic instability, which was enhanced by the localization of electrons created by a collapse in the density of states.

Delaunay et al.[288] compared the magnetic properties of Co−C and CoPt−C thin films with nanogranular morphology and particles sizes between 5 and 25 nm. Selected area diffraction measurements were used to determine the microstructure of the film, which suggested the formation of a CoPt alloy due to the *d* spacing values. A vibrating sample magnetometer was utilized to obtain the magnetic hysteresis curves for the thin films. At an annealing temperature of 350 °C, the coercivities for the Co−C and CoPt−C films were 550 and 1500 Oe, respectively. The change in the magnetic properties may be due to an increase in the magnetocrystalline anisotropy due to a face-centered-cubic to face-centered-tetragonal phase transition.[288,290,291]

Carpenter et al.[249] prepared PtFe nanoparticles using an electroless deposition method. The method utilized separate

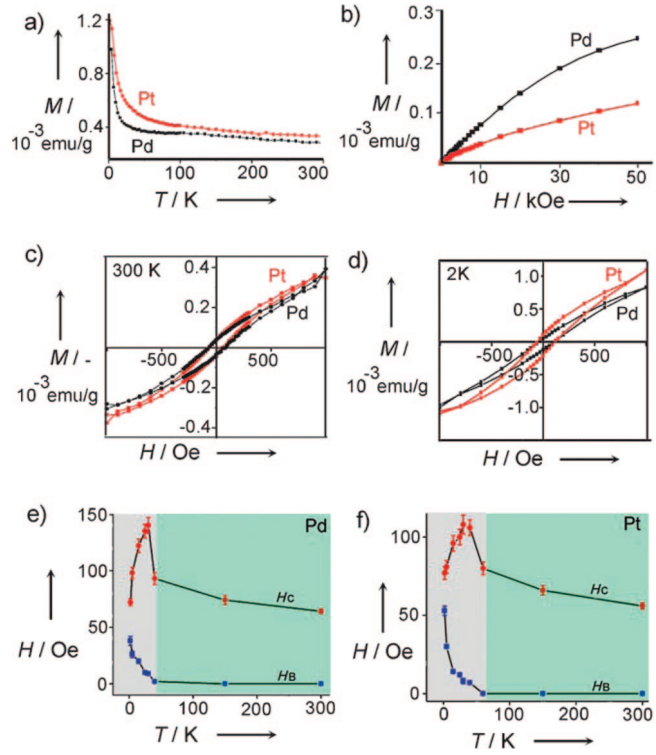

Figure 31. (a) Comparison of the effect of temperature on the magnetization of Pd (black) and Pt (red) nanowires in an external field of 1000 Oe with zero field cooling. Effect of temperature on the field-dependent magnetization of Pd and Pt nanowires: (b) 5, (c) 300, and (d) 2000 K. Effect of temperature on the coercivity (H_C) and biased field (H_B) of (e) Pd and (f) Pt nanowires. Reprinted from Teng, X.; Han, W.; Ku, W.; Hucker, M. *Angew. Chem., Int. Ed.* **2008**, *47*, 2055. Copyright 2008 Wiley-VCH.

water and oil phases containing the surfactants cetyltrimethylammonium bromide (CTAB) and 1-butanol. Different ratios of the Pt and Fe precursors were reduced by sodium borohydride to form the nanoparticles. TEM images revealed that the particles had average diameters of 10 nm and XRD analysis confirmed the formation of a PtFe alloy. A SQUID magnetometer was employed for the magnetic measurements. The addition of Pt to the samples increased the coercivity from 200 Oe for Fe to 1500 Oe for Fe/Pt_3. The increased coercivity of the samples upon the addition of Pt was attributed to an increase in the anisotropy of the system. Interestingly, the Fe/Pt_3 ordered and disordered alloys had coercivities of 400 and 1500 Oe, respectively. The enhanced coercivity of the disordered alloy could be due to exchange coupling between ferromagnetic impurities or a difference in particle size.

The magnetic properties of Pt and Pt-based nanomaterials have been investigated using density functional calculations and SQUID magnetometers. While bulk Pt metal may be paramagnetic, the fabrication of Pt nanomaterials produces ferromagnetic and superparamagnetic properties. Certainly, the magnetic properties of Pt nanomaterials are further enhanced through the addition of ferromagnetic elements such as Fe or Co. The magnetic properties of Pt and Pt-based nanomaterials are dependent on composition and morphology, which can be tuned by optimizing synthesis conditions such as the presence of capping agents and reaction temperature.

4. Applications of Pt and Pt-Based Nanomaterials

4.1. CO Oxidation

The CO oxidation reaction has been extensively investigated on Pt and Pt-based nanomaterials due to its application in hydrogen and small organic molecule based fuel cells. CO is an intermediate/product of methanol, ethanol, and formic acid oxidation and the reformation of hydrocarbons used to synthesize hydrogen. The formation of CO has a significant impact on fuel cell applications because CO may strongly adsorb to the surface of Pt and Pt-based electrodes and occupy catalytic sites, thus slowing the reaction kinetics.[299] Therefore the design of catalysts with high activity toward CO oxidation is vital to fuel cell applications. CO can be removed from sites on Pt and Pt-based electrodes in an oxidative step involving OH species that are formed through the activation of water. On a pure Pt electrode, the water activation step requires high potentials, which is undesirable for fuel cell applications.

Efforts to improve the performance of Pt electrodes toward CO oxidation have focused on the effect of particle size[300−302] as well as coupling other metals with platinum to form various Pt-based nanomaterials, including Au,[303] Co,[20,304] Ir,[21] Ni,[304] Sn,[305] Mo,[306] W,[307] Pb,[21] Pd,[21] and Ru.[246,308,309] For instance, Wang et al.[21] investigated the performance of various nanoporous Pt-based electrocatalysts formed by hydrothermal deposition. Figure 32 compares the performance of various Pt-based nanomaterials toward CO oxidation. As seen in Figure 32, on the first sweep, the CV curve is flat across the hydrogen adsorption region indicating that all the Pt sites were occupied by adsorbed CO. The broad oxidation peaks and subsequent return of the hydrogen adsorption peaks indicate that the CO has been removed from the electrode surface on the first cycle. The PtRu electrode has the best performance of the electrodes in terms of onset potential and peak potential. In an effort to understand the mechanism of CO oxidation on PtRu surfaces, many research groups have used in situ Fourier transform infrared (FTIR) spectroscopy.[310−316] An in situ FTIR study of the CO oxidation characteristics on Ru-modified Pt(111) electrodes by Lin et al.[310] revealed that absorbed CO migrates to Ru where it is preferentially oxidized. Figure 33 shows the FTIR spectra for the Pt, PtRu, and Ru electrodes. The spectra for Pt(111) show two potential-dependent bands around 2070 and 1830 cm^{-1}, which were attributed to linear bonded (CO_L) and 2-fold bridge bonded (CO_B) CO species. The two electrodes containing Ru show a band around 2000 cm^{-1} attributed to linear bonded CO species on Ru. Therefore, when the Ru content of the electrodes was increased from 0.2 to 1.0, the intensity of the CO_L and CO_B bands from Pt(111) decreased. For electrodes with a Ru content greater than 0.6, a red shift of -10 cm^{-1} and a blue shift of $+6$ cm^{-1} were observed for the CO_L bands on the Pt(111) and Ru surfaces, respectively. These results reveal an important electronic effect of the Ru-modified Pt(111) electrode. Two mechanisms have been proposed to account for the enhanced electrocatalytic properties of PtRu toward CO oxidation. The first mechanism is a bifunctional mechanism, whereby oxygen-containing species are adsorbed on Ru atoms, which promote the oxidation of CO to CO_2 on neighboring sites, as summarized below.[309]

$$Pt + CH_3OH \rightarrow Pt(CO)_{ads} + 4H^+ + 4e^- \quad \text{(CO adsorption)}$$

$$Ru + H_2O \rightarrow Ru(OH)_{ads} + H^+ + e^- \quad \text{(OH adsorption)}$$

$$Pt(CO)_{ads} + Ru(OH)_{ads} \rightarrow CO_2 + Pt + Ru + H^+ + e^- \quad \text{(CO oxidation)}$$

The other is a ligand effect whereby the electronic properties of Pt are modified by the PtRu orbital overlap, which weakens the strength of the bond between the Pt and the adsorbed CO.

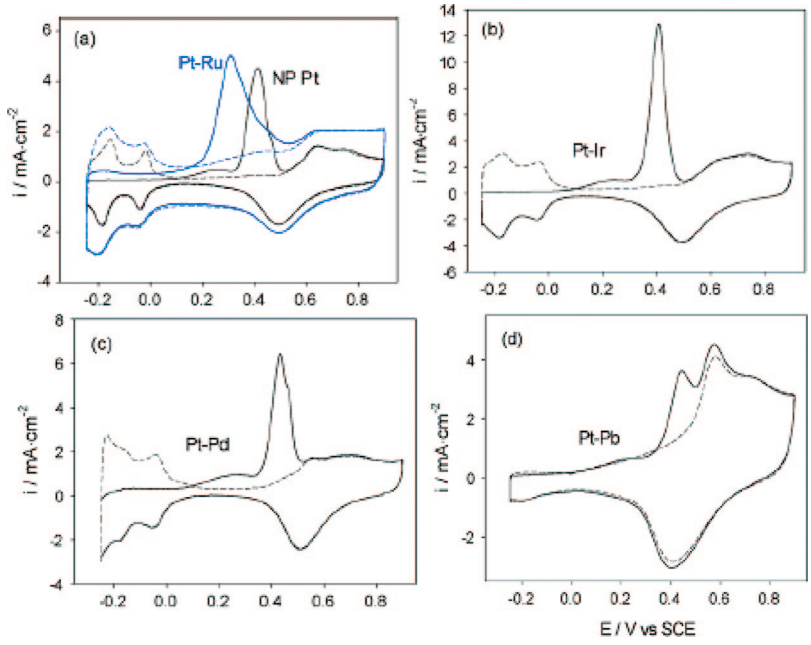

Figure 32. Cyclic voltammograms of CO stripping on nanoporous Pt and Pt-based electrodes: (A) PtRu (blue) and nanoporous Pt (black); (B) PtIr; (C) PtPd; (D) PtPb. Two cycles of the CV were recorded for each electrode in a 0.1 M H_2SO_4 at a potential scan rate of 20 mV/s: the first sweep cycle is shown as solid line, and the second sweep cycle is drawn as dashed line. Reprinted from Wang, J.; Holt-Hindle, P.; MacDonald, D.; Thomas, D. F.; Chen, A. *Electrochim. Acta* **2008**, *53*, 6944. Copyright 2008 Elsevier.

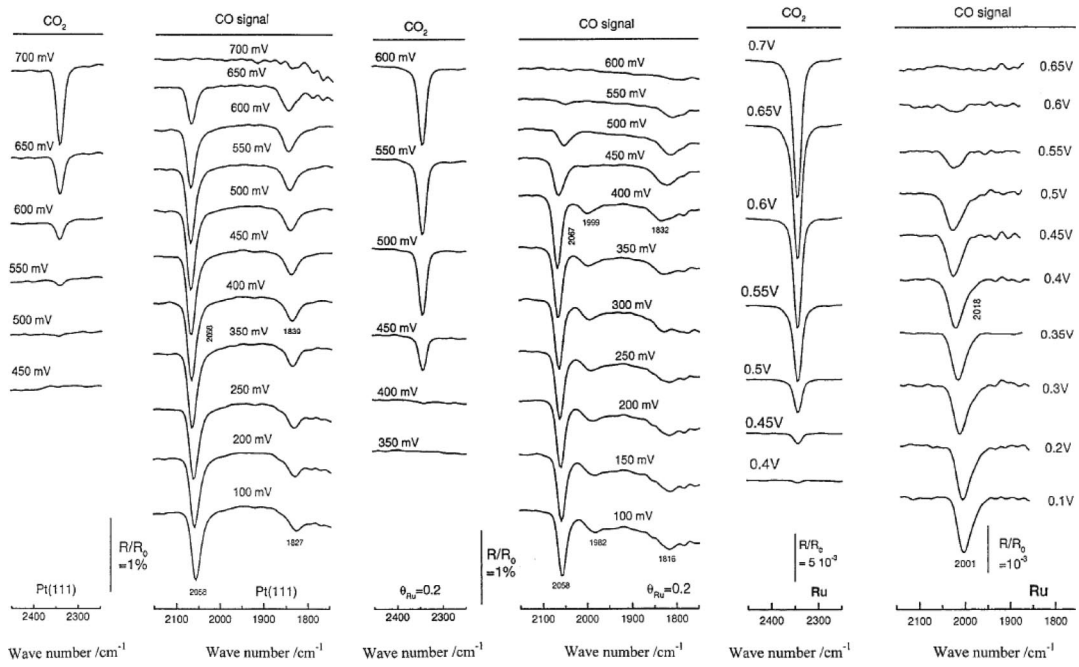

Figure 33. In situ FTIR spectra of Pt(111), Pt(111) with Ru coverage of 0.2, and (C) Ru electrodes showing bands for adsorbed CO and the CO_2 produced during the CO stripping experiment in 0.1 M $HClO_4$. The CO adlayer was formed at 0.1 V, and the potential of the experiment was changed from 0.1 V in +50 mV increments. The reference spectra for CO_2 and CO were taken at 0.1 and 0.8 V, respectively. Reprinted from ref 310. Copyright 1999 American Chemical Society.

Efforts to further enhance the electrocatalytic activity of the fuel cell catalysts toward CO oxidation have focused on the development of ternary Pt-based nanomaterials, such as PtCoW,[307] PtRuMo,[317] PtRuPd,[318] PtRuFe,[319] PtRuNi,[319] and PRuCo.[319] Jeon et al.[319] utilized an electroless deposition method with sodium borohydride as the reducing agent to form various PtRuM (M = Fe, Ni, Co) nanomaterials. All three of the PtRu-based electrocatalysts displayed lower onset potentials for the oxidation of CO compared with PtRu (0.49 V), with values of 0.46, 0.48, and 0.48 V for PtRuFe, PtRuNi, and PtRuCo, respectively. The increased activity of the PtRuFe electrocatalyst in comparison to PtRu may be attributed to alloying between Pt and Fe, which could prevent the electron back-donation from Pt to CO, thereby weakening the Pt−CO bond.

The development of novel Pt-based binary and ternary electrocatalysts has significantly enhanced the electrocatalytic activity of fuel cell catalysts toward CO oxidation. The added benefit to alloying other metals with platinum to form Pt-based nanomaterials is that Pt loading can be significantly reduced, thereby reducing the cost of the application of anodes in small organic molecule and hydrogen fuel cells.

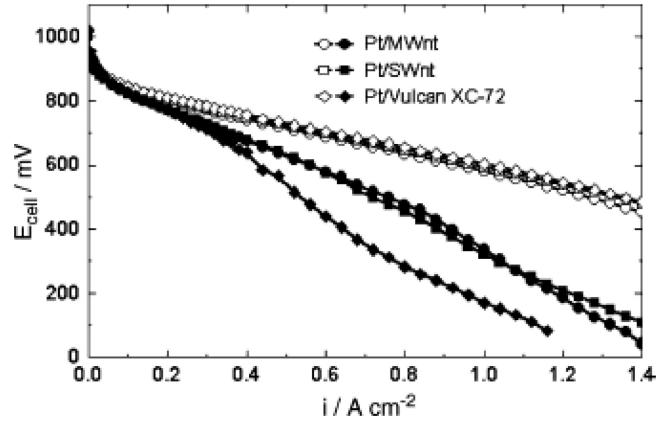

Figure 34. PEMFC performance of Pt electrodes with substrates. The cathode was a Pt/C (E-TEK) with a Pt loading of 0.4 mg cm^{-2} and fed with O_2 humidified at 90 °C and 0.17 MPa. The membrane used was Nafion 115. The anodes were fed with H_2 (open symbols) and H_2 + 100 ppm CO (shaded symbols) humidified at 100 °C and 0.2 MPa. Reprinted from Carmo, M.; Paganin, V. A.; Rosolenb, J. M.; Gonzalez, E. R. *J. Power Sources* **2005**, *142*, 169. Copyright 2005 Elsevier.

4.2. Hydrogen Fuel Cells

The use of hydrogen as a fuel has numerous advantages. It can be produced from the electrolysis of water or from the reformation of methane, methanol, or other liquid fuels, and when consumed in proton exchange membrane fuel cells (PEMFCs) with oxygen, pure water is the product. In addition, some infrastructure exists for the storage, transport, and distribution of compressed hydrogen in the United States. Among the precious metals, platinum is the most active toward the hydrogen oxidation reaction (HOR) that occurs at the anode in PEMFCs. The power density of PEM fuel cells improved substantially from about 0.1 kW L^{-1} in 1989 to 2.3 kW L^{-1} in 2001. In 2004, the cost of PEM fuel cells was \$175 kW^{-1}. The US Department of Energy has set targets of \$45 kW^{-1} for 2010 and \$30 kW^{-1} for 2015 in order to make the PEMFCs competitive with conventional gasoline−electric technology.

In order to meet cost reductions of this magnitude, the Pt catalyst loading must be decreased. Two strategies have been investigated for reducing the Pt loading in PEMFCs: the fabrication of binary and ternary Pt-based alloyed nanomaterials and the dispersion of Pt-based nanomaterials onto high surface area substrates. For example, Carmo et al.[320] investigated the use of SWNTs, MWNTs, and Vulcan XC-72 as electrocatalyst supports for Pt in PEMFCs. The effect of the different electrocatalyst supports on cell performance with and without the presence of CO is shown in Figure 34. The results show that all three catalysts suffered a drop in performance upon the addition of CO. However, the elec-

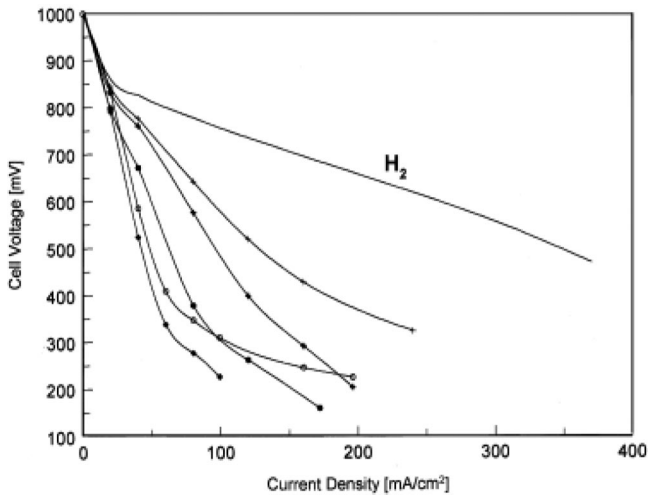

Figure 35. Current−voltage cells of binary Pt-based anodes in H_2/150 ppm CO: (◆) Pt, (+) PtRu, (●) PtW, (○) PtSn. The load of the anode and cathode was 0.4 mg cm^{-2}. Reprinted from Götz, M.; Wendt, H. *Electrochim. Acta* **1998**, *43*, 3637. Copyright 1998 Elsevier.

trodes containing the nanotube supports performed much better than those with the Vulcan XC-72 support. This enhancement could be explained by the Ni, Fe, or other contaminants present in the nanotubes, which could facilitate CO oxidation at lower potentials.

The development of novel binary and ternary Pt-based nanomaterials for PEMFCs aids in the reduction of Pt loading in PEMFCs, as well as increases the carbon monoxide tolerance of the anode. Carbon monoxide is produced during the reformation of hydrocarbons and is typically present at a concentration of several ppm in compressed hydrogen.[218,277] Many binary Pt nanomaterials, such as PtRu,[321−326] PtCo,[322] PtMo,[324] PtSn,[324] and PtW,[324] have been fabricated with the goal of improving the electrocatalytic activity of the anode toward the HOR in the presence of CO. Götz et al.[324] investigated the electrocatalytic activity of PtMo, PtRu, PtSn, and PtW nanoparticles toward the HOR and CO oxidation. Figure 35 compares the effect on the cocatalytic properties of the four elements, Mo, Ru, Sn, and W, through the electrocatalytic activity of the binary Pt-based nanoparticles in the current−voltage curves. While all the electrodes demonstrated a decrease in electrocatalytic activity in the presence of CO, all four binary electrodes had better performance than the pure Pt electrocatalyst. The PtMo, PtRu, PtSn, and PtW electrocatalysts show enhanced CO-tolerance when compared with Pt in the HOR. The PtRu electrode displayed the best performance due to either an electronic effect or the bifunctional mechanism. The Pt−CO bond becomes weaker following the addition of Ru to Pt. The Ru modifies the electronic properties of Pt. In the bifunctional mechanism, Ru facilitates the generation of oxygen-containing species at lower potentials than Pt, which facilitates the oxidation of CO molecules on adjacent sites to form CO_2.[19]

Striving to further improve the electrocatalytic activity of the anode in PEMFCs toward HOR and CO oxidation, many ternary PtRu-based electrocatalysts have been synthesized including PtRuAg,[327] PtRuAu,[327,328] PtRuMo,[324] PtRuOs,[328] PtRuSn,[324] $PtRuSnO_x$,[328] PtRuRh,[327] PtRuW,[324] $PtRuWO_x$,[328] and $PtRuW_2C$.[327] Voltammetric investigations of CO stripping on the electrocatalysts revealed that the $PtRuWO_x$ and $PtRuW_2C$ had lower onset potentials for CO oxidation compared with PtRu. Thus, consensus among these investigations is that the addition of the element W to PtRu resulted in the most active ternary Pt-based electrocatalysts toward hydrogen and CO oxidation.

Significant progress has been made at increasing the performance and decreasing the cost of PEMFCs through the use of high surface area supporting materials and the development of novel binary and ternary Pt-based nanomaterials. PEMFCs are important energy conversion devices in that they have the potential to reduce dependence on fossil fuels and reduce greenhouse gas emissions. The appearance of test automobiles with hydrogen-powered PEMFCs by major car companies such as Honda, GM, Mercedes Benz, Toyota, and Ford are a major step toward achieving both goals.

4.3. Methanol Fuel Cells

Methanol offers several advantages over hydrogen as a fuel including the ease of transportation and storage and high theoretical energy density. The methanol oxidation reaction (MOR) occurs at the anode in direct methanol fuel cells (DMFC). Platinum is the most promising candidate among pure metals for application in DMFCs. Platinum has the highest activity toward the dissociative adsorption of methanol. However, pure Pt surfaces are poisoned by carbon monoxide, a byproduct of methanol oxidation, at room temperature. A simplified reaction scheme for the oxidation of methanol is[248]

$$CH_3OH \rightarrow (CH_3OH)_{ads} \quad \text{(methanol adsorption)}$$

$$(CH_3OH)_{ads} \rightarrow (CO)_{ads} + 4H^+ + 4e^- \quad \text{(C−H bond activation)}$$

$$(CO)_{ads} + H_2O \rightarrow CO_2 + 2H^+ + 2e^- \quad \text{(CO oxidation)}$$

Researchers have focused on dispersing nanostructured catalysts on high surface area supporting materials and the development of Pt-based nanomaterials with high electrocatalytic activity toward MOR to overcome the poisoning effect of CO. Wu et al.[329] used the hydrothermal method to decorate free-standing Ti nanowires with Pt nanoparticles (Pt@Ti). The Pt nanoparticles had an average diameter of 3 nm and coated the surface of the Ti nanowires with diameters of 45 nm. On the Pt@Ti electrode, a huge peak (J_f = 68.83 mA cm^{-2}) appears at 0.57 V during the forward scan, and another large peak (J_b = 62.07 mA cm^{-2}) displays at 0.48 V during the backward scan from 0.80 to −0.225 V, revealing that the J_f/J_b value for the Pt@Ti electrode was 1.11 compared with 0.98 for the polycrystalline Pt electrode. Lower J_f/J_b values indicate the accumulation of carbonaceous species on the catalyst's surface and incomplete oxidation of methanol during the anodic scan. Therefore, the Pt@Ti electrode possessed improved CO tolerance and a peak current density over 190 times higher than the polycrystalline Pt electrode.

Peng et al.[28] compared the electrocatalytic activity of nanoporous Pt networks and bulk Pt toward the oxidation of methanol. The nanoporous Pt networks were synthesized using a seed-assisted hydrothermal deposition technique. Hydrogen adsorption and desorption were used to determine the electroactive surface area of the electrodes and revealed that the nanoporous Pt electrode had an active surface area

20 times higher than the bulk Pt electrode. Cyclic voltammetry and chronoamperometry experiments conducted in a 0.1 M CH_3OH + 0.5 M H_2SO_4 solution demonstrated the enhanced electrocatalytic activity of the nanoporous Pt toward methanol oxidation. The CVs revealed a higher current density and broader oxidation peaks for the nanoporous Pt electrode. In addition, the steady state current density for the nanoporous Pt electrode was over 25 times higher than the bulk Pt electrode at 600 mV. The use of synthesis techniques, such as the hydrothermal method, enables the development of nanostructured Pt materials with large surface areas and enhanced electrocatalytic activity compared with bulk Pt.

One of the disadvantages to using a pure Pt electrocatalyst is that the performance of the catalyst suffers due to the poisoning by carbon monoxide, since Pt requires a potential of at least 0.5 V to generate the OH species necessary to oxidize carbon monoxide.[330] This drawback is often overcome by coupling platinum with other metals, such as Co,[331] Fe,[331] Ir,[21] Ni,[223,331] Pb,[21,332] Pd,[21] Ru,[21,332] V,[333] and Au,[334] that facilitate the generation of the OH species at lower potentials than Pt. Wang et al.[21] studied the electrocatalytic activity of nanoporous Pt, PtRu, PtIr, PtPd, and PtPb networks fabricated with a hydrothermal deposition technique toward methanol oxidation. Chronoamperometric experiments were conducted at 0.3, 0.5, and 0.8 V in a 0.1 M CH_3OH + 0.5 M H_2SO_4 solution. Throughout the potential range, the binary Pt-based nanoporous electrocatalysts exhibited higher current densities than the nanoporous Pt electrode. At low potential, the nanoporous PtRu electrode exhibited the best performance toward methanol oxidation, due to the ability of Ru to generate oxygen-containing species at potentials as low as 0.3 V. The enhanced electrocatalytic properties of the PtRu catalyst are attributed to two mechanisms: the ligand effect mechanism whereby the electronic properties of Pt are modified by the PtRu orbital overlap or the bifunctional mechanism where Ru facilitates the generation of oxygen-containing species on sites adjacent to Pt, thereby aiding in the oxidation of CO.[267] At higher potentials, PtIr exhibited the strongest electrocatalytic activity toward methanol oxidation. The enhanced activity of the nanoporous PtIr electrocatalyst could be attributed to an effect similar to the bifunctional mechanism for Ru.[21]

The electrocatalytic activity of electrocatalysts can be further enhanced through the development of ternary Pt-based nanomaterials, such as PtVFe, PtNiFe, PtRuMo, or PtRuIr.[157,335−337] Bauer et al.[157] compared the electrocatalytic activity of PtRu and PtRuMo electrocatalysts synthesized with electrodeposition. Figure 36 shows the fuel cell polarization curves for the electrodes at higher temperatures. The PtRuMo (2200 W m^{-2}) nanomaterials show enhanced power density versus PtRu (1950 W m^{-2}). Therefore the presence of Mo had a beneficial effect on the fuel cell performance of the anode at high temperatures.

The development of novel Pt-based binary and ternary electrocatalysts has made great strides toward overcoming the challenges of poor anode kinetics and the poisoning effect of CO. While DMFCs suffer from reduced efficiency due to methanol crossover from the anode to the cathode, the advantages methanol has over hydrogen as a fuel suggest that DMFCs have strong potential for practical applications.

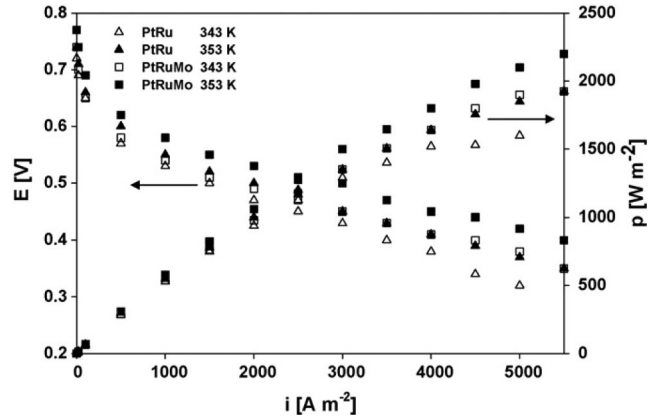

Figure 36. Fuel cell performance of PtRu and PtRuMo electrocatalysts. The anode feed was 1 M CH_3OH + 0.5 M H_2SO_4 at a rate of 5 mL min^{-1} under ambient pressure. The cathode feed was dry O_2 gas at a rate of 500 mL min^{-1} under STP and 2 atm. Reprinted from Bauer, A.; Gyenge, E. L.; Oloman, C. W. *J. Power Sources* **2007**, *167*, 281. Copyright 2007 Elsevier.

4.4. Electrochemical Oxidation of Ethanol

Ethanol offers an attractive alternative to methanol in direct alcohol fuel cells. The advantages of ethanol are a higher theoretical energy density (8.1 kWh kg^{-1}) versus methanol (6.1 kWh kg^{-1}), lower toxicity versus methanol, and ease of production from the fermentation of sugar-containing raw materials.[338−340] The reaction scheme for the oxidation of ethanol in acidic media on Pt surfaces is much more complex than methanol oxidation, since the complete oxidation of ethanol to CO_2 requires the transfer of 12 electrons compared with the 6 required for methanol. Ethanol can be adsorbed through either the −C or −O onto Pt surfaces. Therefore several reaction mechanisms have been proposed to account for the products of ethanol electro-oxidation on Pt surfaces: acetaldehyde, acetic acid, carbon dioxide, and methane. The main products of the oxidation of ethanol are acetaldehyde and acetic acid, which are formed through the direct oxidation of the alcohol group.[339]

Zhang et al.[341] compared the electrocatalytic activities of Pt nanowire arrays to Pt films toward ethanol electro-oxidation. The nanowire arrays were fabricated using the electrochemical deposition of Pt−Cu alloy nanowires onto alumina templates and dealloying the Cu component. CV experiments were used to compare the electrocatalytic activity of the Pt film, Pt nanowire array, and porous Pt nanowire array electrodes toward ethanol oxidation. Both of the Pt nanowires arrays exhibited higher anodic peak current densities toward ethanol oxidation than the Pt film electrode. The porous Pt nanowire arrays had higher electrocatalytic activity toward ethanol oxidation than the Pt nanowire arrays despite lower Pt loading, 0.79 vs 4.7 mg cm^{-2}. The enhanced electrocatalytic activity of the porous Pt nanowire arrays may be attributed to more efficient mass and electron transport as well as a larger number of three-phase boundary reactive sites.

Ethanol electro-oxidation on Pt surfaces suffers from the same drawback as methanol oxidation, the adsorbed CO decreases the performance of the electrocatalyst. To overcome this drawback, numerous binary Pt-based electrocatalysts have been studied, such as PtW,[342] PtPd,[342] PtRu,[340,342,343] PtSn,[342,344−346] and PtIr.[347] Zhou et al.[342] prepared Pt, PtRu, PtSn, PtW, and PtPd nanomaterials on carbon vulcan XC-72R. Figure 37 shows the CVs of the performance of the

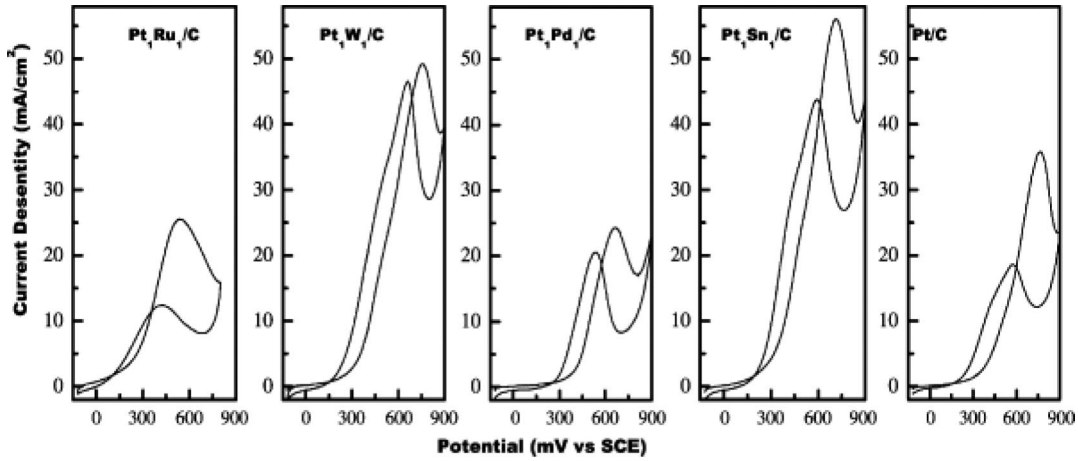

Figure 37. CVs of carbon-supported binary Pt-based electrodes in 0.5 M H_2SO_4 + 1.0 M ethanol at 25 °C and a scan rate was 10 mV/s. Reprinted from Zhou, W.; Zhou, Z.; Song, S.; Li, W.; Sun, G.; Tsiakaras, P.; Xin, Q. *Appl. Catal., B* **2003**, *46*, 273. Copyright 2003 Elsevier.

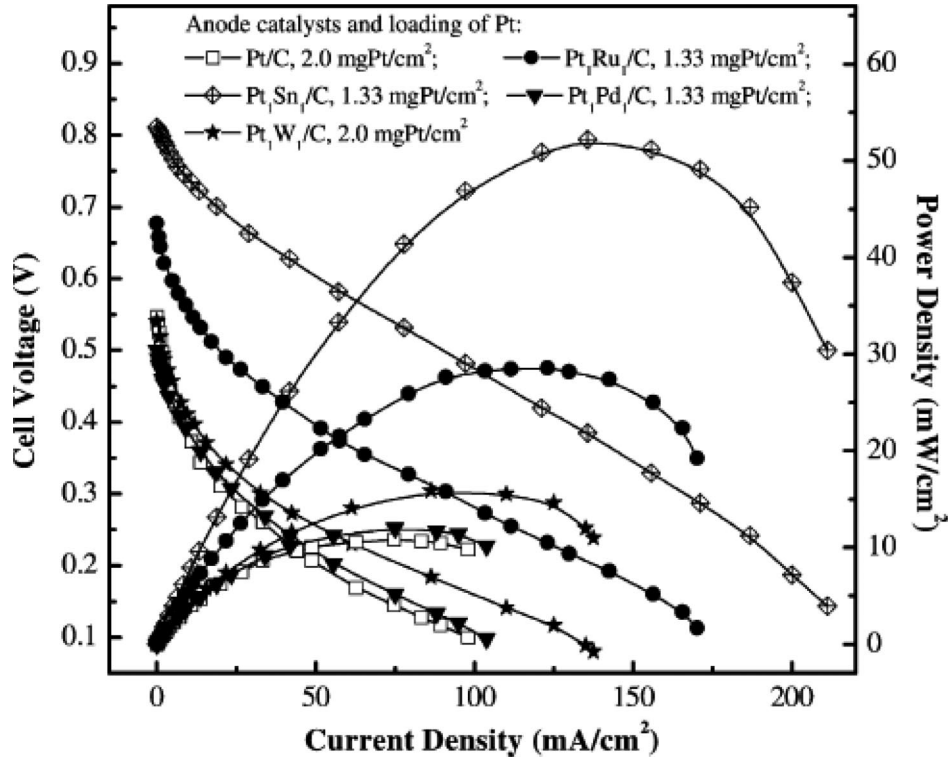

Figure 38. Comparison of binary Pt-based anode catalysts in an ethanol fuel cell. The cathode was a Pt/C from Johnson Matthey Co with a Pt loading of 1.0 mg cm^{-2}, the solid electrolyte was a Nafion-115 membrane, and the electrolyte was 1.0 M ethanol at a flow rate of 1.0 mL min^{-1} and temperature of 90 °C. Reprinted from Zhou, W.; Zhou, Z.; Song, S.; Li, W.; Sun, G.; Tsiakaras, P.; Xin, Q. *Appl. Catal., B* **2003**, *46*, 273. Copyright 2003 Elsevier.

binary Pt-based electrocatalysts toward ethanol oxidation. The addition of the second metal to Pt resulted in increased peak current density and a shift in the potential of the oxidation peak to more negative potentials. Overall, the addition of Sn, Ru, and W to Pt had significant effects on the electrocatalytic activity of the Pt-based electrocatalysts toward ethanol oxidation. The PtSn electrocatalyst had the highest current density and PtRu had the lowest overpotential. However, the peak current density of the PtSn electrocatalyst was at a comparable potential to Pt. The enhanced effect of the Sn, Ru, and W can be partially attributed to the ability of these elements to provide oxygen-containing species at lower potentials than Pt. The oxidation of the adsorbed CO intermediates can be facilitated by these oxygen-containing species. However, the bifunctional mechanism alone cannot account for the large variations in the fuel cell performance of the catalysts, shown in Figure 38. While the addition of W and Ru enhances the electrocatalytic activity of Pt toward ethanol oxidation, PtSn has the highest open circuit potential and power density. A number of factors have been proposed to account for the performance of the PtSn electrocatalyst including changes in Pt lattice parameters, charge transfers between Pt and Sn, a decrease in the oxidic state of Pt, and an electronic interaction between Pt and Sn. Ternary electrocatalysts such as PtRuW, PtRuMo, PtSnIr, and $PtRhSnO_2$ have shown enhanced electrocatalytic activity toward ethanol oxidation compared with their binary counterparts.[342,346−348]

Ethanol is the smallest alcohol containing a C−C bond. These bonds present a great challenge in the design of oxidation catalysts because they are strong and difficult to

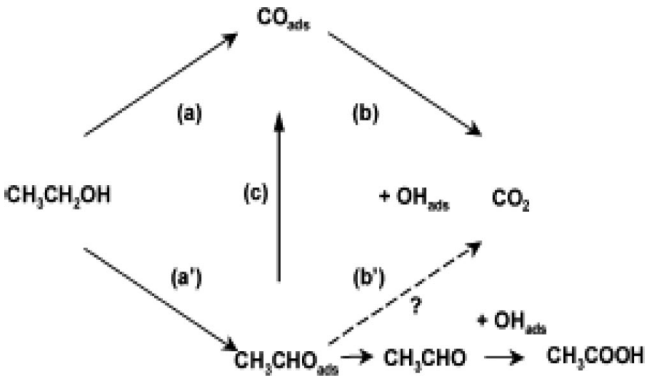

Figure 39. Ethanol oxidation mechanism. Reprinted from Léger, J.-M.; Rousseau, S.; Coutanceau, C.; Hahn, F.; Lamy, C. *Electrochim. Acta* **2005**, *50*, 5118. Copyright 2005 Elsevier.

break. Figure 39 shows the proposed schematic representation for the ethanol oxidation mechanism.[350] FTIR experiments reveal that the main pathways for Pt electrocatalysts are paths a and b, whereas PtRu and PtSn electrocatalysts favor the a′ and b′ pathways leading to the formation of acetic acid.[339,349,350] The key to unlocking the energy density of ethanol lies in the design of electrocatalysts that favor the reaction pathways that break the C−C bond, which results in the complete oxidation of ethanol.

Direct ethanol fuel cells have attracted considerable attention from researchers because they are much more compact in comparison to hydrogen PEMFCs. Ethanol offers several advantages over methanol as a fuel for direct alcohol fuel cells because it has higher theoretical energy density and lower toxicity. It also suffers from similar problems including decreased performance due to adsorbed CO intermediates and fuel crossover. The development of binary and ternary Pt-based nanomaterials with high electrocatalytic activity toward ethanol oxidation is promising for the future application of DEFCs as power sources for portable applications and automobiles.

4.5. Electrochemical Oxidation of Formic Acid

Formic acid is another attractive fuel for use in PEM-based fuel cells, such as direct formic acid fuel cells (DFAFC). In contrast to hydrogen, formic acid is liquid at room temperature and therefore much less hazardous to store and transport.[351] Although formic acid (2086 Wh L^{-1}) has a lower energy density than methanol (4690 Wh L^{-1}), DFAFCs are competitive with DMFCs. DFAFCs have a lower fuel crossover than DMFCs due to the repulsion between the sulfuric acid groups of Nafion and the formate anions, which enables the use of high concentrations of formic acid.[352] The low fuel crossover allows for the use of thinner membranes. This reduces the cost of DFAFCs, as well as allowing higher concentrations of formic to boost the energy density of the cell.[341] The mechanism for formic acid electro-oxidation on platinum surfaces involves dehydrogenation and dehydration pathways:

$$HCOOH \rightarrow CO_2 + 2H^+ + 2e^- \quad \text{(dehydrogenation path)}$$

$$HCOOH \rightarrow CO_{ads} + H_2O \rightarrow CO_2 + 2H^+ + 2e^- \quad \text{(dehydration path)}$$

The dehydrogenation pathway is preferred due to the complete oxidation of formic acid to CO_2 through the formation of adsorbed intermediates such as $COOH_{ads}$. The dehydration pathway produces adsorbed carbon monoxide, which requires higher electrode potentials to be oxidized to CO_2. Park et al.[353] compared the electrocatalytic activity of bulk Pt and Pt nanoparticle films toward formic acid oxidation. Figure 40 shows the CVs of the different Pt electrodes in different concentrations of formic acid. At high concentrations of formic acid, the negative going sweeps of the CV have much higher current densities, an indication that CO production was more extensive. The CVs also reveal that the smaller the particle size of the Pt nanoparticle films, the lower the onset potential for methanol oxidation and the higher the current densities.

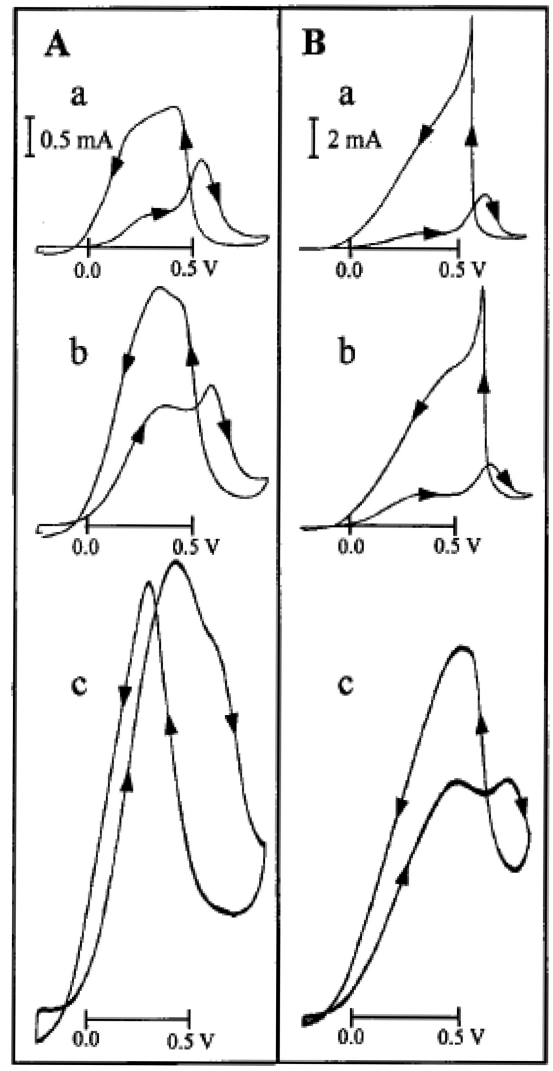

Figure 40. CVs of (a) polycrystalline Pt, (b) Pt nanoparticle (8.8 nm) film/C, (c) Pt nanoparticle (2.0 nm) film/C in (A) 10 mM and (B) 0.1 M formic acid + 0.05 M H_2SO_4. The current densities are normalized to the 1 cm^2 geometric surface area, which corresponds to a H adsorption/desportion charge of 240 $\mu C\ cm^{-2}$. Reprinted from ref 353. Copyright 2002 American Chemical Society.

A number of binary Pt-based nanomaterial electrocatalysts have been investigated for enhanced electrocatalytic activity toward formic acid oxidation including PtPd,[354−357] PtAu,[358] PtAg,[359] PtBi,[260] PtCo,[355] PtFe,[356] PtPd,[354,356,357] and PtPb.[260,360] Wang et al.[21] studied the electrocatalytic activity of nanoporous Pt, PtRu, PtIr, PtPd, and PtPb networks synthesized by a hydrothermal deposition technique toward formic acid oxidation. Figure 41 shows the electrocatalytic activity of the binary Pt-based electrocatalysts toward formic acid

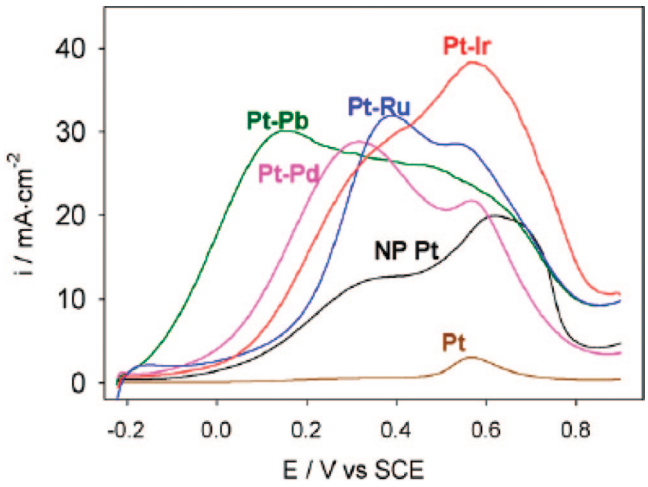

Figure 41. Forward sweep of CVs for nanoporous Pt electrodes in 0.1 M HCOOH+ 0.1 M H_2SO_4 at a potential scan rate of 20 mV s^{-1}. Reprinted from Wang, J.; Holt-Hindle, P.; MacDonald, D.; Thomas, D. F.; Chen, A. *Electrochim. Acta* **2008**, *53*, 6944. Copyright 2008 Elsevier.

electro-oxidation. The bulk Pt electrode displays small current densities at low electrode potentials since formic acid oxidation occurred mainly through the dehydration pathway. In contrast, the binary Pt-based electrocatalysts exhibit enhanced electrocatalytic activity toward formic acid oxidation throughout the potential range. Therefore, formic acid oxidation occurred on the nanoporous binary Pt-based electrocatalysts through both the dehydration and dehydrogenation pathways. Overall, the PtPb electrode had the best performance due to its high current density at low electrode potentials, indicating that the oxidation of formic acid occurred mainly via the preferential dehydrogenation route. Thus, the variation of the composition in bimetallic Pt-based electrocatalysts can tune the mechanism of formic acid oxidation and their resulting electrocatalytic activities.

Jayashree et al.[354] found that the addition of Pd significantly enhanced the power density of Pt-based electrocatalysts toward formic acid oxidation in DFAFCs. Figure 42 shows the power density and polarization curves for the Pt, Pd, and PtPd electrocatalysts prepared via electrodeposition. At cell potentials above 0.5 V, the PtPd has the highest current density and a power density over 6 times higher than that of the Pt electrocatalyst. Formic acid oxidation on Pd surfaces occurs by the dehydrogenation pathway where no CO species are formed. Thus, formic acid oxidation takes place at low potentials, which results in better cell performance. The enhanced cell performance of the PtPd electrocatalyst was attributed to a change in the mechanism of formic acid oxidation from the dehydration pathway for pure Pt electrocatalysts to both the dehydration and dehydrogenation pathways.

The composition of binary Pt-based nanomaterials plays a key role in the formic acid oxidation mechanism and thus the performance of the resulting fuel cell. DFAFCs offer several advantages over H_2 powered PEMFCs and DMFCs, including that the fuel is recognized as safe by the US Food and Drug Administration, has low temperature operation, ease of transport and storage of the fuel, and low fuel crossover.[351] These advantages make DFAFCs attractive candidates to replace batteries as the power sources for portable electronics in the future.

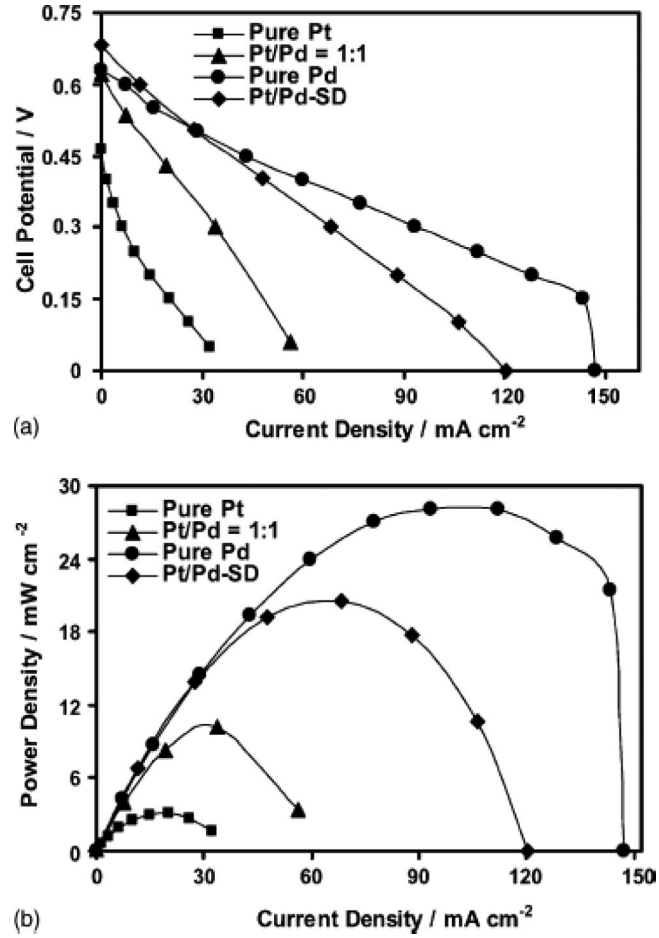

Figure 42. (a) Polarization and (b) power density graphs for the fuel cell testing of pure Pt, PtPd (1:1), PtPd-SD, and pure Pd electrocatalysts as anode and pure Pt as the cathode. The current densities correspond to the geometric surface area of the various electrodes. Reprinted from Jayashree, R. S.; Spendelow, J. S.; Yeom, J.; Rastogi, C.; Shannon, M. A.; Kenis, P. J. A. *Electrochim. Acta* **2005**, *50*, 4674. Copyright 2005 Elsevier.

4.6. Oxygen Reduction

The oxygen reduction reaction (ORR) has been widely investigated due to the application of oxygen cathodes in fuel cells. The electrocatalytic performance of the cathode is a key factor for optimizing the power output of fuel cells. Among the pure precious metals, platinum has the highest electrocatalytic activity toward oxygen reduction.[269] The ORR on Pt surfaces in aqueous solutions occurs via one of two mechanisms:

$$O_2 + 4H^+ + 4e^- \rightarrow 2H_2O$$

$$O_2 + 4H^+ + 2e^- \rightarrow H_2O_2 + 2H^+ + 2e^- \rightarrow 2H_2O$$

The direct four-electron reduction of oxygen to water is preferred due to its enhanced power generation;[361] also it avoids the generation of H_2O_2, which is corrosive toward the electrolyte membrane. The formation of intermediates such as O_{ads}, OH_{ads}, and O_2H_{ads} indicates that multiple reaction pathways exist.[361−363] The formation of intermediates on the electrode surface block O_2 adsorption sites, which reduce the performance of the electrocatalyst. The use of Pt and Pt-based nanomaterials as cathodes helps to inhibit the formation of adsorbed oxygenated species at potentials above

0.8 V and improve ORR kinetics via lower energy pathways.[362] For instance, Geniès et al.[364] studied the mechanism of the ORR on Pt nanoparticles of various sizes. The experiments revealed that as the particle size of the Pt nanoparticles decreased, the specific activity (current density related to real surface area) decreased by a factor of 3. The loss of activity may be related to stronger adsorption of the oxygenated species. Their experimental results also revealed that oxygen was reduced via the direct four-electron pathway on the Pt nanoparticles.

The commercialization of fuel cells is hindered by the high Pt loadings required to achieve the desired electrocatalytic activity toward ORR. Efforts to improve the electrocatalytic performance of Pt catalysts have focused on improving the catalytic effectiveness of Pt by dispersing catalyst materials onto an electrode support with high surface area or by forming Pt[362−368] and Pt-based nanomaterials.[369−381] Tang et al.[269] compared the electrocatalytic activity of Pt nanoparticles dispersed on CNT arrays and graphite substrates. Linear sweep voltammograms conducted on the electrocatalysts with low Pt loadings revealed that the peak current density of the Pt/CNT electrode was 1.4 times higher than the Pt/graphite electrode, despite having a lower Pt loading mass. At high Pt mass loadings, the Pt/CNT electrode had a peak current density two times higher than the Pt/graphite electrode. The high electrocatalytic activity of the Pt/CNT electrode toward the ORR could be attributed to either the structural and electrical properties of the CNTs or the high dispersion of the Pt nanoparticles on the CNTs. The linear relationship between E_p and $\log(\nu)$ was investigated using the formula:

$$E_p = A - [(2.3RT/(\alpha nF))(\log \upsilon)]$$

where A is a constant related to the formal electrode potential (E^0) and the standard rate constant at E^0, and α is the transfer coefficient, which describes the effect of potential on the activation energy of the reaction. The α values calculated for the Pt/CNT and Pt/graphite electrodes were 0.124 and 0.097, respectively. The values reveal that the ORR is irreversible and that the Pt/CNT electrode had lower activation energy for the reaction, implying that CNTs could have a positive effect on the kinetics of the reaction.

Kongkanand et al.[365] conducted similar experiments with Pt/SWCNT and commercial Pt/C (40 wt % Pt on Vulcan XC-72) electrodes. The Tafel plots shown in Figure 43 demonstrate that both electrodes have the same Tafel slopes, in the low current region where oxygen reduction occurs in the presence of hydroxyl species adsorbed to the Pt surface. However, the high current region reveals that the Pt/SWCNT electrode has a slightly higher Tafel slope than the commercial Pt/C catalyst. The enhanced activity of the Pt/SWCNT electrode toward oxygen reduction could be related to the high porosity of the nanotubes, which allows the diffusion of the reagents.

The electrocatalytic activity of various binary Pt-based electrocatalysts toward ORR have been investigated including PtAu,[379] PtCo,[369,371] PtCr,[372,373] PtCu,[369] PtFe,[369,378] PtFeO,[380] PtIr,[377] PtMoO,[381] PtNi,[369,370,374] PtRu,[375] PtTi,[376] PtTiO,[381] and PtW.[377] Xiong et al.[369] investigated the electrocatalytic activity of nanostructured PtCo, PtCu, PtFe, and PtNi alloyed catalysts toward the ORR. The galvanostatic-polarization curves in Figure 44 reveal that the nanostructured PtCu and PtCo electrocatalysts exhibit better performance and lower polarizations than Pt at current densities lower than 0.5 A cm^{-2}. The PtNi electrocatalyst also exhibits this trend but

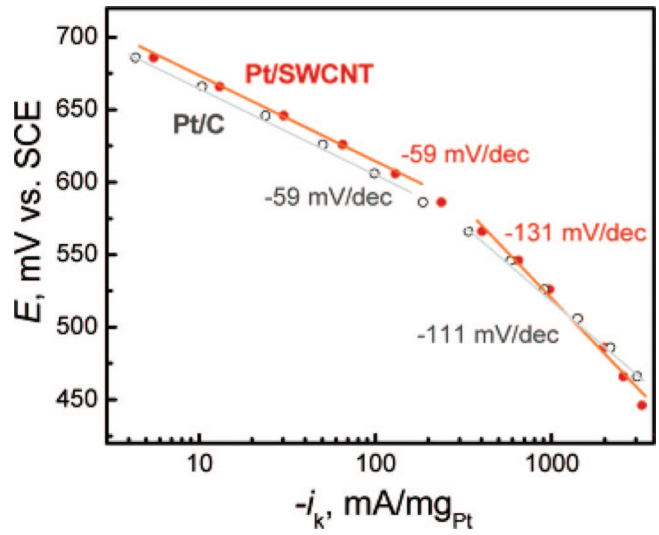

Figure 43. Tafel plots from the rotating disk voltammograms of Pt/SWCNT and Pt/C with the following conditions: O_2 saturated 0.1 M $HClO_4$ solution, temperature 24 °C, scan rate 20 mV s^{-1}, and rotation rate 1600 rpm. Reprinted from ref 365. Copyright 2006 American Chemical Society.

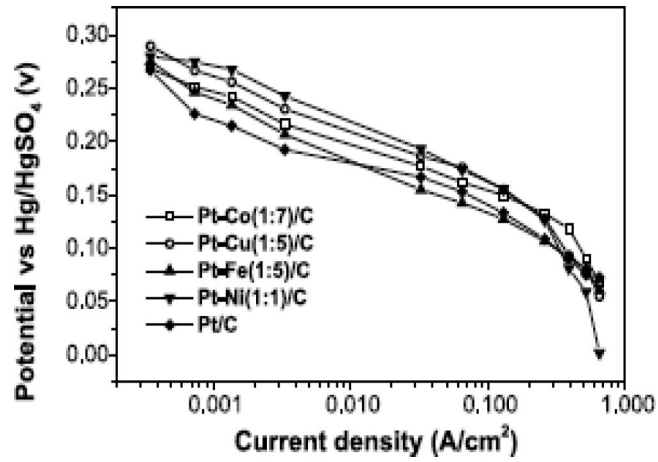

Figure 44. Galvanostatic-polarization curves of various Pt-based nanomaterials with catalyst loadings of 4.7 mg cm^{-2} in a 0.5 M H_2SO_4 solution at room temperature. Reprinted from Xiong, L.; Kannan, A. M.; Manthiram, A. *Electrochem. Commun.* **2002**, *4*, 898. Copyright 2002 Elsevier.

has the largest polarization at high current densities. Spectroscopic studies indicated that the enhanced electrocatalytic activity of the Pt alloy electrocatalysts could be due to changes in the Pt−Pt bond distances, Pt−Pt coordination numbers, or electron density in the Pt 5d orbitals or surface oxide layers.

In the case of DMFCs, the methanol crossover from the anode to the Pt-based cathode causes a considerable decrease in charge and voltage efficiencies. It is thus one of the key problems hindering the application of Pt-based cathodes in DMFCs. Efforts to reduce the effect of methanol crossover on the performance of DMFCs have focused on designing membranes that are less permeable to methanol and the development of novel Pt-based electrocatalysts with high methanol tolerance or inactivity toward methanol. Maillard et al.[366] found that a decrease in the size of Pt nanoparticles from 4.6 to 2.3 nm resulted in enhanced mass activity for ORR in the presence of methanol. In addition, synthesized PtCr nanosized electrocatalysts showed increased tolerance toward methanol competition during the ORR compared with

a Pt/C electrocatalyst. Similarly, Yang et al.[370] discovered that PtNi alloyed nanoparticles had considerably higher electrocatalytic activity toward ORR than Pt/C electrocatalysts. The high methanol tolerance of the PtNi electrocatalysts could be due to low activity of the catalyst toward methanol oxidation as a result of the disordered structure or the composition of the alloy electrocatalyst.

Several factors hinder the practical application of Pt-based cathodes in fuel cells, including Pt loading, reaction kinetics, and intermediates produced from the ORR and methanol tolerance. Researchers have confronted these challenges by investigating methods to improve the electrocatalytic performance of Pt-based nanomaterials through the design of Pt nanomaterials with small sizes, the dispersion of Pt-nanomaterials onto substrates with high surface area and good electronic properties and the development of bimetallic Pt-based nanomaterials. Significant progress in addressing these challenges is evident through the appearance of automobiles powered by fuel cells.

4.7. Glucose Detection

Despite the advances from over 40 years of development, enzymatic glucose sensors have drawbacks that originate from the nature of the enzyme. Temperature, chemical and thermal instabilities, pH, and humidity are all potentially damaging factors that can denature the enzymes and cause the loss of sensor activity.[382] The use of inert metals as electrocatalysts for glucose oxidation overcomes these problems. Thus the development of nonenzymatic catalysts for the electro-oxidation of glucose is of great interest for the development of biosensors for diabetic patients. Mechanistic studies of the electrochemical oxidation of α- and β-glucose on Pt surfaces in a neutral phosphate buffer solution indicate that glucono-δ-lactone is the product of the two-electron oxidation of glucose via dehydrogenation at the C1 carbon, which is hydrolyzed to form the final product, gluconic acid.[382] Several challenges hinder the practical application of Pt electrocatalysts in nonenzymatic glucose sensors, including the slow kinetics of glucose oxidation, which result in low sensitivity, the presence of adsorbed chloride ions and chemisorbed intermediates, which hinder the activity of Pt, and endogenous species, which can be oxidized in the same potential range as glucose causing poor selectivity.

Efforts to improve the catalytic activity of Pt have focused on dispersing nanoparticles onto CNTs[383−385] and fabricating high surface area Pt nanodendrites[386] and nanotubules or nanowire arrays.[169,387] For example, Yuan et al.[387] compared the electrocatalytic activity of bulk Pt and Pt nanotubule arrays fabricated with electrochemical deposition onto a modified alumina membrane. Figure 45 shows the amperometric response of the electrodes toward glucose and various endogenous species at 0.4 V vs SCE. The Pt nanotubule arrays exhibited a much higher current response to the successive additions of 2 mM glucose compared with the bulk Pt electrode. In addition, the Pt nanotubule arrays had a much lower current response to the additions of the endogenous species.

Subsequent investigations have sought to further improve the sensitivity and selectivity of the Pt nanomaterials by modifying Pt with Ir,[16] Bi,[388] WO_3,[389] Pb,[25,390,393] Au,[391,394] Ru,[392,393] Pd,[393] and Rh.[393] Wang et al.[25] synthesized nanoporous PtPb networks with different compositions and examined their sensitivity and selectivity toward glucose

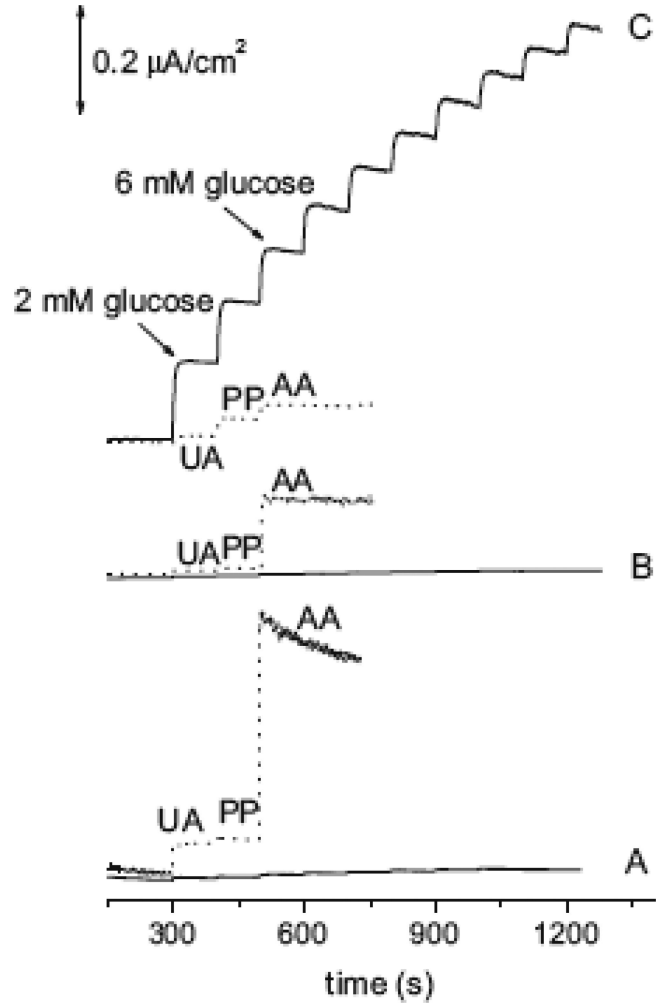

Figure 45. Amperometric response of (A) smooth Pt disk electrode (R_f = 30 A), (B) direct deposited Pt electrode (R_f = 183 A), and Pt nanotubule array electrode (R_f = 286 A) toward successive additions of 2 mM glucose or 0.02 mM UA, 0.1 mM PP, or 0.1 mM AA at 0.4 V vs SCE. All three electrodes had identical geometric surface areas of 0.1256 cm^2. Reprinted from Yuan, J.; Wang, K.; Xia, X. *Adv. Funct. Mater.* **2005**, *15*, 803. Copyright 2005 Wiley-VCH.

oxidation. A comparison of the amperometric responses of the various nanoporous PtPb networks toward successive 1 mM additions of glucose revealed that the PtPb (50:50) electrocatalyst had the best performance at −80 and +400 mV. The current response at −80 mV was much higher than that at +400 mV, which indicated a better sensitivity to glucose concentrations between 0 and 16 mM. Figure 46a presents the CVs of the nanoporous PtPb electrode recorded in a glucose solution and in a solution containing 5 mM ascorbic acid (AA), which is one of the most serious interfering agents. The onset of the ascorbic acid oxidation is at around −50 mV; the peak potential of glucose oxidation is −80 mV, which is 30 mV lower than the onset potential of ascorbic acid oxidation. This indicates that sensing glucose at −80 mV on the nanoporous PtPb electrode would successfully avoid the interfering current signal contributed from ascorbic acid. Given the high sensitivity of the nanoporous PtPb electrodes at −80 mV, their response toward successive additions of endogenous species and glucose was also investigated at −80 mV as seen in Figure 46b. At a potential of −80 mV the nanoporous PtPb networks exhibited no response to the endogenous species, for instance,

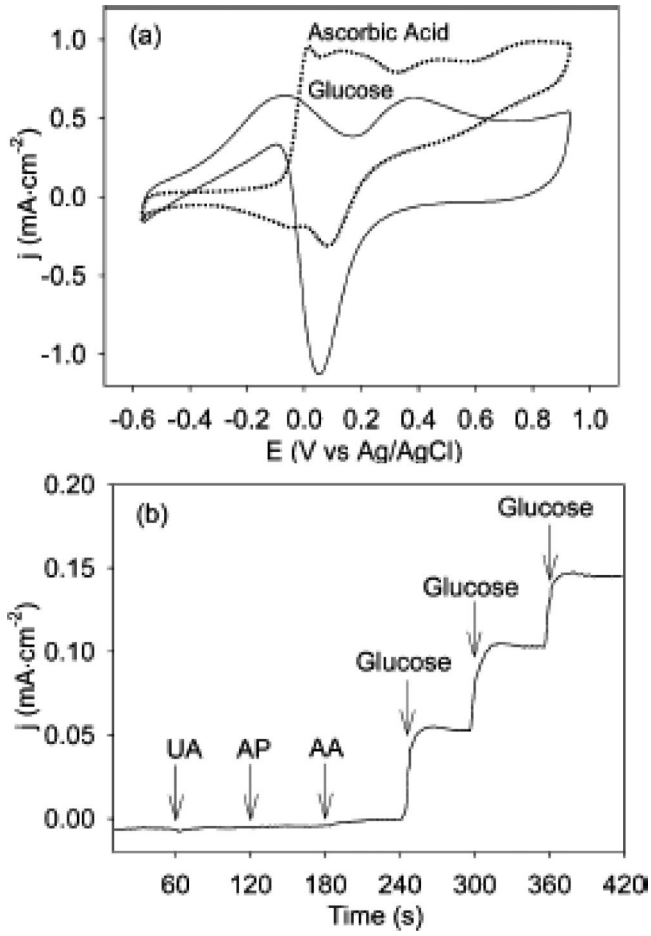

Figure 46. (a) CVs of the nanoporous PtPb (50:50) electrode in solution of 0.1 M phosphate buffer (pH 7.40), 0.15 M NaCl, and 5 mM ascorbic acid (dotted line) and 10 mM glucose (solid line), at a potential scan rate of 10 mV s^{-1}. (b) Amperometric response of the nanoporous PtPb (50:50) electrode toward successive additions of 0.02 mM UA, 0.1 mM AP, 0.1 mM AA, and 1 mM glucose at 60 s intervals in a 0.1 M phosphate buffer solution (pH 7.4) at −80 mV. Reprinted from ref 25. Copyright 2008 American Chemical Society.

AA, uric acid (UA) and 4-acetamidophenol (AP), and a good current response upon successive additions of glucose. Overall the PtPb electrocatalysts had good sensitivity and selectivity toward glucose and remarkable tolerance toward the common interfering species of AA, AP, and UA.

Nonenzymatic glucose sensors with Pt-based electrocatalysts offer several advantages over enzymatic glucose sensors, including high stability and ease of fabrication. Many novel Pt and binary Pt-based nanomaterials have been developed to overcome the challenges of glucose oxidation on Pt surfaces, such as low selectivity, poor sensitivity, and poisoning from interfering species.

4.8. Other Applications

Besides the key electrocatalytic role they serve in fuel cells and glucose sensors, platinum catalysts are important components of automotive catalytic converters, CO gas sensors, petroleum refining, hydrogen production, and anticancer drugs. These applications utilize platinum nanomaterials due to their catalytic ability to oxidize CO and NO_x, dehydrogenate hydrocarbons, and electrolyze water and their ability to inhibit the division of living cells.

Carbon monoxide is a colorless and odorless gas produced via the incomplete combustion of fossil fuels. CO can inhibit the human body's capacity to transport oxygen by combining with hemoglobin in blood. Thus, CO is capable of causing health problems such as headaches, nausea, and death. The US Environmental Protection Agency reports that CO exposure over 35 ppm for longer than one hour is dangerous. Therefore portable devices are needed to monitor CO pollution. CO monitoring devices require high stability and low detection limits. Electrochemical gas sensors employing platinum catalysts have low power requirements, quick response, high sensitivity, high stability, and linear ouput. The formation of oxygenated species at Pt sites on the electrode surface aids in the oxidation of CO to CO_2. While bulk Pt electrodes show modest CO oxidation characteristics at low concentrations, electrodes synthesized with Pt nanomaterials show enhanced electrocatalytic activity toward CO oxidation. The enhanced activity of nanostructured Pt electrodes toward CO oxidation can be attributed to the higher electroactive surface area of Pt nanomaterials, which have more Pt sites available to form oxygenated species.[395,396] In the future, the development of electrochemical CO gas sensors with binary Pt-based nanostructured electrodes may help to increase sensitivity and decrease the production costs via increased Pt utilization and decreased Pt loading.

Automotive pollution control systems use catalysts containing Pt, Pd, and Rh to oxidize carbon monoxide and hydrocarbons and reduce oxides of nitrogen. In 2005, this application accounted for 50% of the platinum-group metal (PGM) usage in the world. Stricter emission standards and increased demand for vehicles in developing nations are expected to increase the usage of PGM metals in the future. A test of a new automotive catalytic converter by General Motors revealed that only 50% of PGM metals are exposed to a vehicle's exhaust gases and the dispersion decreases significantly during the life of the catalytic converter to below 5% after 25 000 miles. The deterioration was the result of particle agglomeration and sintering due to exposure to high temperatures and vehicular vibrations. Current emission standards require the participation of just 5% of PGM in catalytic reactions during 80% of a vehicle's life. Employing precise fabrication techniques to synthesize well-dispersed, efficient, and highly stable Pt nanomaterials could help to significantly reduce Pt loading and meet the increasingly stringent emission standards of the future.[397] The use of smart nanostructured Pt catalysts, which are rejuvenated back into active state through a self-regeneration function, may also help to reduce the usage of PGM metals and prevent the deterioration of catalyst performance over a vehicle's life.[398]

The appearance of hydrogen infrastructure and fuel cell powered automobiles in the US suggests that demand for hydrogen will increase substantially in the future. The most common method used to produce hydrogen is a multistep process involving the production of synthesis gas and its subsequent conversion to CO_2 and H_2. This method produces a small amount of residual CO, which hinders the performance of the hydrogen-powered PEMFCs. Pure hydrogen can be produced by two processes employing nanostructured Pt catalysts, the electrolysis of water and a direct one-step process involving the nonoxidative catalytic decomposition of hydrocarbons. Wang et al.[399] found that 0.1−1 wt % Pt nanoparticles dispersed on stacked-cone carbon nanotubes (SC-CNT) showed 100% selectivity for the dehydrogenation of methylcyclohexane to hydrogen and toluene and cyclo-

hexane to hydrogen and benzene. The activity of the 0.25 wt % Pt/SC-CNT catalyst was almost identical to a commercial 1% Pt/Al_2O_3 catalyst, which demonstrated the high Pt utilization of the as-synthesized electrocatalysts. Yoshida et al.[400] employed Pt/TiO_2 catalysts to produce hydrogen gas via the photocatalytic steam reforming of methane. The reaction was initiated using UV light produced from a 300 W xenon lamp at room temperature. Only 0.1 wt % Pt was needed for the photocatalyst to exhibit high activity. The role of Pt in the photocatalyst was to prevent the separation of the photoexcited electrons and holes, preventing their recombination. Nanostructured Pt-based electrocatalysts synthesized by Petrik et al.[401] showed high stability and activity toward hydrogen evolution comparable to commercial Johnson Matthey Pt/C electrocatalysts.

Platinum nanomaterials play a key role in the production of gasoline, through their catalysis of reforming and isomerization processes used to create higher octane components for gasoline. Cyclic hydrocarbons such as cyclohexane and cyclohexene undergo platinum-catalyzed dehydrogenation reactions to form benzene, which is used to blend higher octane gasoline.[402,403] Extensive research into these reactions has revealed the effect of symmetry, particle size, and temperature on the performance of the Pt catalysts.[404,405] While platinum catalysts are normally less than 1.3 wt %, bimetallic Pt-based catalysts such as PtSn help to improve performance and decrease the Pt loading requirements.[406,407]

Platinum is inert and does not corrode inside the human body, and it has certain forms that inhibit division in living cells. These properties have led to the development of Pt-based nanomaterials for biomedical applications. The most well-known platinum-based drug for cancer treatment is *cis*-diamminedichloroplatinum (cisplatin). It is used to treat testicular and ovarian cancer and has annual sales worth almost 500 million US dollars.[408] The application of bimetallic Pt-based nanoparticles is more prevalent than pure Pt nanoparticles.[409] For instance, yolk−shell $PtFe@CoS_2$ nanocrystals synthesized by Gao et al.[410] demonstrated much lower IC_{50} (concentration needed to inhibit cell growth by 50% versus control) compared with cisplatin. Overall, the use of nanoscale drugs for biomedical applications has several advantages over small molecule based drugs, such as lower toxicity, increased accumulation in the target tissue, and a surface functionalization capacity with targeting and passivating moieties.[410,411]

Aside from fuel cells, catalytic converters, petroleum refining, hydrogen production, anticancer drugs, and sensors, in the future, the development of innovative synthesis techniques will undoubtedly lead to the discovery of more unique properties of Pt-based nanomaterials and applications that have the potential to be beneficial for society and industry alike.

5. Conclusions and Future Outlook

This review has described the common methods of synthesizing Pt and Pt-based nanostructured materials including the sol−gel method, electrodeposition, electroless deposition, and physical methods as well as hydrothermal and solvothermal techniques. The properties section examined the influence of composition and morphology of the Pt and Pt-based nanomaterials on their catalytic, magnetic, and optical properties. The applications section discussed the catalytic properties of Pt and Pt-based nanomaterials toward applications such as fuel cells, biosensors, chemical sensors, automotive catalytic converters, petroleum refining, hydrogen production, and anticancer drugs. In light of the rarity and price of platinum, researchers have made significant strides toward reducing Pt loading in these applications by design and synthesis of Pt-based nanomaterials. The use of diverse synthesis techniques to tune the properties of Pt-based nanomaterials will continue to play a vital role in improving existing technologies and discovering new applications.

The future of platinum nanomaterials involves a mixture of challenges and opportunities. The threat of climate change and decreasing reserves of natural resources has driven the search for economical and environmentally sustainable energy conversion processes. Fuel cells are at the forefront of this quest, which presents researchers with the key challenges of increasing Pt efficiency and decreasing Pt loading in fuel cell catalysts. Future progress in this area hinges on enhancing our understanding of how synthesis techniques, composition, and morphology affect the catalytic activity of Pt-based nanomaterials. The development of novel and improved synthesis methods that allow precise control over product morphology and composition will undoubtedly present the opportunity to decrease the cost and improve the performance of Pt-based catalysts in applications such as nonenzymatic glucose sensors and automotive catalytic converters. In addition, as greater knowledge is acquired about the properties of Pt-based nanomaterials, there will be more opportunities to exploit individual characteristics in magnetic and optical based applications. Certainly the development of novel Pt and Pt-based nanomaterials will help to improve existing technologies, and further research will produce innovations that will benefit industries and society.

6. Acknowledgments

This work was supported by a Discovery Grant from the Natural Sciences and Engineering Research Council of Canada (NSERC). A. Chen acknowledges NSERC and the Canada Foundation of Innovation (CFI) for the Canada Research Chair Award in Material and Environmental Chemistry.

7. References

(1) Shao, Y.; Liu, J.; Wang, Y.; Lin, Y. *J. Mater. Chem.* **2009**, *19*, 46.
(2) Liu, H.; Song, C.; Zhang, L.; Zhang, J.; Wang, H.; Wilkinson, P. *J. Power Sources* **2006**, *155*, 95.
(3) Tian, N.; Zhou, Z.-Y.; Sun, S.-G. *J. Phys. Chem. C* **2008**, *112*, 19801.
(4) Shiju, N. R.; Guliants, V. V. *Appl. Catal., A* **2009**, *356*, 1.
(5) (a) Subhramannia, M.; Pillai, V. K. *J. Mater. Chem.* **2008**, *18*, 5858. (b) Liao, S.; Holmes, K.; Tsaprailis, H.; Birss, V. I. *J. Am. Chem. Soc.* **2006**, *128*, 3504.
(6) Rigsby, M. A.; Zhou, W. P.; Lewera, A.; Duong, H. T.; Bagus, P. S.; Jaegermann, W.; Hunger, R.; Wieckowski, A. *J. Phys. Chem. C* **2008**, *112*, 15595.
(7) (a) Hu, X.; Dong, S. *J. Mater. Chem.* **2008**, *18*, 1279. (b) Koczkur, K.; Yi, Q.; Chen, A. *Adv. Mater.* **2007**, *19*, 2648. (c) Peng, X.; Koczkur, K.; Chen, A. *Nanotechnology* **2007**, *18*, 305605.
(8) Peng, Z. M.; Yang, H. *Nano Today* **2009**, *4*, 143.
(9) (a) Manthiram, A.; Murugan, A. V.; Sarkar, A.; Muraliganth, T. *Energy Environ. Sci.* **2008**, *1*, 621. (b) Antolini, E. *Appl. Catal., B* **2007**, *94*, 324.
(10) (a) Ahmadi, T. S.; Wang, Z. L.; Green, T. C.; Henglein, A.; El-Sayed, M. A. *Science* **1996**, *272*, 1924. (b) Burda, C.; Chen, X.; Narayanan, R.; El-Sayed, M. A. *Chem. Rev.* **2005**, *105*, 1025. (c) Narayanan, R.; El-Sayed, M. A. *J. Phys. Chem. B* **2005**, *109*, 12663. (d) Liao, H.-G.; Jiang, Y.-X.; Zhou, Z.-Y.; Chen, S.-P.; Sun, S.-G. *Angew. Chem., Int. Ed.* **2008**, *47*, 9100. (e) Zhou, Z. Y.; Tian, N.; Huang, Z. Z.; Chen, D. J.; Sun, S.-G. *Faraday Discuss.* **2008**, *140*, 81.
(11) Masala, O.; Seshadri, R. *Annu. Rev. Mater. Res.* **2004**, *34*, 41.

(12) Demazeau, G. *J. Mater. Sci.* **2008**, *43*, 2104.
(13) Byrappa, K.; Adschiri, T. *Prog. Cryst. Growth Charact. Mater.* **2007**, *53*, 117.
(14) Yi, Q.; Li, L.; Yu, W.; Zhou, Z.; Liu, X.; Xu, G. *J. Alloys Compd.* **2008**, *466*, 52.
(15) Holt-Hindle, P.; Yi, Q.; Wu, G.; Koczkur, K.; Chen, A. *J. Electrochem. Soc.* **2008**, *155*, K5.
(16) Holt-Hindle, P.; Nigro, S.; Asmussen, M.; Chen, A. *Electrochem. Commun.* **2008**, *10*, 1438.
(17) Wang, J.; Thomas, D. F.; Chen, A. *Chem. Commun.* **2008**, 5010.
(18) Hong, D. U.; Han, C.-H.; Park, S. H.; Kim, I.-J.; Gwak, J.; Han, S.-D.; Kim, H. J. *Curr. Appl. Phys.* **2009**, *9*, 172.
(19) Yi, Q.; Huang, W.; Liu, X.; Xu, G.; Zhou, Z.; Chen, A. *J. Electroanal. Chem.* **2008**, *197*, 619.
(20) Lepró, X.; Terrés, E.; Vega-Cantú, Y.; Rodríguez-Macías, F. J.; Muramatsu, H.; Kim, Y. A.; Hayahsi, T.; Endo, M.; Torres, M. R.; Terrones, M. *Chem. Phys. Lett.* **2008**, *463*, 124.
(21) Wang, J.; Holt-Hindle, P.; MacDonald, D.; Thomas, D. F.; Chen, A. *Electrochim. Acta* **2008**, *53*, 6944.
(22) Chen, L.; Lu, G. *Electrochim. Acta* **2008**, *53*, 4316.
(23) Yi, Q.; Zhang, J.; Chen, A.; Liu, X.; Xu, G.; Zhou, Z. *J. Appl. Electrochem.* **2008**, *38*, 695.
(24) Zheng, L.; Xiong, L.; Sun, J.; Li, J.; Yang, S.; Xia, J. *Catal. Commun.* **2008**, *9*, 624.
(25) Wang, J.; Thomas, D. F.; Chen, A. *Anal. Chem.* **2008**, *80*, 997.
(26) Han, C.-H.; Hong, D.-W.; Kim, I.-J.; Gwak, J.; Han, S.-D.; Singh, K. C. *Sens. Actuators, B* **2007**, *128*, 320.
(27) Yi, Q.; Chen, A.; Huang, W.; Zhang, J.; Liu, X.; Xu, G.; Zhou, Z. *Electrochem. Commun.* **2007**, *9*, 1513.
(28) Peng, X.; Koczkur, K.; Nigro, S.; Chen, A. *Chem. Commun.* **2004**, 2872.
(29) Chen, H.; Wang, Y.; Dong, S. *Inorg. Chem.* **2007**, *46*, 10587.
(30) Zhang, Z.; Blom, D. A.; Gai, Z.; Thompson, J. R.; Shen, J.; Dai, S. *J. Am. Chem. Soc.* **2003**, *125*, 7528.
(31) Hou, Y.; Kondoh, H.; Che, R.; Takeguchi, M.; Ohta, T. *Small* **2006**, *2*, 235.
(32) Wen, M.; Qi, H.; Zhao, W.; Chen, J.; Li, L.; Wu, Q. *Colloids Surf., A* **2008**, *312*, 73.
(33) Schubert, U. *J. Chem. Soc., Dalton Trans.* **1996**, 3343.
(34) Hench, L. L.; West, J. K. *Chem. Rev.* **1990**, *90*, 33.
(35) Lembacher, C.; Schubert, U. *New J. Chem.* **1998**, 721.
(36) Breitscheidel, B.; Zieder, J.; Schubert, U. *Chem. Mater.* **1991**, *3*, 559.
(37) Shiga, H.; Okubo, T.; Sadakata, M. *Ind. Eng. Chem. Res.* **1996**, *35*, 4479.
(38) Hippe, C.; Wark, M.; Lork, E.; Schulz-Ekloff, G. *Microporous Mesoporous Mater.* **1991**, *31*, 235.
(39) Facchin, G.; Caruran, G.; Campostrini, R.; Gialanella, S.; Lutterotti, L.; Armelao, L.; Marcí, G.; Palmisano, L.; Sclafani, A. *J. Sol-Gel Sci. Technol.* **2000**, *18*, 29.
(40) Bae, D.; Han, K.; Adair, J. H. *J. Am. Ceram. Soc.* **2002**, *85*, 1321.
(41) Yu, K. M. K.; Thompsett, D.; Tsang, S. C. *Chem. Commun.* **2003**, 1522.
(42) Yang, M.; Yang, Y.; Liu, Y.; Shen, G.; Yu, R. *Biosens. Bioelectron.* **2006**, *21*, 1125.
(43) Kang, X.; Mai, Z.; Zou, X.; Cai, P.; Mo, J. *Talanta* **2008**, *74*, 879.
(44) Hippe, C.; Lamber, R.; Schulz-Ekloff, G.; Schubert, U. *Catal. Lett.* **1997**, *43*, 195.
(45) Hu, L.; Boateng, K. A.; Hill, J. M. *J. Mol. Catal. A: Chem.* **2006**, *259*, 51.
(46) Malenovska, M.; Martinez, S.; Neouze, M.; Schubert, U. *Eur. J. Inorg. Chem.* **2007**, 2609.
(47) Jena, B. K.; Raj, C. R. *J. Phys. Chem. C* **2008**, *112*, 3496.
(48) Suffredini, H. B.; Tricoli, V.; Vatistas, N.; Avac, L. A. *J. Power Sources* **2006**, *158*, 124.
(49) Beakley, L. W.; Yost, S. E.; Cheng, R.; Chandler, B. D. *Appl. Catal., A* **2005**, *292*, 124.
(50) Kim, J. Y.; Yang, Z. G.; Chang, C.-C.; Valdez, T. I.; Narayanan, S. R.; Kumta, P. N. *J. Electrochem. Soc.* **2003**, *150*, A1421.
(51) Sault, A. G.; Jeffrey, A. M.; Kawola, S.; Boespflug, E. *J. Catal.* **2000**, *191*, 474.
(52) Kim, H.; Kim, W.; Park, T.; Park, H.; Suh, D. J. *Carbon* **2008**, *46*, 1393.
(53) Courtheou, L.; Popa, F.; Gautron, E.; Rossignol, S.; Kappenstein, C. *J. Non-Cryst. Solids* **2004**, *350*, 113.
(54) Balakrishnan, K.; Gonzalez, R. D. *Langmuir* **1994**, *10*, 2487.
(55) Bass, R. J.; Dunn, T. M.; Lin, Y.; Hohn, K. L. *Ind. Eng. Chem. Res.* **2008**, *47*, 7184.
(56) Anders, A. *J. Phys. D: Appl. Phys.* **2007**, *40*, 2272.
(57) Wee, J.; Lee, K.; Kim, S. H. *J. Power Sources* **2007**, *165*, 667.
(58) Taguchi, A.; Inoue, M.; Hiromi, C.; Tanizawa, M.; Kitami, T.; Abe, T. *Vacuum* **2008**, *83*, 575.
(59) Rabat, H.; Andreazza, C.; Brault, P.; Caillard, A.; Béguin, F.; Charles, C.; Boswell, R. *Carbon* **2009**, *47*, 209.
(60) You, T.; Niwa, O.; Horiuchi, T.; Tomita, M.; Iwasaki, Y.; Ueno, Y.; Hirono, S. *Chem. Mater.* **2002**, *14*, 4796.
(61) Miyauchi, M. *Phys. Chem. Chem. Phys.* **2008**, *10*, 6258.
(62) Kang, S. H.; Sung, Y.; Smyrl, W. H. *J. Electrochem. Soc.* **2008**, *155*, B1128.
(63) Rabat, H.; Andreazza, C.; Brault, P.; Thomann, A.; Cavarroc, M.; Tessier, Y.; Caillard, A.; Charles, C.; Boswell, R. W. *IEEE Trans. Plasma Sci.* **2008**, *36*, 872.
(64) Caillard, A.; Charles, C.; Boswell, R.; Brault, P. *J. Phys. D: Appl. Phys.* **2008**, *41*, 185307.
(65) Lee, W.; Alhosan, M.; Yohe, S. L.; Macy, N. L.; Smyrl, W. H. *J. Electrochem. Soc.* **2009**, *155*, B915.
(66) Wang, H.; Zhang, M.; Cheng, F.; Xu, C. *Int. J. Electrochem. Sci.* **2008**, *3*, 946.
(67) Kim, H.; Lee, J.; Kim, J. *J Power Sources* **2008**, *180*, 191.
(68) Rabat, H.; Brault, P. *Fuel Cells* **2008**, *2*, 81.
(69) Yoo, S. J.; Cho, Y.; Park, H.; Lee, J. K.; Sung, Y. *J. Power Sources* **2008**, *178*, 547.
(70) Yamamoto, H.; Hirakawa, K.; Abe, T. *Mater. Lett.* **2008**, *62*, 2118.
(71) O'Hare, R.; Lee, S.; Cha, S.; Prinz, F. B. *J. Power Sources* **2002**, *109*, 483.
(72) Wan, C.; Zhuang, Q. *Int. J. Hydrogen Energy* **2007**, *32*, 4402.
(73) Park, K.; Song, Y.; Lee, J.; Han, S. *Electrochem. Commun.* **2007**, *9*, 2111.
(74) Park, K.; Han, S.; Lee, J. *Electrochem. Commun.* **2007**, *9*, 1578.
(75) Caillard, A.; Charles, C.; Boswell, R.; Brault, P. *Nanotechnology* **2007**, *18*, 305603.
(76) Zacharia, R.; Rather, S.-U.; Hwang, S. W.; Nahm, K. S. *Chem. Phys. Lett.* **2007**, *434*, 286.
(77) Baranov, A.; Fanchenko, S.; Calliari, L.; Speranza, G.; Minati, L.; Kharitonov, S.; Fedoseenkov, D.; Shorokhov, A.; Nefedov, A. *Surf. Interface Anal.* **2006**, *38*, 823.
(78) Park, K.; Sung, Y.; Toney, M. F. *Electrochem. Commun.* **2006**, *83*, 59.
(79) Alvisi, M.; Galtieri, G.; Giorgi, L.; Giorgi, R.; Serra, E.; Signore, M. A. *Surf. Coat. Technol.* **2005**, *200*, 1325.
(80) Caillard, A.; Brault, P.; Mathias, T. J.; Charles, C.; Boswell, R. W.; Sauvage, T. *Surf. Coat. Technol.* **2005**, *200*, 391.
(81) Brault, P.; Caillard, A.; Thomann, A. L.; Mathias, J.; Charles, C.; Boswell, R. W.; Escribano, S.; Durand, J.; Sauvage, T. *J. Phys. D: Appl. Phys.* **2004**, *37*, 3419.
(82) Bonakdarpour, A.; Wenzel, J.; Stevens, D. A.; Sheng, S.; Monchesky, T. L.; Lobel, R.; Atanasoski, R. T.; Schmoeckel, A. K.; Vernstrom, G. D.; Debe, M. K.; Dahn, J. R. *J. Electrochem. Soc.* **2005**, *152*, A61.
(83) Xiu, Y. K.; Nakagawa, N. *J. Electrochem. Soc.* **2004**, *151*, A1483.
(84) Serventi, A. M.; Rickerby, D. G.; Horrillo, M. C.; Saint-Jacques, R. G. *Thin Solid Films* **2003**, *445*, 38.
(85) Xu, Y.; Sun, Z. G.; Qiang, Y.; Sellmyer, D. J. *J. Magn. Magn. Mater.* **2003**, *266*, 164.
(86) Matsumiya, M.; Shin, W.; Izu, N.; Murayama, N. *Sens. Actuators, B* **2003**, *93*, 309.
(87) Plank, H.; Gspan, C.; Dienstleder, M.; Kothleitner, G.; Hofer, F. *Nanotechnology* **2008**, *19*, 485302.
(88) Liao, Z.; Xu, J.; Zhang, X.; Yu, D. *Nanotechnology* **2008**, *19*, 305402.
(89) Reguer, A. F.; Bedu, F.; Tonneau, D.; Dallaporta, H.; Prestigiacomo, M.; Houel, A.; Sudraud, P. *J. Vac. Sci. Technol. B* **2008**, *26*, 175.
(90) Inkson, B. J.; Dehm, G.; Peng, Y. *Nanotechnology* **2007**, *18*, 415601.
(91) Langford, R. M.; Wang, T.-X.; Ozkaya, D. *Microelectron. Eng.* **2007**, *84*, 784.
(92) Penate-Quesada, L.; Mitra, J.; Dawson, P. *Nanotechnology* **2007**, *18*, 215203.
(93) Barry, J. D.; Ervin, M.; Molstad, J.; Wickenden, A.; Brintlinger, T.; Hoffman, P.; Meingailisa, J. *J. Vac. Sci. Technol. B* **2006**, *24*, 3165.
(94) Hannour, A.; Bardotti, L.; Prevel, B.; Bernstein, E.; Melinon, P.; Perez, A.; Gierak, J.; Bourhis, E.; Mailly, D. *Surf. Sci.* **2005**, *594*, 1.
(95) Withrow, S. P.; White, C. W.; Budai, J. D.; Boatner, L. A.; Sorge, K. D.; Thompson, J. R.; Kalyanaraman, R. *J. Magn. Magn. Mater.* **2003**, *260*, 319.
(96) Eppler, A. S.; Zhu, J.; Anderson, E. A.; Somorjai, G. A. *Top. Catal.* **2000**, *13*, 33.
(97) Hu, X.; Cahill, D. G.; Averback, R. S. *Appl. Phys. Lett.* **2000**, *76*, 3215.
(98) Frabboni, S.; Gazzadi, G. C.; Felisari, L.; Spessot, A. *Appl. Phys. Lett.* **2006**, *88*, 213116.
(99) Bommersbach, P.; Chaker, M.; Mohamedi, M.; Guay, D. *J. Phys. Chem. C* **2008**, *112*, 14672.
(100) Rakshit, R. K.; Bose, S. K.; Sharma, R.; Budhani, R. C.; Vijaykumar, T.; Neena, S. J.; Kulkarni, G. U. *J. Appl. Phys.* **2008**, *103*, 023915.
(101) Kawabata, S.; Naono, Y.; Taguchi, Y.; Huh, S. H.; Nakajima, A. *Appl. Surf. Sci.* **2007**, *253*, 6690.

(102) Dobrynin, A. N.; Ievlev, D. N.; Verschoren, G.; Swerts, J.; Van Bael, M. J.; Temst, K.; Lievens, P.; Piscopiello, E.; Van Tendeloo, G.; Zhou, S. Q.; Vantomme, A. *Phys. Rev. B* **2006**, *73*, 104421.
(103) Dolbec, R.; Irissou, E.; Chaker, M.; Guay, D.; Rosei, F.; El Khakani, M. A. *Phys. Rev. B* **2004**, *70*, 201406.
(104) Serventi, A. M.; Dolbec, R.; El Khakani, M. A.; Saint-Jacques, R. G.; Rickerby, D. G. *J. Phys. Chem. Solids* **2003**, *64*, 2097.
(105) Leuchtner, R. E.; Horwitz, J. S.; Chrisey, D. B. *J. Appl. Phys.* **1998**, *83*, 5477.
(106) Nichols, W. T.; Sasaki, T.; Koshizakia, N. *J. Appl. Phys.* **2006**, *100*, 114913.
(107) Deivaraj, T. C.; Chen, W.; Lee, J. Y. *J. Mater. Chem.* **2003**, *13*, 2555.
(108) Fukuoka, A.; Higashimoto, N.; Sakamoto, Y.; Inagaki, S.; Fukushima, Y.; Ichikawa, M. *Microporous Mesoporous Mater.* **2001**, *48*, 171.
(109) Caruso, R. A.; Ashokkumar, M.; Grieser, F. *Colloids Surf., A* **2000**, *169*, 219.
(110) Park, J.-E.; Atobe, M.; Fuchigami, T. *Electrochim. Acta* **2005**, *51*, 849.
(111) Mallikarjuna, N. N.; Varma, R. S. *Cryst. Growth Des.* **2007**, *7*, 686.
(112) Perkas, N.; Minh, D. P.; Gallezot, P.; Gedanken, A.; Besson, M. *Appl. Catal., B* **2005**, *59*, 121.
(113) Remita, H.; Keita, B.; Torigoe, K.; Belloni, J.; Nadjo, L. *Surf. Sci.* **2004**, *572*, 301.
(114) Mafuné, F.; Kondow, T. *Chem. Phys. Lett.* **2004**, *383*, 343.
(115) Ng, Y. H.; Ikeda, S.; Harada, T.; Park, S.; Sakata, T.; Mori, H.; Matsumura, M. *Chem. Mater.* **2008**, *20*, 1154.
(116) Luo, X.; Imae, T. *J. Mater. Chem.* **2007**, *17*, 567.
(117) Kapoor, S.; Palit, D.; Mukherjee, T. *Chem. Phys. Lett.* **2001**, *349*, 19.
(118) Harada, M.; Okamoto, K.; Terazima, M. *Langmuir* **2006**, *22*, 9142.
(119) Oh, S.-D.; Yoon, K. R.; Choi, S.-H.; Gopalan, A.; Lee, K.-P.; Sohn, S.-H.; Kang, H.-D.; Choi, I. S. *J. Non-Cryst. Solids* **2006**, *352*, 355.
(120) Wang, H.; Sun, X.; Ye, Y.; Qiu, S. *J. Power Sources* **2006**, *161*, 839.
(121) Oh, S.-D.; Kim, M.-R.; Choi, S.-H.; Chun, J.-H.; Lee, K.-P.; Gopalan, A.; Hwang, C.-G.; Sang-Ho, K.; Hoon, O. J. *J. Ind. Eng. Chem.* **2008**, *14*, 687.
(122) Ozkaraoglu, E.; Tunc, I.; Suzer, S. *Polymer* **2009**, *50*, 462.
(123) Shironita, S.; Mori, K.; Shimizu, T.; Ohmichi, T.; Mimura, N.; Yamashita, H. *Appl. Surf. Sci.* **2008**, *254*, 7604.
(124) Lee, K.; Zhang, J.; Wang, H.; Wilkinson, D. *J. Appl. Electrochem.* **2006**, *36*, 507.
(125) Tiwari, J. N.; Pan, F.-M.; Tiwari, R. N.; Nandi, S. K. *Chem. Commun.* **2008**, 6516.
(126) Zhong, Y.; Xu, C.-L.; Kong, L.-B.; Li, H.-L. *Appl. Surf. Sci.* **2008**, *255*, 3388.
(127) Saejeng, Y.; Tantavichet, N. *J. Appl. Electrochem.* **2009**, *39*, 123.
(128) Rajalakshmi, N.; Dhathathreyan, K. S. *Int. J. Hydrogen Energy* **2008**, *33*, 5672.
(129) Nagle, L. C.; Rohan, J. F. *J. Power Sources* **2008**, *185*, 411.
(130) Liu, F.-J.; Huang, L.-M.; Wen, T.-C.; Li, C.-F.; Huang, S.-L.; Gopalan, A. *Synth. Met.* **2008**, *158*, 603.
(131) Paoletti, C.; Cemmia, A.; Leonardo Giorgi, L.; Giorgi, R.; Pilloni, L.; Serra, E.; Pasquali, M. *J. Power Sources* **2008**, *18*, 84.
(132) Song, Y.-J.; Oh, J.-K.; Park, K.-W. *Nanotechnology* **2008**, *19*, 355602.
(133) Tsai, Y.-C.; Hong, Y.-H. *J. Solid State Electrochem.* **2008**, *12*, 1293.
(134) Zhang, L.; Fang, Z.; Zhao, G.-C.; Wei, X.-W. *Int. J. Electrochem. Sci.* **2008**, *3*, 746.
(135) Zhang, J.; Ma, H.; Zhang, D.; Liu, P.; Tian, F.; Ding, Y. *Phys. Chem. Chem. Phys.* **2008**, *10*, 3250.
(136) Tsai, M.-C.; Yeh, T.-K.; Tsai, C.-H. *Mater. Chem. Phys.* **2008**, *109*, 422.
(137) Kima, S.; Park, S.-J. *Electrochim. Acta* **2008**, *53*, 4082.
(138) Li, P.; Wu, J.; Lin, J.; Huang, M.; Lan, Z.; Li, Q. *Electrochim. Acta* **2008**, *53*, 4161.
(139) Zhu, Z.-Z.; Wang, Z.; Li, H.-L. *Appl. Surf. Sci.* **2008**, *254*, 2934.
(140) Zhao, G.-Y.; Li, H.-L. *Appl. Surf. Sci.* **2008**, *254*, 3232.
(141) Montilla, F.; Morallo'n, E.; Duo, I.; Comninellis, C.; Vázquez, J. L. *Electrochim. Acta* **2003**, *48*, 3891.
(142) Cherstiouk, O. V.; Gavrilov, A. N.; Plyasova, L. M.; Molina, I. Y.; Tsirlina, G. A.; Savinova, E. R. *J. Solid State Electrochem.* **2008**, *12*, 497.
(143) Zou, Y.; Xiang, C.; Sun, L.-X.; Xu, R. *Biosens. Bioelectron.* **2008**, *23*, 1010.
(144) Qu, M.; Zhao, G.; Wang, Q.; Cao, X.; Zhang, J. *Nanotechnology* **2008**, *19*, 055707.
(145) Dominguez-Dominguez, S.; Arias-Pardilla, J.; Berenguer-Murcia, A.; Morallon, E.; Cazorla-Amoró, D. *J. Appl. Electrochem.* **2008**, *38*, 259.
(146) Wu, G.; Xu, B.-Q. *J. Power Sources* **2007**, *174*, 148.
(147) El Roustom, B.; Siné, G.; Foti, G.; Comninellis, Ch. *J. Appl. Electrochem.* **2007**, *37*, 1227.
(148) Napolskii, K. S.; Barczuk, P. J.; Vassiliev, S. Yu.; Veresov, A. G.; Tsirlina, G. A.; Kulesza, P. J. *Electrochim. Acta* **2007**, *52*, 7910.
(149) Kang, X.; Mai, Z.; Zou, X.; Cai, P.; Mo, J. *Anal. Biochem.* **2007**, *369*, 71.
(150) Ayyadurai, S. M.; Choi, Y.-S.; Ganesan, P.; Kumaraguru, S. P.; Popov, B. N. *J. Electrochem. Soc.* **2007**, *154*, B1063.
(151) Abdel Rahim, M. A.; Hassan, H. B.; Abdel Hameel, R. M. *Fuel Cells* **2007**, *4*, 298.
(152) Cui, H.-F.; Ye, J.-S.; Zhang, W.-D.; Li, C.-M.; Luong, J. H. T.; Sheu, F.-S. *Anal. Chim. Acta* **2007**, *594*, 175.
(153) Chen, X.; Li, N.; Eckhard, K.; Stoica, L.; Xia, W.; Assmann, J.; Muhler, M.; Schuhmann, W. *Electrochem. Commun.* **2007**, *9*, 1348.
(154) Xu, Y.; Lin, X. *J. Power Sources* **2007**, *170*, 13.
(155) Zhao, Y.; Fan, L.; Zhong, H.; Li, Y.; Yang, S. *Adv. Funct. Mater.* **2007**, *17*, 1537.
(156) Zhao, Y.; E, Y.; Fan, L.; Qiu, Y.; Yang, S. *Electrochim. Acta* **2007**, *52*, 5873.
(157) Bauer, A.; Gyenge, E. L.; Oloman, C. W. *J. Power Sources* **2007**, *167*, 281.
(158) Yu, P.; Yan, J.; Zhang, J.; Mao, L. *Electrochem. Commun.* **2007**, *9*, 1139.
(159) Xu, Y.; Lin, X. *Electrochim. Acta* **2007**, *52*, 5140.
(160) Zhao, Y.; Fan, L.; Zhong, H.; Li, Y. *Microchim. Acta* **2007**, *158*, 327.
(161) Chu, X.; Duan, D.; Shen, G. *Talanta* **2007**, *71*, 2040.
(162) Massoni, N.; Beaumont-Martinent, A.; Laurent, J.-Y. *J. Power Sources* **2007**, *166*, 68.
(163) Qu, F.; Yang, M.; Shen, G.; Yu, R. *Biosens. Bioelectron.* **2007**, *22*, 1749.
(164) Lee, J.; Seo, J.; Han, K.; Kim, H. *J. Power Sources* **2006**, *163*, 349.
(165) Tsai, M.-C.; Yeh, T.-K.; Juang, Z.-Y.; Tsai, C.-H. *Carbon* **2007**, *45*, 383.
(166) Zhao, G.-Y.; Xu, C.-L.; Guo, D.-J.; Li, H.; Li, H.-L. *Appl. Surf. Sci.* **2007**, *253*, 3242.
(167) Lee, U.-H.; Lee, J. H.; Jung, D.-Y.; Kwon, Y.-U. *Adv. Mater.* **2006**, *18*, 2825.
(168) Zhao, G.-Y.; Xu, C.-L.; Guo, D.-J.; Li, H.; Li, H.-L. *J. Power Sources* **2006**, *162*, 492.
(169) Yang, M.; Qu, F.; Lu, Y.; He, Y.; Shen, G.; Yu, R. *Biomaterials* **2006**, *27*, 5944.
(170) Wang, Z.-H.; Zhang, L.-L.; Qiu, K.-Y. *J. Power Sources* **2006**, *161*, 133.
(171) Liu, F.; Lee, J. Y.; Zhou, W. *J. Electrochem. Soc.* **2006**, *153*, A2133.
(172) Tsai, M.-C.; Yeh, T.-K.; Tsai, C.-H. *Electrochem. Commun.* **2006**, *8*, 1445.
(173) Bauer, A.; Gyenge, E. L.; Oloman, C. W. *Electrochim. Acta* **2006**, *51*, 5356.
(174) Gloaguen, F.; Leager, J. M.; Lamy, C.; Marmann, A.; Stimming, U.; Vogela, R. *Electrochim. Acta* **1999**, *44*, 1805.
(175) Siné, G.; Duo, I.; Elroustom, B.; Fóti, G.; Comninellis, Ch. *J. Appl. Electrochem.* **2006**, *36*, 847.
(176) Plyasova, L. M.; Molina, I. Yu.; Gavrilov, A. N.; Cherepanova, S. V.; Cherstiouk, O. V.; Rudin, N. A.; Savinova, E. R.; Tsirlina, G. A. *Electrochim. Acta* **2006**, *51*, 4477.
(177) Zhang, J.; Li, W.; Jones, G. A.; Shen, T. H. *J. Appl. Phys.* **2006**, *99*, Q502.
(178) Lu, G.; Zangari, G. *Electrochim. Acta* **2006**, *51*, 2531.
(179) Ye, J.-S.; Cui, H.-F.; Wen, Y.; Zhang, W. D.; Xu, G. Q.; Sheu, F.-S. *Microchim. Acta* **2006**, *152*, 267.
(180) Qian, L.; Liu, Y.; Song, Y.; Zhuang Li, Z.; Yang, X. *Electrochem. Commun.* **2005**, *7*, 1209.
(181) Selvaraju, T.; Ramaraj, R. *J. Electroanal. Chem.* **2005**, *585*, 290.
(182) Liu, F.; Yang Lee, J.; Zhou, W. *Adv. Funct. Mater.* **2005**, *15*, 1459.
(183) He, P.; Liu, H.; Li, Z.; Li, J. *J. Electrochem. Soc.* **2005**, *152*, E146.
(184) Cui, H.-F.; Ye, J.-S.; Zhang, W.-E.; Wang, F.; Sheu, F.-S. *J. Electroanal. Chem.* **2005**, *577*, 295.
(185) Wei, Z. D.; Chan, S. H.; Li, L. L.; Cai, H. F.; Xia, Z. T.; Sun, C. X. *Electrochim. Acta* **2005**, *50*, 2279.
(186) Guo, Y.-G.; Hu, J.-S.; Zhang, H.-M.; Liang, H.-P.; Wan, L.-J.; Bai, C.-L. *Adv. Mater.* **2005**, *17*, 746.
(187) Maillard, F.; Schreier, S.; Hanzlik, M.; Savinova, E. R.; Weinkauf, S.; Stimming, U. *Phys. Chem. Chem. Phys.* **2005**, *7*, 385.
(188) Tusseeva, E. K.; Mikhaylova, A. A.; Khazova, O. A.; Kourtakis, K.-D. *J. Electrochem. Soc.* **2004**, *40*, 1146.
(189) Wang, F.; Hosoiri, K.; Doi, S.; Okamoto, N.; Kuzushima, T.; Totsuka, T.; Watanabe, T. *Electrochem. Commun.* **2004**, *6*, 1149.
(190) He, Z.; Chen, J.; Liu, D.; Zhou, H.; Kuang, Y. *Diamond Relat. Mater.* **2004**, *13*, 1764.
(191) Mascaro, L. H.; Goncalves, D.; Bulhões, L. O. S. *Thin Solid Films* **2004**, *461*, 243.
(192) Wang, S.; Yin, Y.; Lin, X. *Electrochem. Commun.* **2004**, *6*, 259.
(193) Zhou, H. H.; Jiao, S. Q.; Chen, J. H.; Wei, W. Z.; Kuang, Y. F. *J. Appl. Electrochem.* **2004**, *34*, 455.

(194) Tang, H.; Chen, J.; Nie, L.; Liu, D.; Deng, W.; Kuang, Y.; Yao, S. *J. Colloid Interface Sci.* **2004**, *269*, 26.
(195) Gao, T.-R.; Chen, Z.-Y.; Peng, Y.; Li, F.-S. *Chin. Phys.* **2002**, *11*, 1307.
(196) Xiao, F.; Zhao, F.; Zhang, Y.; Guo, G.; Zeng, B. *J. Phys. Chem. C* **2009**, *113*, 849.
(197) Suzuki, T.; Miyata, H.; Noma, T.; Kuroda, K. *J. Phys. Chem. C* **2008**, *112*, 1831.
(198) Day, T. M.; Unwin, P. R.; Wilson, N. R.; Macpherson, J. V. *J. Am. Chem. Soc.* **2005**, *127*, 10639.
(199) Tian, N.; Zhou, Z.-Y.; Sun, S.-G.; Ding, Y.; Wang, Z. L. *Science* **2007**, *316*, 732.
(200) Tsakova, V. *J. Solid State Electrochem.* **2008**, *12*, 1421.
(201) Ron, I.; Friedman, N.; Cahen, D.; Sheves, M. *Small* **2008**, *4*, 2271.
(202) Qin, F.; Shen, W.; Wang, C.; Xu, H. *Catal. Commun.* **2008**, *9*, 2095.
(203) Lohmueller, T.; Bock, E.; Spatz, J. P. *Adv. Mater.* **2008**, *20*, 2297.
(204) Chu, S. Z.; Kawamura, H.; Mori, M. *J. Electrochem. Soc.* **2008**, *155*, D414.
(205) Lombardi, I.; Marchionna, S.; Zangari, G.; Pizzini, S. *Langmuir* **2007**, *23*, 12413.
(206) Yae, S.; Nasu, N.; Matsumoto, K.; Hagihara, T.; Fukumuro, N.; Matsud, H. *Electrochim. Acta* **2007**, *53*, 35.
(207) Tegou, A.; Papadimitriou, S.; Pavlidou, E.; Kokkinidis, G.; Sotiropoulos, S. *J. Electroanal. Chem.* **2007**, *608*, 67.
(208) Zhu, J.; Su, Y.; Cheng, F.; Chen, J. *J. Power Sources* **2007**, *166*, 331.
(209) Metz, K. M.; Goel, D.; Hamers, R. J. *J. Phys. Chem. C* **2007**, *111*, 7260.
(210) Yae, S.; Kobayashi, T.; Abe, M.; Nasu, N.; Fukumuro, N.; Ogawa, S.; Yoshida, N.; Nonomura, S.; Nakato, Y.; Matsuda, H. *Sol. Energy Mater. Sol. Cells* **2007**, *91*, 224.
(211) Travitsky, N.; Ripenbein, T.; Golodnitsky, D.; Rosenberg, Y.; Burshtein, L.; Peleb, E. *J. Power Sources* **2006**, *161*, 782.
(212) Fujii, T.; Ito, M. *Fuel Cells* **2006**, *5*, 356.
(213) Díaz, D. J.; Williamson, T. L.; Guo, X.; Sood, A.; Bohn, P. W. *Thin Solid Films* **2006**, *514*, 120.
(214) Qu, L.; Dai, L.; Osawa, E. *J. Am. Chem. Soc.* **2006**, *128*, 5523.
(215) Daz, R.; Arbiol, J.; Sanz, F.; Cornet, A.; Morante, J. R. *Chem. Mater.* **2002**, *14*, 3277.
(216) Chen, J.; Lim, B.; Lee, E. P.; Xia, Y. *Nano Today* **2009**, *4*, 81.
(217) Elechiguerra, J. L.; Larios-Lopez, L.; Jose-Yacaman, M. *Appl. Phys. A: Mater. Sci. Process.* **2006**, *84*, 11.
(218) Elezović, N. R.; Gajić-Krstaji, L.; Radmilović, V.; Vračard, L.; Krstajić, N. V. *Electrochim. Acta* **2009**, *54*, 1375.
(219) Jeyabharathi, C.; Mathiyarasu, J.; Phani, K. L. N. *J. Appl. Electrochem.* **2009**, *39*, 45.
(220) Wang, Z.-C.; Zhao, D.-D.; Zhao, G.-Y.; Li, H.-L. *J. Solid State Electrochem.* **2009**, *13*, 371.
(221) Hwang, B.-J.; Sarma, L. S.; Chen, C.-H.; Bock, C.; Lai, F.-J.; Chang, S.-H.; Yen, S.-C.; Liu, D.-G.; Sheu, H.-S.; Lee, J. F. *J. Phys. Chem. C* **2008**, *112*, 19922.
(222) Knupp, S. L.; Li, W.; Paschos, O.; Murray, T. M.; Snyder, J.; Haldar, P. *Carbon* **2008**, *46*, 1276.
(223) Jiang, Q.-Z.; Wu, X.; Shen, M.; Ma, Z.-F.; Zhu, X.-Y. *Catal. Lett.* **2008**, *124*, 434.
(224) Susut, C.; Nguyena, T. D.; Chapman, G. B.; Tong, Y. *Electrochim. Acta* **2008**, *53*, 6135.
(225) Formo, E.; Peng, Z.; Lee, E.; Lu, X.; Yang, H.; Xia, Y. *J. Phys. Chem. C* **2008**, *112*, 9970.
(226) Ren, L.; Xing, Y. *Electrochim. Acta* **2008**, *53*, 5563.
(227) Li, H.; Sun, G.; Gao, Y.; Jiang, Q.; Jia, Z.; Xin, Q. *J. Phys. Chem. C* **2007**, *111*, 15192.
(228) Oh, H.-S.; Oh, J.-G.; Hong, Y.-G.; Kim, H. *Electrochim. Acta* **2007**, *52*, 7278.
(229) Lee, E. P.; Peng, Z.; Cate, D. M.; Yang, H.; Campbell, C. T.; Xia, Y. *J. Am. Chem. Soc.* **2007**, *129*, 10634.
(230) Nitani, H.; Nakagawa, T.; Daimon, H.; Kurobe, Y.; Ono, T.; Honda, Y.; Koizumi, A.; Seino, S.; Yamamoto, T. A. *Appl. Catal., A* **2007**, *326*, 194.
(231) Song, S.; Wang, Y.; Shen, P. K. *J. Power Sources* **2007**, *170*, 46.
(232) Guo, J.; Sun, G.; Sun, S.; Yan, S.; Yang, W.; Qi, J.; Yan, Y.; Xin, Q. *J. Power Sources* **2007**, *168*, 299.
(233) Liu, Z.; Ling, X. Y.; Guo, B.; Hong, L.; Lee, J. Y. *J. Power Sources* **2007**, *167*, 272.
(234) Li, H.; Sun, G.; Li, N.; Sun, S.; Su, D.; Xin, Q. *J. Phys. Chem. C* **2007**, *111*, 5605.
(235) Yan, S.; Sun, G.; Tian, J.; Jiang, L.; Qi, J.; Xin, Q. *Electrochim. Acta* **2006**, *52*, 1692.
(236) Rioux, R. M.; Song, H.; Grass, M.; Habas, S.; Niesz, K.; Hoefelmeyer, J. D.; Yang, P.; Somorjai, G. A. *Top. Catal.* **2006**, *39*, 167.
(237) Tseng, C.-H.; Lo, S.-T.; Lo, S.-C.; Chu, P. P. *Mater. Chem. Phys.* **2006**, *100*, 385.
(238) Chen, J.; Xiong, Y.; Yin, Y.; Xia, Y. *Small* **2006**, *2*, 1340.
(239) Roychowdhury, C.; Matsumoto, F.; Mutolo, P. F.; Abrua, H. D.; DiSalvo, F. J. *Chem. Mater.* **2005**, *17*, 5871.
(240) Jiang, L.; Sun, G.; Sun, S.; Liu, J.; Tang, S.; Li, H.; Zhou, B.; Xin, Q. *Electrochim. Acta* **2005**, *50*, 5384.
(241) Li, X.; Chen, W.-X.; Zhao, J.; Xing, W.; Xu, Z.-D. *Carbon* **2005**, *43*, 2168.
(242) Chen, J.; Herricks, T.; Xia, Y. *Angew. Chem., Int. Ed.* **2005**, *44*, 2589.
(243) Chen, W.; Zhao, J.; Lee, J. Y.; Liu, Z. *Mater. Chem. Phys.* **2005**, *91*, 124.
(244) Herricks, T.; Chen, J.; Xia, Y. *Nano Lett.* **2004**, *4*, 2367.
(245) Chen, W.-X.; Lee, J. Y.; Liu, Z. *Mater. Lett.* **2004**, *58*, 3166.
(246) Liu, Z.; Lee, J. Y.; Chen, W.; Han, M.; Gan, M. L. *Langmuir* **2004**, *20*, 181.
(247) Iwaki, T.; Kakihara, Y.; Toda, T.; Abdulla, M.; Okuyama, K. *J. Appl. Phys.* **2003**, *94*, 6807.
(248) Antolini, E.; Lopes, T.; Gonzalez, E. R. *J. Alloys Compd.* **2008**, *461*, 253.
(249) Carpenter, E. E.; Sims, J. A.; Wienmann, J. A.; Zhou, W. L.; O'Connor, C. J. *J. Appl. Phys.* **2000**, *87*, 5615.
(250) Malheiro, A. R.; Perez, J.; Villullas, H. M. *J. Electrochem. Soc.* **2009**, *156*, B51.
(251) Lim, D.-H.; Lee, W.-D.; Choi, D.-H.; Park, D.-R.; Lee, H.-I. *J. Power Sources* **2008**, *185*, 159.
(252) Matsumoto, F.; Roychowdhury, C.; DiSalvo, F. J.; Abruña, H. D. *J. Electrochem. Soc.* **2008**, *155*, B148.
(253) Song, Y.; Garcia, R. M.; Dorin, R. M.; Wang, H.; Qiu, Y.; Coker, E. N.; Steen, W. A.; Miller, J. E.; Shelnutt, J. A. *Nano Lett.* **2007**, *7*, 3650.
(254) Xue, X.; Ge, J.; Tian, T.; Liu, C.; Xing, W.; Lu, T. *J. Power Sources* **2007**, *172*, 560.
(255) Wang, J. J.; Yin, G. P.; Zhang, J.; Wang, Z. B.; Gao, Y. Z. *Electrochim. Acta* **2007**, *52*, 7042.
(256) Wang, J.; Yin, G.; Shao, Y.; Wang, Z.; Gao, Y. *J. Electrochem. Soc.* **2007**, *154*, B687.
(257) Yao, W.; Yang, J.; Wang, J.; Nuli, Y. *Electrochem. Commun.* **2007**, *9*, 1029.
(258) Harada, M.; Einaga, H. *J. Colloid Interface Sci.* **2007**, *308*, 568.
(259) Prabhuram, J.; Zhao, T. S.; Liang, Z. X.; Chen, R. *Electrochim. Acta* **2007**, *52*, 2649.
(260) Roychowdhury, C.; Matsumoto, F.; Zeldovich, V. B.; Warren, S. C.; Mutolo, P. F.; Ballesteros, M. J.; Wiesner, U.; Abrua, H. D.; DiSalvo, F. J. *Chem. Mater.* **2006**, *18*, 3365.
(261) Nagao, D.; Shimazaki, Y.; Kobayashi, Y.; Konno, M. *Colloids Surf., A* **2006**, *273*, 97.
(262) Guo, J. W.; Zhao, T. S.; Prabhuram, J.; Chen, R.; Wong, C. W. *Electrochim. Acta* **2005**, *51*, 754.
(263) Guo, J. W.; Zhao, T. S.; Prabhuram, J.; Wong, C. W. *Electrochim. Acta* **2005**, *50*, 1973.
(264) Solla-Gullon, J.; Vidal-Iglesias, F. J.; Montiel, V.; Alda, A. *Electrochim. Acta* **2004**, *49*, 5079.
(265) Eklund, S. E.; Cliffel, D. E. *Langmuir* **2004**, *20*, 6012.
(266) Kumbhar, A.; Spinu, L.; Agnoli, F.; Wang, K.-Y.; Zhou, W.; O'Connor, C. J. *IEEE Trans. Magn.* **2001**, *37*, 2216.
(267) Zhang, X.; Chan, K.-Y. *Chem. Mater.* **2003**, *15*, 451.
(268) Park, J.-I.; Cheon, J. *J. Am. Chem. Soc.* **2001**, *123*, 5743.
(269) Tang, H.; Chen, J. H.; Huang, Z. P.; Wang, D. Z.; Ren, Z. F.; Nie, L. H.; Kuang, Y. F.; Yao, S. Z. *Carbon* **2004**, *42*, 191.
(270) Teranishi, T.; Hosoe, M.; Miyake, M. *Adv. Mater.* **1997**, *9*, 65.
(271) He, Z.; Chen, J.; Liu, D.; Tang, H.; Deng, W.; Kuang, Y. *Mater. Chem. Phys.* **2004**, *85*, 396.
(272) Guo, D.-J.; Li, H.-L. *J. Electroanal. Chem.* **2004**, *573*, 197.
(273) Jeyadevan, B.; Hobo, A.; Urakawa, K.; Chinnasamy, C. N.; Shinoda, K.; Tohji, K. *J. Appl. Phys.* **2003**, *93*, 7574.
(274) Luo, J.; Maye, M. M.; Petkov, V.; Kariuki, N. N.; Wang, L.; Njoki, P.; Mott, D.; Lin, Y.; Zhong, C.-J. *Chem. Mater.* **2005**, *17*, 3086.
(275) Guo, J.; Sun, G.; Wang, Q.; Wang, G.; Zhou, Z.; Tang, S.; Jiang, L.; Zhou, B.; Xin, Q. *Carbon* **2006**, *44*, 152.
(276) Wu, M.-L.; Chen, D.-H.; Huang, T.-C. *J. Colloid Interface Sci.* **2001**, *243*, 102.
(277) Liang, Y.; Zhang, H.; Yi, B.; Zhang, Z.; Tan, Z. *Carbon* **2005**, *43*, 3144.
(278) Yashima, M.; Falk, L. K. L.; Palmqvist, A. E. C.; Holmberg, K. *J. Colloid Interface Sci.* **2003**, *268*, 348.
(279) Bensebaa, F.; Patrito, N.; Le Page, Y.; L'Ecuyer, P.; Wang, D. *J. Mater Chem.* **2004**, *14*, 3378.
(280) (a) Sun, S.-G.; Chen, A.; Huang, T. S.; Li, J. B.; Tian, Z. W. *J. Electroanal. Chem.* **1992**, *340*, 213. (b) Tian, N.; Zhou, Z.-Y.; Sun, S.-G. *Chem. Commun.* **2009**, 1502.
(281) Bartlett, P. N.; Baumberg, J. J.; Coyle, S.; Abdelsalam, M. E. *Faraday Discuss.* **2004**, *125*, 117.
(282) Kim, S. J.; Ah, C. S.; Jang, D.-J. *Adv. Mater.* **2007**, *19*, 1064.

(283) Grzelczak, M.; Prez-Juste, J.; Garca de Abajo, F. J.; Liz-Marzn, L. M. *J. Phys. Chem. C* **2007**, *111*, 6183.
(284) Tong, X. L.; Lin, K.; Lv, D. J.; Yang, M. H.; Liu, Z. X.; Zhang, D. S. *Appl. Surf. Sci.* **2009**, *255*, 7995.
(285) Bigall, N. C.; Hartling, T.; Klose, M.; Simon, P.; Eng, L. M.; Eychmuller, A. *Nano Lett.* **2008**, *8*, 4588.
(286) Kim, S. H.; Kim, K. C.; Kim, Y. S.; Kim, H. L. *Curr. Appl. Phys.* **2006**, *6*, 1036.
(287) Tian, N.; Zhou, Z.-Y.; Sun, S.-G.; Cui, L.; Ren, B.; Tian, Z.-Q. *Chem. Commun.* **2006**, 4090.
(288) Delaunay, J.-J.; Hayashi, T.; Tomita, M.; Hirono, S.; Umemura, S. *Appl. Phys. Lett.* **1997**, *71*, 3427.
(289) Sun, X.; Kang, S.; Harrell, J. W.; Nikles, D. E. *J. Appl. Phys.* **2003**, *93*, 7337.
(290) Chinnasamy, C. N.; Jeyadevan, B.; Shinoda, K.; Tohji, K. *J. Appl. Phys.* **2003**, *93*, 7583.
(291) Petit, C.; Rusponi, S.; Brune, H. *J. Appl. Phys.* **2004**, *95*, 4251.
(292) Delin, A.; Tosatti, E. *Surf. Sci.* **2004**, *262*, 566.
(293) Liu, X.; Bauer, M.; Bertagnolli, H.; Roduner, E.; van Slageren, J.; Phillipp, F. *Phys. Rev. Lett.* **2006**, *97*, 253401.
(294) (a) Yang, X. M.; Liu, C.; Ahner, J.; Yu, J.; Klemmer, T.; Johns, E.; Weller, D. *J. Vac. Sci. Technol. B* **2004**, *22*, 31. (b) Latham, A. H.; Williams, M. E. *Acc. Chem. Res.* **2008**, *41*, 411.
(295) Du, X.; Inokuchi, M.; Toshima, N. *J. Magn. Magn. Mater.* **2006**, *299*, 21.
(296) Zhang, H.-T.; Ding, J.; Chow, G.-M. *Langmuir* **2008**, *24*, 375.
(297) Yamamoto, Y.; Miura, T.; Nakae, Y.; Teranishi, T.; Miyake, M.; Hori, H. *Physica B* **2003**, *1183*, 329.
(298) Teng, X.; Han, W.-Q.; Ku, W.; Hucker, M. *Angew. Chem., Int. Ed.* **2008**, *47*, 2055.
(299) (a) Arenz, M.; Mayrhofer, K. J. J.; Stamenkovic, V.; Blizanac, B. B.; Tomoyuki, T.; Ross, P. N.; Markovic, N. M. *J. Am. Chem. Soc.* **2005**, *127*, 6819. (b) Chen, A.; La Russa, D.; Miller, B. *Langmuir* **2004**, *20*, 9695.
(300) Mayrhofer, K. J. J.; Arenz, M.; Blizanac, B. B.; Stamenkovic, V.; Ross, P. N.; Markovic, N. M. *Electrochim. Acta* **2005**, *50*, 5144.
(301) Maillard, F.; Savinova, E. R.; Stimming, U. *J. Electroanal. Chem.* **2007**, *599*, 221.
(302) Maillard, F.; Eikerling, M.; Cherstiouk, O. V.; Schreier, S.; Savinova, E.; Stimmin, U. *Faraday Discuss.* **2004**, *125*, 357.
(303) Mott, D.; Luo, J.; Njoki, P. N.; Lin, Y.; Wang, L.; Zhong, C.-J. *Catal. Today* **2007**, *122*, 378.
(304) Antolini, E.; Salgado, J. R. C.; Gonzalez, E. R. *Appl. Catal., B* **2006**, *63*, 137.
(305) Colmati, F.; Antolini, E.; Gonzalez, E. R. *Electrochim. Acta* **2005**, *50*, 5496.
(306) Ordóñeza, L. C.; Roquero, P.; Sebastian, P. J.; Ramírez, J. *Int. J. Hydrogen Energy* **2007**, *32*, 3147.
(307) Zeng, J.; Lee, J. Y. *Int. J. Hydrogen Energy* **2007**, *32*, 4389.
(308) Tong, Y. Y.; Kim, H. S.; Babu, P. K.; Waszczuk, P.; Wieckowski, A.; Oldfield, E. *J. Am. Chem. Soc.* **2002**, *124*, 468.
(309) Waszczuk, P.; Solla-Gullon, J.; Kim, H.-S.; Tong, Y. Y.; Montiel, V.; Aldaz, A.; Wieckowski, A. *J. Catal.* **2001**, *203*, 1.
(310) Lin, W. F.; Zei, M. S.; Eiswirth, M.; Ertl, G.; Iwasita, T.; Vielstich, W. *J. Phys. Chem. B* **1999**, *103*, 6968.
(311) Batista, E. A.; Hoster, H.; Iwasita, T. *J. Electroanal. Chem.* **2003**, *554*−*555*, 265.
(312) Lin, W. F.; Iwasita, T.; Vielstich, W. *J. Phys. Chem. B* **1999**, *103*, 3250.
(313) Zheng, M.-S.; Sun, S.-G.; Chen, S.-P. *J. Appl. Electrochem.* **2001**, *31*, 749.
(314) Sato, T.; Kunimatsu, K.; Uchida, H.; Watanabe, M. *Electrochim. Acta* **2007**, *53*, 1265.
(315) Chen, Q.-S.; Sun, S.-G.; Zhou, Z.-Y.; Chen, Y.-X.; Deng, S.-B. *Phys. Chem. Chem. Phys.* **2008**, *10*, 3645.
(316) Maillard, F.; Savinova, E. R.; Simonov, P. A.; Zaikovskii, V. I.; Stimming, U. *J. Phys. Chem. B* **2004**, *108*, 17893.
(317) Tsiouvaras, N.; Martínez-Huerta, M. V.; Moliner, R.; Lázaro, M. J.; Rodríguez, J. L.; Pastor, E.; Pena, M. A.; Fierroa, J. L. G. *J. Power Sources* **2009**, *186*, 299.
(318) Garcia, A. C.; Paganin, V. A.; Ticianelli, E. A. *Electrochim. Acta* **2008**, *53*, 4309.
(319) Jeon, M. K.; Lee, K. R.; Daimon, H.; Nakahara, A.; Woo, S. I. *Catal. Today* **2008**, *132*, 123.
(320) Carmo, M.; Paganin, V. A.; Rosolen, J. M.; Gonzalez, E. R. *J. Power Sources* **2005**, *142*, 169.
(321) Stolbov, S.; Ortigoza, M. A.; Adzic, R.; Rahman, T. S. *J. Chem. Phys.* **2009**, *130*, 124714.
(322) Uchida, H.; Izumi, K.; Aoki, K.; Watanabe, M. *Phys. Chem. Chem. Phys.* **2009**, *11*, 1771.
(323) Adzic, R. R.; Zhang, J.; Sasaki, K.; Vukmirovic, M. B.; Shao, M.; Wang, J. X.; Nilekar, A. U.; Mavrikakis, M.; Valerio, J. A.; Uribe, F. *Top. Catal.* **2007**, *46*, 249.
(324) Götz, M.; Wendt, H. *Electrochim. Acta* **1998**, *43*, 3637.
(325) Mazurek, M.; Benker, N.; Roth, C.; Fuess, H. *Fuel Cells* **2006**, *3*−*4*, 208.
(326) Camara, G. A.; Ticianelli, E. A.; Mukerjee, S.; Lee, S. J.; McBreen, J. *J. Electrochem. Soc.* **2002**, *149*, A748.
(327) Venkataraman, R.; Kunz, H. R.; Fenton, J. M. *J. Electrochem. Soc.* **2003**, *150*, A278.
(328) He, C.; Kunz, H. R.; Fenton, J. M. *J. Electrochem. Soc.* **2003**, *150*, A1017.
(329) Wu, G.; Adams, B.; Tian, M.; Chen, A. *Electrochem. Commun.* **2009**, *11*, 736.
(330) Leger, J.-M. *J. Appl. Electrochem.* **2001**, *31*, 767.
(331) Hsieh, C.-T.; Lin, J.-Y. *J. Power Sources* **2009**, *188*, 347.
(332) Ghosh, T.; Matsumoto, F.; McInnis, J.; Weiss, M.; Abrunã, H. D.; DiSalvo, F. J. *J. Nanopart. Res.* **2009**, *11*, 965.
(333) Justin, P.; Rao, G. R. *Catal. Today* **2009**, *141*, 138.
(334) Tang, W.; Jayaraman, S.; Jaramillo, T. F.; Stucky, G. D.; McFarland, E. W. *J. Phys. Chem. C* **2009**, *113*, 5014.
(335) Lima, A.; Coutanceau, C.; Leãger, J.-M.; Lamy, C. *J. Appl. Electrochem.* **2001**, *31*, 379.
(336) Liag, Y.; Zhang, H.; Zhong, H.; Zhu, X.; Tian, Z.; Xu, D.; Yi, B. *J. Catal.* **2006**, *238*, 468.
(337) Zhong, C.-J.; Luo, J.; Njoki, P. N.; Mott, D.; Wanjala, B.; Loukrakpam, R.; Lim, S.; Wang, L.; Fang, B.; Xu, Z. *Energy Environ. Sci.* **2008**, *1*, 454.
(338) Vigier, F.; Coutanceau, C.; Perrard, A.; Belgsir, E.; Lamy, C. *J. Appl. Electrochem.* **2004**, *34*, 439.
(339) Lamy, C.; Rousseau, S.; Belgsir, E. M.; Coutanceau, C.; Léger, J.-M. *Electrochim. Acta* **2004**, *49*, 3901.
(340) Wang, Q.; Sun, G. Q.; Jiang, L. H.; Xin, Q.; Sun, S.-G.; Jiang, Y. X.; Chen, S. P.; Jusys, Z.; Behm, R. J. *Phys. Chem. Chem. Phys.* **2007**, *9*, 2686.
(341) Zhang, X.; Lu, W.; Da, J.; Wang, H.; Zhao, D.; Webley, P. A. *Chem. Commun.* **2009**, 195.
(342) Zhou, W.; Zhou, Z.; Song, S.; Li, W.; Sun, G.; Tsiakaras, P.; Xin, Q. *Appl. Catal., B* **2003**, *46*, 273.
(343) Liu, Z.; Ling, X. Y.; Su, X.; Lee, J. Y.; Gan, L. M. *J. Power Sources* **2005**, *149*, 1.
(344) Léger, J.-M. *Electrochim. Acta* **2005**, *50*, 3123.
(345) Purgato, F. L. S.; Olivi, P.; Léger, J.-M.; de Andrade, A. R.; Tremiliosi-Filho, G.; Gonzalez, E. R.; Lamym, C.; Kokoh, K. B. *J. Electroanal. Chem.* **2009**, *628*, 81.
(346) Zhou, W. J.; Li, W. Z.; Song, S. Q.; Zhou, Z. H.; Jiang, L. H.; Sun, G. Q.; Xin, Q.; Poulianitis, K.; Kontou, S.; Tsiakaras, P. *J. Power Sources* **2004**, *131*, 217.
(347) Ribeiro, J.; dos Anjos, D. M.; Kokoh, K. B.; Coutanceau, C.; Léger, J.-M.; Olivi, P.; de Andrade, A. R.; Tremiliosi-Filho, G. *Electrochim. Acta* **2007**, *52*, 6997.
(348) Kowal, A.; Li, M.; Shao, M.; Sasaki, K.; Vukmirovic, M. B.; Zhang, J.; Marinkovic, N. S.; Liu, P.; Frenkel, A. I.; Adzic, R. R. *Nat. Mater.* **2009**, *8*, 325.
(349) Camara, G. A.; de Lima, R. B.; Iwasita, T. *J. Electroanal. Chem.* **2005**, *585*, 128.
(350) Léger, J.-M.; Rousseau, S.; Coutanceau, C.; Hahn, F.; Lamy, C. *Electrochim. Acta* **2005**, *50*, 5118.
(351) Yu, X.; Pickup, P. G. *J. Power Sources* **2008**, *182*, 124.
(352) Chetty, R.; Scott, K. *J. New Mater. Electr. Sys.* **2007**, *10*, 135.
(353) Park, S.; Xie, Y.; Weaver, M. J. *Langmuir* **2002**, *18*, 5792.
(354) Jayashree, R. S.; Spendelowa, J. S.; Yeom, J.; Rastogi, C.; Shannon, M. A.; Kenis, P. J. A. *Electrochim. Acta* **2005**, *50*, 4674.
(355) Chi, N.; Chan, K.-Y.; Phillips, D. L. *Catal. Lett.* **2001**, *71*, 21.
(356) Chen, W.; Kim, J.; Sun, S.; Chen, S. *Phys. Chem. Chem. Phys.* **2006**, *8*, 2779.
(357) Lee, H. J.; Habas, S. E.; Somorjai, G. A.; Yang, P. D. *J. Am. Chem. Soc.* **2008**, *130*, 5406.
(358) Xu, J. B.; Zhao, T. S.; Liang, Z. X. *J. Power Sources* **2008**, *185*, 857.
(359) Xu, J. B.; Zhao, T. S.; Liang, Z. X. *J. Phys. Chem. C* **2008**, *112*, 17362.
(360) Wang, J.; Asmussen, R. M.; Adams, B.; Thomas, D. F.; Chen, A. *Chem. Mater.* **2009**, *21*, 1716.
(361) Zhang, T.; Anderson, A. B. *Electrochim. Acta* **2007**, *53*, 982.
(362) Murthi, V. S.; Urian, R. C.; Mukerjee, S. *J. Phys. Chem. B* **2004**, *108*, 11011.
(363) Antoine, O.; Bultel, Y.; Durand, R. *J. Electroanal. Chem.* **2001**, *499*, 85.
(364) Genies, L.; Faure, R.; Durand, R. *Electrochim. Acta* **1998**, *44*, 1317.
(365) Kongkanand, A.; Kuwabata, S.; Girishkumar, G.; Kamat, P. *Langmuir* **2006**, *22*, 2392.
(366) Maillard, F.; Martin, M.; Gloaguen, F.; Léger, J.-M. *Electrochim. Acta* **2002**, *4*, 7–3431.
(367) Zhou, H.; Zhou, W.-P.; Adzic, R. R.; Wong, S. S. *J. Phys. Chem. C* **2009**, *113*, 5460.

(368) Yang, W.; Yang, C.; Sun, M.; Yang, F.; Ma, Y.; Zhang, Z.; Yang, X. *Talanta* **2009**, *78*, 557.
(369) Xiong, L.; Kannan, A. M.; Manthiram, A. *Electrochem. Commun.* **2002**, *4*, 898.
(370) Yang, H.; Coutanceau, C.; Léger, J.-M.; Alonso-Vante, N.; Lamy, C. *J. Electroanal. Chem.* **2005**, *576*, 305.
(371) Chen, S.; Ferreira, P. J.; Sheng, W.; Yabuuchi, N.; Allard, L. F.; Shao-Horn, Y. *J. Am. Chem. Soc.* **2008**, *130*, 13818.
(372) Antolini, E.; Salagado, J. R. C.; Santos, L. G. R. A.; Garcia, G.; Ticianelli, E. A.; Pastor, E.; Gonzalez, E. R. *J. Appl. Electrochem.* **2006**, *36*, 355.
(373) Yang, H.; Alonso-Vante, N.; Leger, J.-M.; Lamy, C. J. *J. Phys. Chem. B* **2004**, *108*, 1938.
(374) Yang, H.; Vogel, W.; Lamy, C.; Alonso-Vante, N. *J. Phys. Chem B* **2004**, *108*, 11024.
(375) Chen, G.; Delafuente, D.; Pani, S.; Mallouk, T. E. *Catal. Today* **2001**, *67*, 341.
(376) He, T.; Kreidler, E.; Xiong, L.; Luo, J.; Zhong, C. J. *J. Electrochem. Soc.* **2006**, *153*, A1637.
(377) Ioroi, T.; Yasuda, K. *J. Electrochem. Soc.* **2005**, *152*, A1917.
(378) Shimizu, K.; Cheng, I. F.; Wai, C. M. *Electrochem. Commun.* **2009**, *11*, 691.
(379) Zhang, J.; Sasaki, K.; Sutter, R.; Adzic, R. R. *Science* **2007**, *315*, 220.
(380) Wang, C.; Daimon, H.; Sun, S. *Nano Lett.* **2009**, *9*, 1493.
(381) Elezovic, N. R.; Babic, B. M.; Radmilovic, V. R.; Vracard, L. M.; Krstajic, N. V. *Electrochim. Acta* **2009**, *54*, 2404.
(382) Park, S.; Boo, H.; Chung, T. D. *Anal. Chim. Acta* **2006**, *556*, 46.
(383) Xie, J.; Wang, S.; Aryasomayajula, L.; Varadan, V. K. *Nanotechnology* **2007**, *18*, 065503.
(384) Pang, X.; He, D.; Luo, S.; Cai, Q. *Sens. Actuators B* **2009**, *137*, 134.
(385) Rong, L.-Q.; Yang, C.; Qian, Q.-Y.; Xia, X.-H. *Talanta* **2007**, *72*, 819.
(386) Shen, Q.; Jiang, L.; Zhang, H.; Min, Q.; Hou, W.; Zhu, J.-J. *J. Phys. Chem. C* **2008**, *112*, 16385.
(387) Yuan, J.; Wang, K.; Xia, X. *Adv. Funct. Mater.* **2005**, *15*, 803–809.
(388) Wittstock, G.; Strubing, A.; Azargan, R.; Werner, G. *J. Electroanal. Chem.* **1998**, *444*, 61.
(389) X. Zhang, X.; Chan, K.-Y.; You, J.-K.; Lin, Z.-G.; Tseung, A. C. C. *J. Electroanal. Chem.* **1997**, *430*, 147.
(390) Bai, Y.; Sun, Y.; Sun, C. *Biosens. Bioelectron.* **2008**, *24*, 579.
(391) Kang, Q.; Yang, L.; Cai, Q. *Biolectrochemistry* **2008**, *74*, 62.
(392) Li, L.-H.; Zhang, W.-D.; Ye, J.-S. *Electroanalysis* **2008**, *20*, 2212.
(393) Sun, Y.; Buck, H.; Mallouk, T. E. *Anal. Chem.* **2001**, *73*, 1599.
(394) Jin, C.; Chen, Z. *Synth. Met.* **2007**, *157*, 592.
(395) Chou, C.-H.; Chang, J.-L.; Zen, J.-M. *Electroanalysis* **2009**, *21*, 206.
(396) Sathe, B. R.; Risbud, M. S.; Patil, S.; Ajayakumar, K. S.; Naik, R. C.; Mulla, I. S.; Pillai, V. K. *Sens. Actuators A* **2007**, *138*, 376.
(397) Lloyd, S. M.; Lave, L. B.; Matthews, H. S. *Environ. Sci. Technol.* **2005**, *39*, 1384.
(398) Tanaka, H.; Uenishi, M.; Taniguchi, M.; Tan, I.; Narita, K.; Kimura, M.; Kaneko, K.; Nishihata, Y.; Mizuki, J. *Catal. Today* **2006**, *117*, 321.
(399) Wang, Y.; Shah, N.; Huffman, G. P. *Energy Fuels* **2004**, *18*, 1429.
(400) Yoshida, H.; Hirao, K.; Nishimoto, J.-I.; Shimura, K.; Kato, S.; Itoh, H.; Hattori, T. *J. Phys. Chem. C* **2008**, *112*, 5542.
(401) Petrik, L. F.; Godongwana, Z. G.; Iwuoha, E. I. *J. Power Sources* **2008**, *185*, 838.
(402) Velichkina, L. M.; Pestryakov, A. N.; Vosmerikov, A. V.; Tuzovskaya, I. V.; Bogdanchikova, N. E.; Avalos, M.; Farias, M.; Tiznado, H. *Petrol. Chem.* **2008**, *48*, 201.
(403) Velichkina, L. M.; Pestryakov, A. N.; Vosmerikov, A. V.; Tuzovskaya, I. V.; Bogdanchikova, N. E.; Avalos, M.; Farias, M.; Tiznado, H. *Petrol. Chem* **2008**, *48*, 355.
(404) Sartale, S. D.; Shiu, H.-W.; Wen, W.-H.; Luo, M.-F.; Lin, Y. C.; Hsu, Y.-J. *Catal. Lett.* **2007**, *119*, 95.
(405) Molnar, E.; Tasi, G.; Konya, Z.; Kiricsi, I. *Catal. Lett.* **2005**, *101*, 159.
(406) Connor, H. *Platinum Met. Rev.* **1961**, *5*, 9.
(407) Bond, G. C. *Platinum Met. Rev.* **2007**, *51*, 63.
(408) Bhattacharya, R.; Mukherjee, P. *Adv. Drug Delivery Rev.* **2008**, *60*, 1289.
(409) Welch, C. M.; Compton, R. G. *Anal. Bioanal. Chem.* **2006**, *384*, 601.
(410) Gao, J.; Liang, G.; Zhang, B.; Kuang, Y.; Zhang, X.; Xu, B. *J. Am. Chem. Soc.* **2007**, *129*, 1428.
(411) Rieter, W. J.; Pott, K. M.; Taylor, K. M. L.; Lin, W. *J. Am. Chem. Soc.* **2008**, *130*, 11584.

CR9003902